Road scene understanding from multisensorial data

Abderrahim KASMI [1,2], Dieumet DENIS [1], Romuald Aufrère [2], Roland CHAPUIS[2]

(1) Sherpa Engineering, 12 Avenue de Verdun 1916, 92250 La Garenne-Colombes
(2) Institut PASCAL, Campus Universitaire des Cézeaux, 4 Avenue Blaise Pascal, 63178 Aubière

Ecole doctorale Sciences Pour l'Ingénieur

Objectives

Road scene understanding has been the subject of different researches. Generally the elements of the road scene are recognized independently of each other.
The main goal of this thesis is to develop a generic algorithm for road scene understanding, that takes into account the reliance between the road elements.

Global Scheme

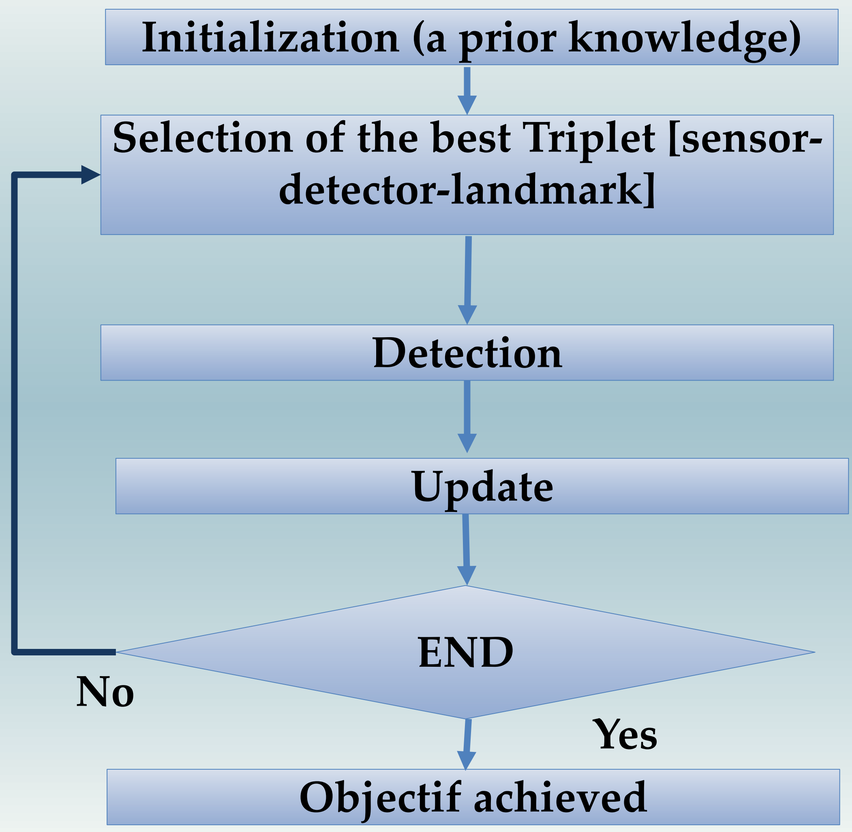

Methods

- Using a prior knowledge about the road scene
- Selection of the Triplet [sensor-detector-landmark] in terms of an entropic criterion
- Taking into account the fact that detectors are not perfect
- The main goal is to have an estimation not only accurate but reliable too

Road scene modeling

- Each element of the road is described by a vector of N parameters **X**, and an associated covariance matrix **Cx**
- Detect the element = estimate the N parameter of **X**

Triplet sensor-detector-landmark

- Set consisting of a sensor, detector and landmark
- For ego lane detection, the ROI are described as triplet sensor-detector-landmark

Selection of the best triplet sensor-detector-Landmark

Bayesian Network

Before update: selection of the best triplet
After update: confidence update

- Confidence in the estimation before update
- Observability
- Occlusion
- Detector reliability
- Ambiguity
- Confidence in the estimation after update

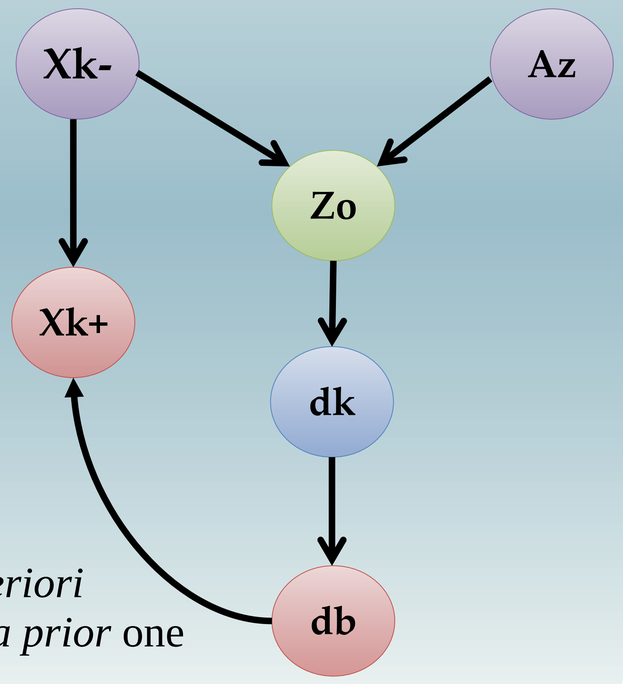

Entropic Criterion

- Difference between *posteriori* information content and *a prior* one

Some Results

Ego lane detection

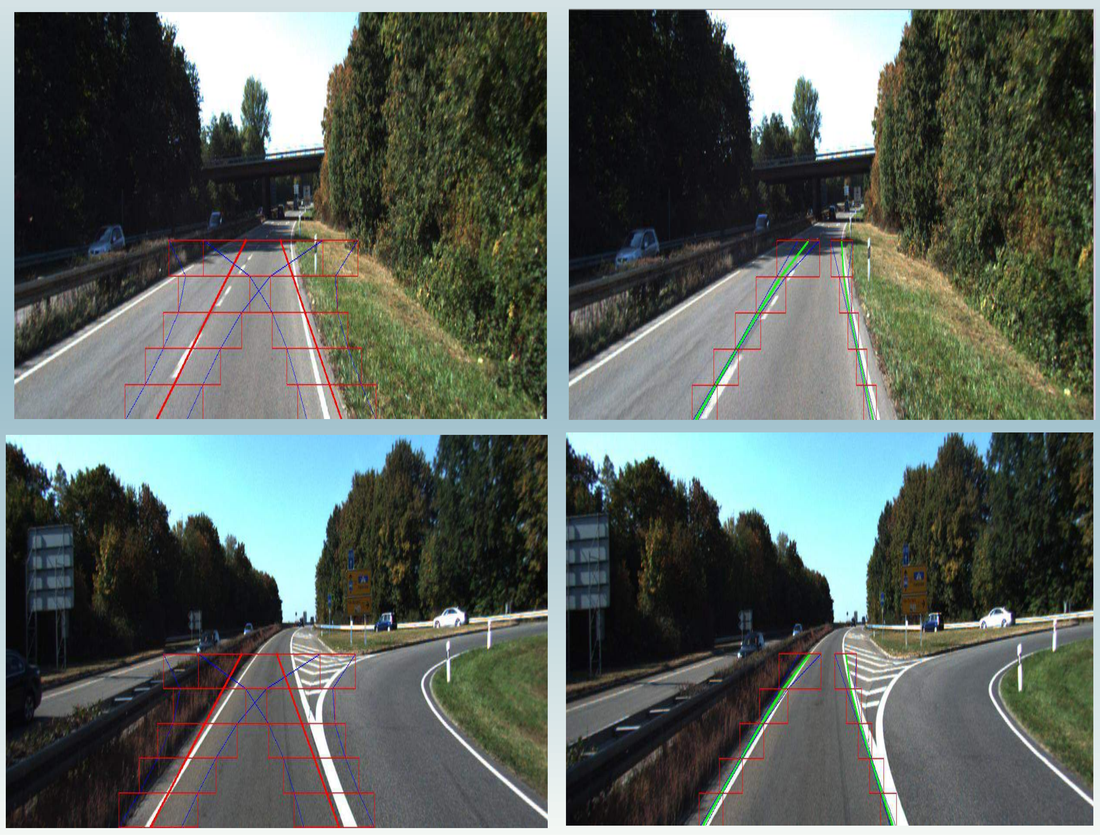

Update

Extended Kalman Filter

- Update **X** and **Cx**
- Update occurs only if the detection succeeded

Future Works

- Using data from multiple detectors
- Using a prior information from maps (OpenStreetMap)
- Testing our algorithm on a benchmark (KITTI)

Recognition and Localization Based on Local and Global Maps

Student name : Achref ELouni
Supervised by : Michel Dhome ,Eric royer , Marc chevaldonne

Institut Pascal

Ecole doctorale
Sciences Pour
l'Ingénieur

Introduction

Visual-Based Localization (VBL) consists of retrieving the pose (position + orientation) of a visual query material within a known space representation. For instance, recovering the pose of a camera that took a given photography according to a set of geo-localized images or a 3D model is a simple illustration of such a localization system.

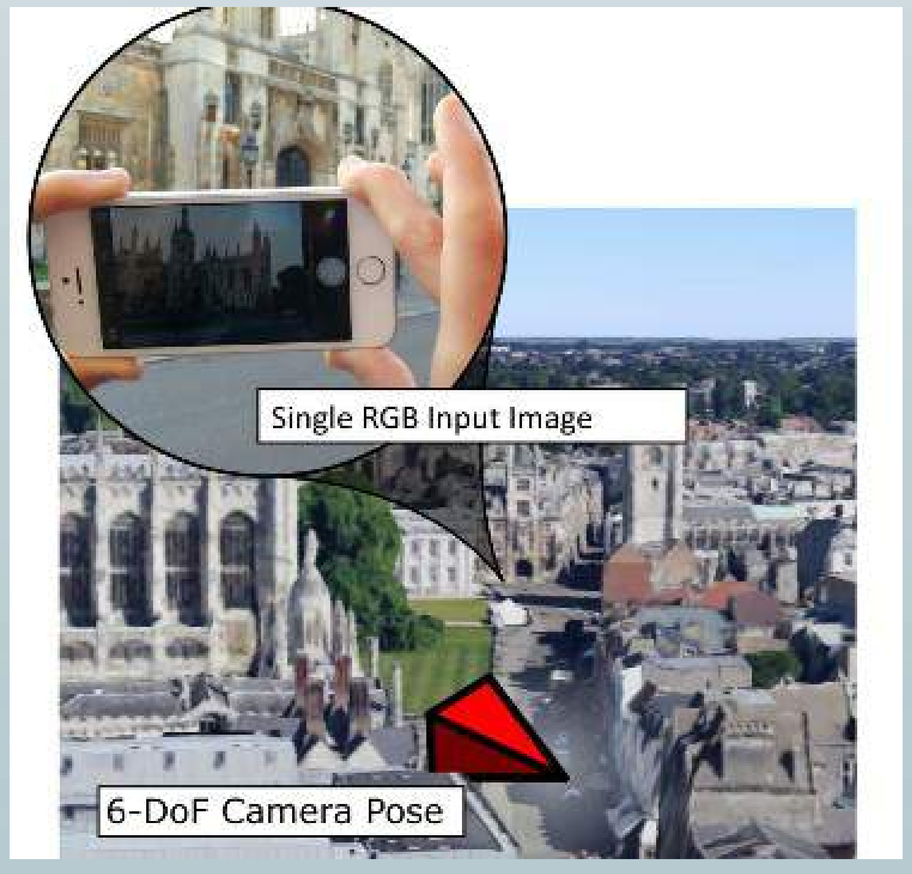

Methods

- Indirect VBL Methods[1]
  - Methods based on Key-point
  - Methods based on CNN
- Direct VBL Methods[2,3]
  - Methods based on Key-point
  - Methods based on CNN

Results

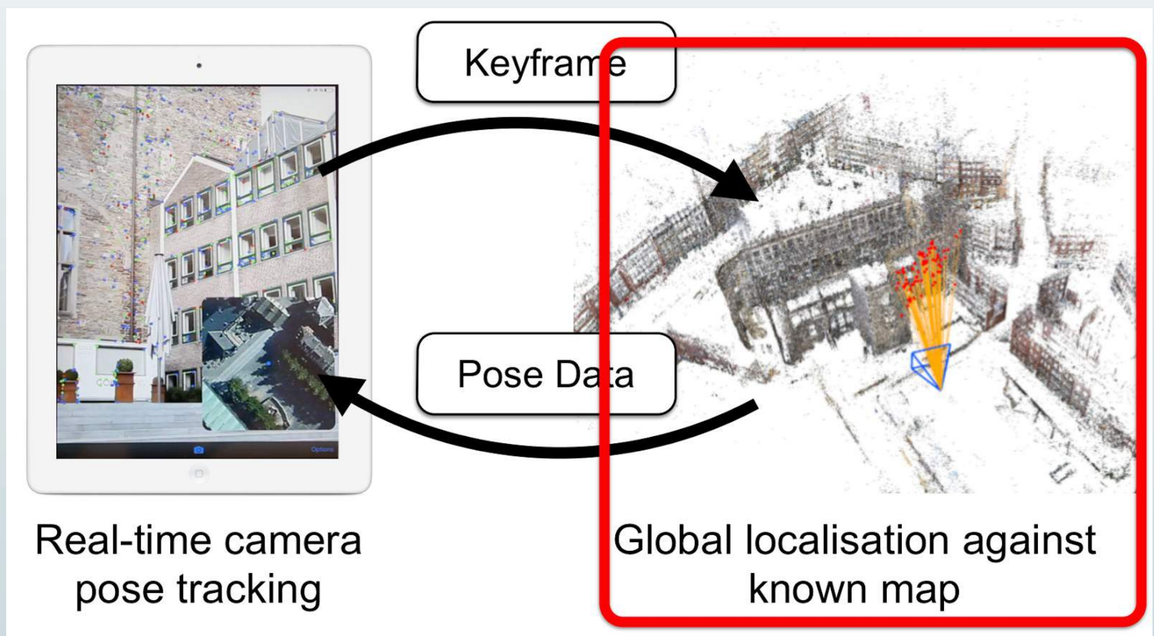

Conclusions

Two families of methods[1,2,3] have been explained to highlight the current capabilities of existing localization systems and to address the remaining challenges in the domain.

Bibliography

[1] Arandjelović, R., Zisserman, A., 2012. Three things everyone should know to improve object retrieval. Proceedings of the IEEE Conference on Computer Vision and Pattern Recognition (CVPR) (April), 2911–2918

[2] Arandjelović, R., Zisserman, A., 2013. All About VLAD. Proceedings of the IEEE Conference on Computer Vision and Pattern Recognition (CVPR),

[3] Arandjelović, R., Zisserman, A., 2014. DisLocation : Scalable descriptor. In: Proceedings of the Asian Conference on Computer Vision (ACCV)

Taking into account the skill level of an operator in adjusting the level of autonomy of a technical system

Adrian Couvent, Nicolas Tricot, Christophe Debain

Irstea, UR TSCF, 9 Avenue Blaise Pascal, 63170 Aubière

Ecole doctorale Sciences Pour l'Ingénieur

Context

The human-machine interaction is a key point for suitable robot integration. Indeed Human-Robot Interaction (HRI) currently receives considerable attention because humans and robots are more and more cooperating in many fields (transport, agriculture, industrial field…). For this purpose, having an efficient repartition task between the human and the robot, both seen as agents, seems important. An efficient repartition could be a dynamic repartition based on the skills of agents regarding the task. The convergence of automated fields together with human sciences allows an adaptation of the machine to the human activity, a leverage of human skills and capacities, and an answer to the human failure. At the moment humans and robots are two entities which can act autonomously and flexibly.

Research question:

❖ *How can they cooperate, while considering the respective performance of each other in a dynamic way ?*

Elements of language:

The activity is the realization of the task based on the skills of the operator. The performance ensues from the activity. When humans and robots are cooperating, the performance is impacted by the autonomy of each agent.

Scientific questions:

- ✓ **With the analysis of the activity of an operator, can we define his level of skills and knowledge regarding the task?**
- ✓ **How can they a priori and dynamically with an automated process be assessed ?**
- ✓ **How can we adapt a priori the behavior of a robot to the estimated level of skills and knowledge?**

Method

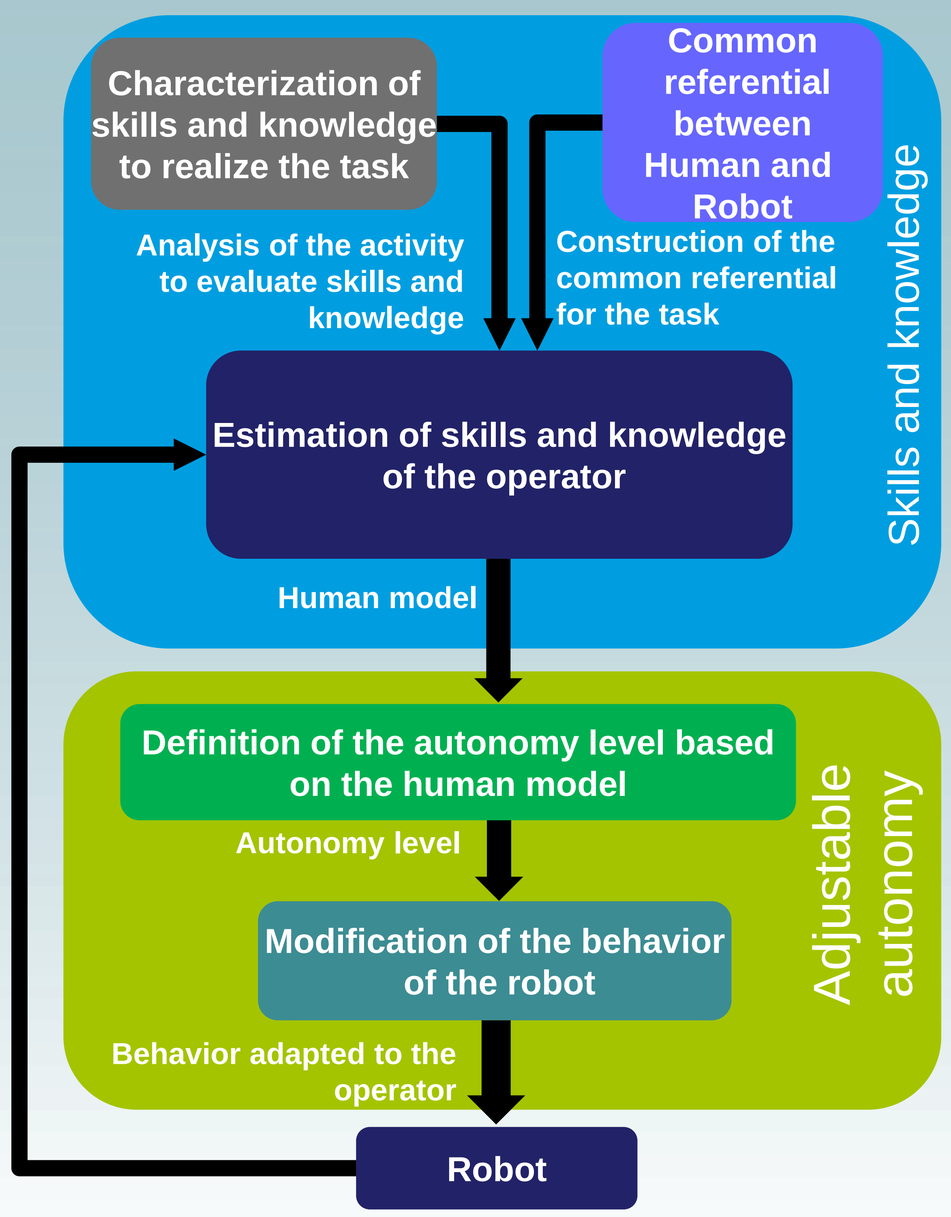

Characterization of skills and knowledge to achieve the task:

- ➢ Knowledge about technology and task
- ➢ Know how to realize the task
- ➢ Know how to cooperate with the robot
- ➢ Situations awareness of the operator
- ➢ Trust in the robot and himself

Common referential between Human and Robot:

- ➢ Robot capacities to realize the task
- ➢ Indicators to compare robot capacities and human skills
- ➢ Construction of patterns

Estimation of skills and knowledge of the operator:

- ➢ Analysis of the activity of the operator
- ➢ Estimation of the indicators used in the common referential
- ➢ Comparison with the pattern
- ➢ Determination of operator model

Definition of the autonomy level based on the human model:

- ➢ Autonomy level defined according to the autonomy of the robot
- ➢ Definition of the autonomy level depending on human model

Modification of the behavior of the robot:

- ➢ Activation of the robot functions based on the autonomy level
- ➢ Adaptation of the function based on the human model
- ➢ Interaction adaptation to improve the performance

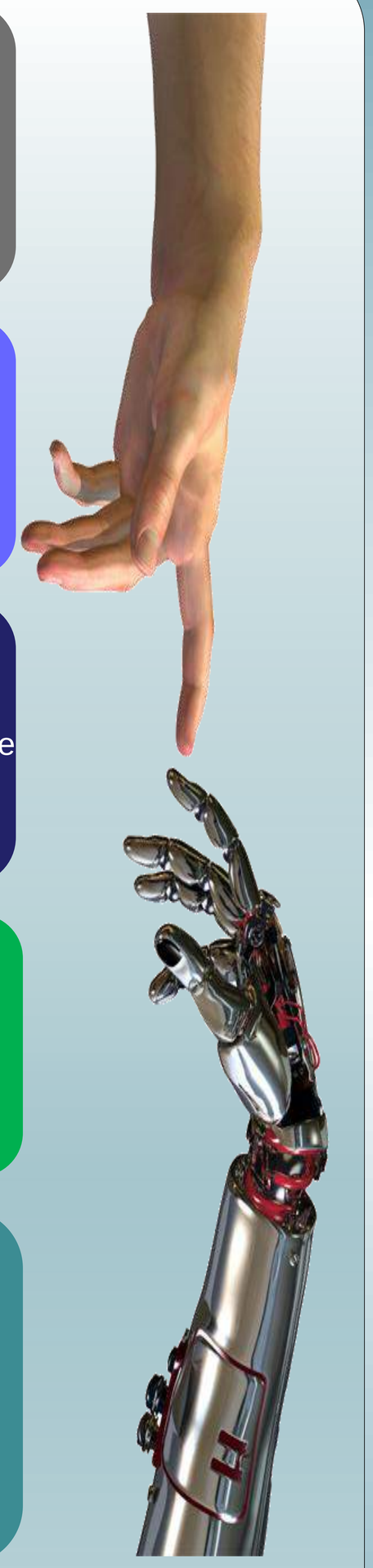

Current works:

Analysis of the activity of an operator when achieving a picking task in complex situations . As a first step, this analysis is made with image processing to create indicators. Then, the previous indicators will be transposed to the robot capacities. This work is implemented on ROS.

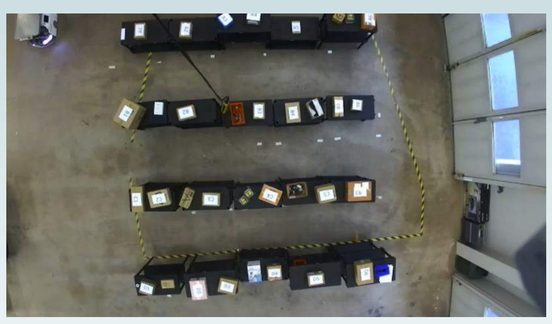

Picture of the picking area

Robot used for experimentation

Active shaping of an electromagnetic field- EMC applications

A. Al Ibrahim, C. Chauvière and P. Bonnet

Institut Pascal - Université Clermont Auvergne

Objectives

To control an electromagnetic field (or voltage) in different environments (transmission lines (TL), free space).

1. Control an electromagnetic field in a TL network
   - ▷ Software correction of a defective network
   - ▷ Detection and localization of defects
2. Control an electromagnetic field in free space environment

Introduction

- The idea of identifying a source that produces a specified electromagnetic field at a given point in space has received a considerable attention over the past 20 years or so. It has been popularized by the time reversal (TR) method, first applied in acoustic and has since spread in various other domains, including electromagnetic compatibility (EMC).
  The advantage of such method is its simplicity. However, its major drawback comes from the fact that it becomes less reliable when imposing complex conditions on the time duration, the target field or when dealing with multiple points in space. Consequently, the need for novel techniques dedicated to accurately tackle such problems is necessary.

Methods

- The methods to control an EM field are:
  - ▷ Time Reversal (TR)
  - ▷ Linear Combination of Configuration Fields (LCCF)

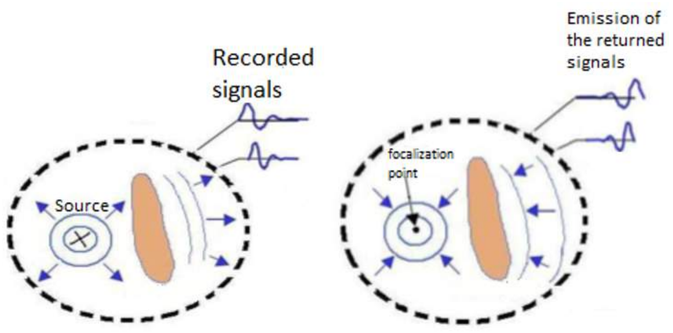

Figure: TR principle

TR	LCCF
Inaccurate due to numerical errors	Compensates numerical errors
Tackle only lossless problems	Tackle problems with arbitrary losses
Less reliable with a complex EM field	Reliable with a complex EM field
Requires perfect Huygens surface	Perfect Huygens surface is not required

Table: Comparison between TR and LCCF

Mathematical Section: LCCF theory

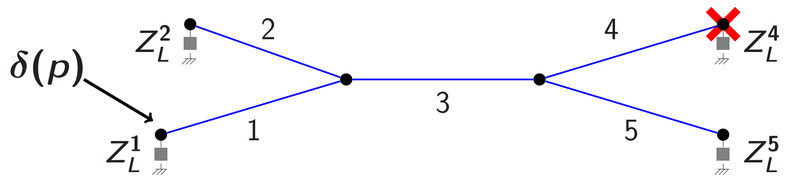

Figure: The configuration of the TL network used

- The LCCF steps are:
  1. Construct the LCCF transfer matrix A: Inject an impulsion and record at a specified point.
  2. Construct the vector b: Inject a signal $\mathfrak{z}_1$ and record at the same point considered in the 1^{st} step.
  3. Solve the linear system:
     $$As = -b + F$$
     to find s the signal to be injected after $\mathfrak{z}_1$ in order to obtain the target field F.
- Nullifying at several points requires the following system to be solved:
$$\begin{pmatrix} A_1 \\ \vdots \\ A_M \end{pmatrix} s = - \begin{pmatrix} b_1 \\ \vdots \\ b_M \end{pmatrix} + \begin{pmatrix} F \\ \vdots \\ F \end{pmatrix} \Leftrightarrow \mathscr{A} s = -\mathscr{b} + \mathscr{F} \qquad (1)$$
- The system (1) is not square and has to be solved in the least square sense.
- (1) requires to be regularized (Tikhonov), it takes the form:
$$\left(\mathscr{A}^T \mathscr{A} + \epsilon I\right) s = \mathscr{A}^T (-\mathscr{b} + \mathscr{F}), \epsilon > 0$$

Results: Null Voltage ($F = 0$) / Defect Detection

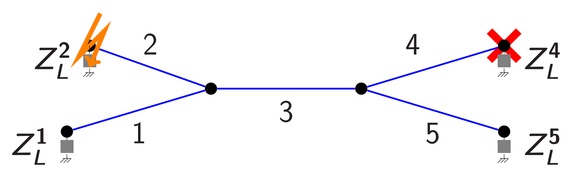

Branch nb	1	2	3	4	5
Length	5	6	4	2	5
Z_C	50	50	50	50	50
Z_L	0	45	0	50	0

Table: Characteristics of the TL network

Figure: The LCCF source

Figure: Nullifying at the the end of line 4

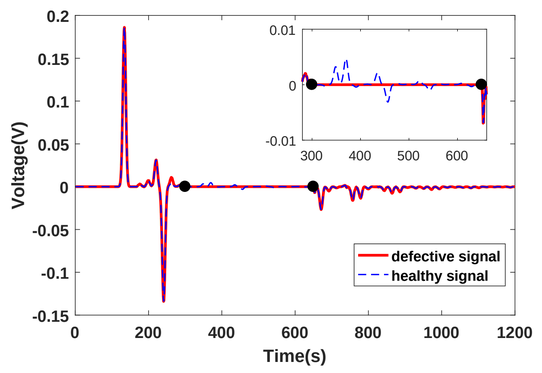

Figure: Detecting a defect in the TL network

- The LCCF source characteristics:
  - ▷ Non-trivial
  - ▷ Its amplitude remains in the same order of magnitude as the Gaussian pulse (1V).
- A non-null voltage implies that a defect is presented in the TL network.
- The LCCF method outperforms the reflectometry technique due to its high sensitivity to soft defects.

Results: Software Defect Correction

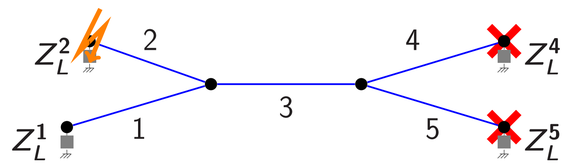

Branch nb	1	2	3	4	5
Length	5	6	4	2	5
Z_C	50	50	50	50	50
Z_L	0	10	0	50	0

Table: Characteristics of the TL network

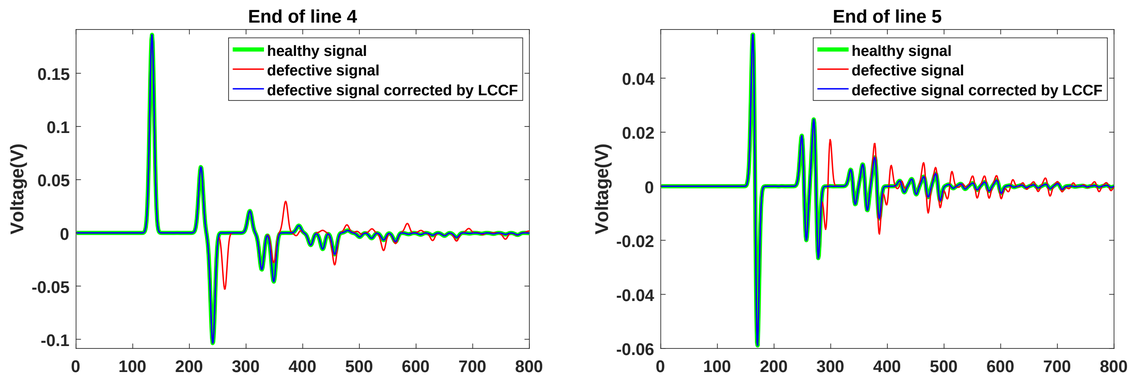

Figure: Software correction at the end lines 4 and 5

- By the LCCF method, we can compute the new voltage source to be injected in order to obtain the voltages of the healthy network.

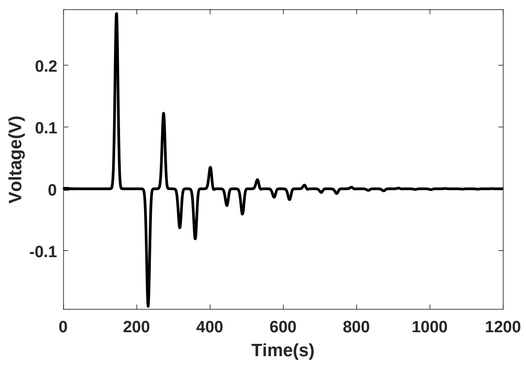

Figure: The LCCF source

Conclusion

- To summarize, using the LCCF technique we can:
  - ▷ Detect defects (hard or soft).
  - ▷ Bring a software correction to defective complex TL networks.
- Future work:
  - ▷ Locate the defects in TL networks
  - ▷ Control an electromagnetic field in 3D
  - ▷ Control an electromagnetic field in the frequency domain
  - ▷ Experimental Tests

Contact info: ali.al_ibrahim@etu.uca.fr +33 (0)4 73 40 77 65

Analysis and modelling of the reaction-mixture interaction on the extrapolation of the aerobic and anaerobic fermenters

Amaury Danican[1], Jean-Pierre Fontaine[1], Christophe Vial[1]

[1] Institut Pascal UMR 6602 CNRS / UCA / SIGMA Clermont
Campus des Cézeaux, 2 avenue Blaise Pascal, 63178 Aubière France

Ecole doctorale Sciences Pour l'Ingénieur

Introduction

Context

The massive use of **fossil fuels** for industrial development and human activities leads to a **pollution of soils, air and water**. This source of energy is also **limited in quantity unlike "renewable" energies**, which are now **real sources** to be exploited.

Within this framework, we are interested in the **"dark fermentation"** process, which consists in the **decomposition of organic substrates** thanks to **microorganisms** in agitated bioreactors (***figure 1***). They are also called **fermenters**, and are used to **produce biohydrogen and other molecules** of commercial interest. It is a well-known process but still needs to be optimized.

An **optimum process** needs a **good homogeneity** of the reactional environment while **limiting the energy consumption** by the impellers. Hence, it is necessary to better understand the **hydrodynamics** and the concomitant **heat and mass transfer** within the fermenter in order to select the **best operating conditions** of the bioreactor and their impact on the mixture.

Objectives

- To develop and validate a numerical tool based on **CFD (*Computational Fluid Dynamics*)** (***figure 6***), based on **Navier-Stokes** equations, leading to assist in the **design of gas-liquid reactors** by including all of the involved physical phenomena.
- The simulations will have to take into account the **multiphase flows** as well as the of **heat and mass transfer**.
- To develop a method of **optical trajectography** to measure the Lagrangian velocity field (***figure 9***), and a method of **PIV (*Particle Image Velocimetry*)** to measure the Eulerian velocity field (***figure 5***).
- Estimate the **quality of the mixing and the mass transfer** in fermenters of **variable size and design** to understand the scale effects in Newtonian and non-Newtonian fluids.

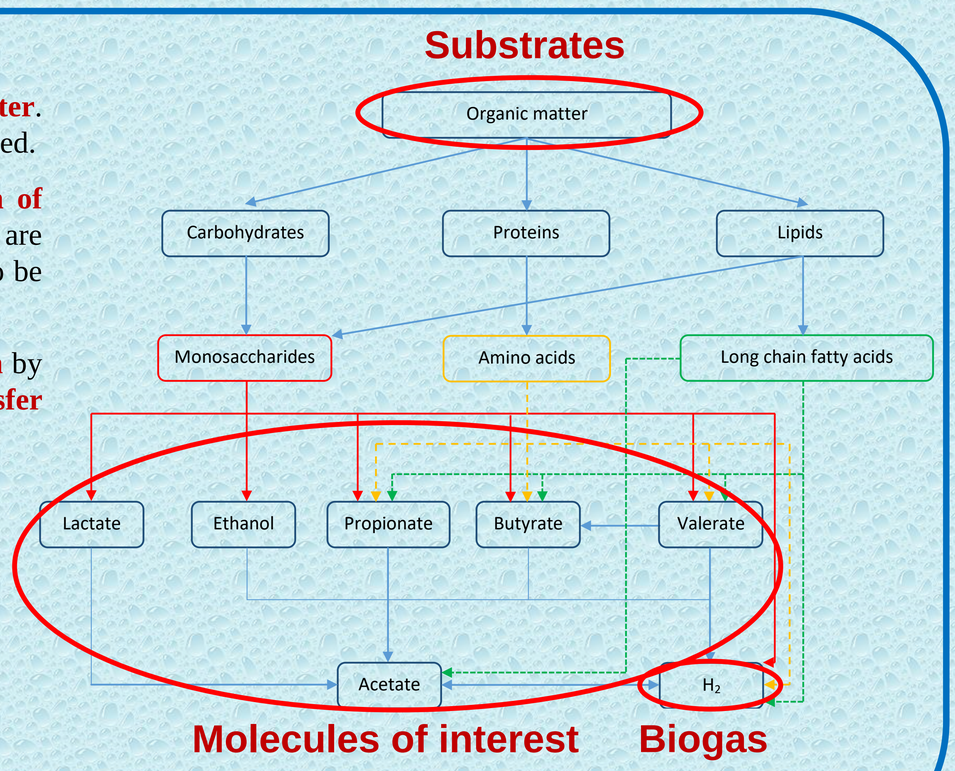

***Figure 1**. Simplified chemical mechanisms which govern dark fermentation process*

Implementation of the CFD model

- ***Definition of the physical domain***
  Implementation of the **domain limits** and the **objects** within it (***figure 2***).
- ***Mesh Grid***
  Definition of the **mesh size and structure** around the objects and the physical domain limits (***figure 3***).
- ***Turbulence model***
  Choosing the most suitable turbulent model for this simulation. A variant of the ***k-ε* model** was chosen in our case.
- ***Boundary conditions***
  Selection of the **boundary conditions** of the flow configuration and the **fluid properties** (ex : ***Newtonian***). **No-slip** on the solid boundaries and **stress free** at the upper liquid-air interface.
- ***Numerical parameters***
  Choosing the **parameters of calculation** (ex: number of iterations, relaxation control, output,…).

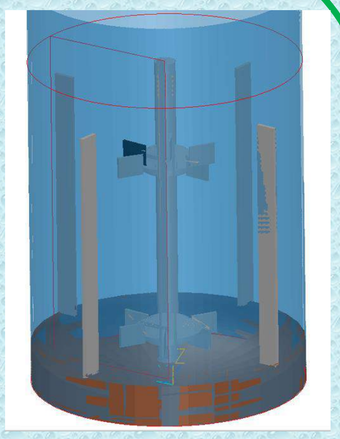

***Figure 2**. Modelling of the bioreactor*

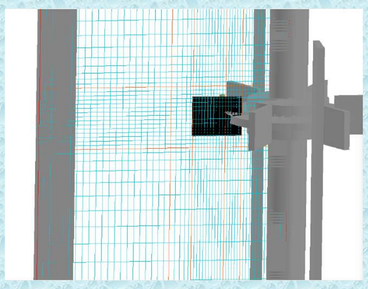

***Figure 3**. Mesh grid of the bioreactor*

Results of the model reliability

- ***Grid independent***
  Choosing the **mesh grid** that allows computing solutions that do **not depend** significantly on the **mesh resolution**.

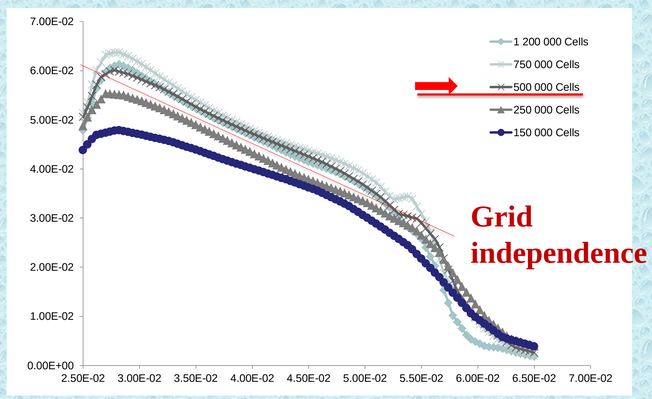

***Figure 4**. Flow speed profile out of the high impeller for each mesh size*

- ***Convergence***
  Stabilization of the values.
- ***Negligible Residuals :***
  The **smallest possible** values of the residuals, which measure **numerical error**.

- ***Comparison to experiments :***
  Comparison with the **PIV data**

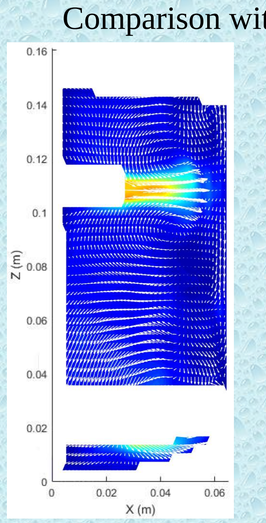

***Figure 5**. Velocity field from PIV at 40 rpm (experimental)*

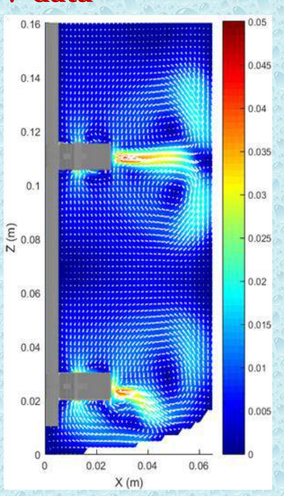

***Figure 6**. Velocity field from CFD at 40 rpm (simulation)*

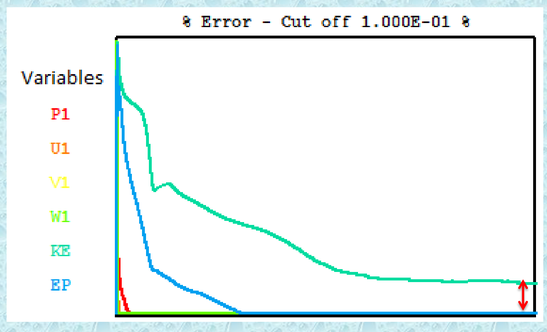

***Figure 7**. Residuals plotted against the number of iterations at 40 rpm*

Conclusions and perspectives

Conclusions

- As it can be seen in the ***figures 4 ,5, 6 and 7***, the **model** has been **correctly set up**, with a good agreement between experimental and numerical data.
- Hence, the first **test on complex fluids** (ex: ***non-Newtonian***) can be performed with a strong basis, which needs to be **reinforced by new PIV measurement** for these types of fluids.
- The new experimental tool of **optical trajectography**, coupled with the study of **heat and mass transfer** should allow us to **better characterize real media** which are complex fluids in order to **enhance biohydrogen production** in this bioreactor.

Complexification of the model

- ***Material and heat transfer***
  Study of **distributive mixing** within the liquid phase (*ex: **mixing time***) and the **dispersive mixing** at the interface, as well as **heat transfer**.
- ***Power consumption***
  Study of the **torque on impellers**, comparing it to the experimental data in order to estimate **power consumption** due to mechanical mixing in the reactor.
- ***Multiphase simulation***
  Study of a **solid suspension** (simulating microorganisms) in the liquid phase.

- ***Non-Newtonian fluids***
  New simulations where the **viscosity** is a function of the **shear rate**.

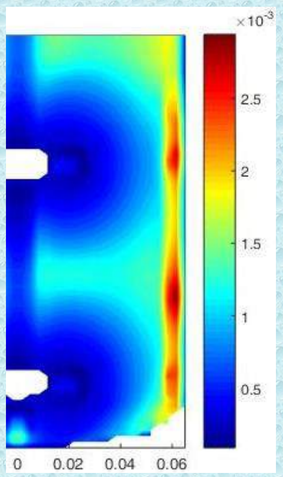

***Figure 8**. Viscosity field in CFD (simulation)*

- ***GENTRA (CFD particle tracking)***
  Simulation of **particle tracking** in the reactor and comparison with **optical trajectography**.

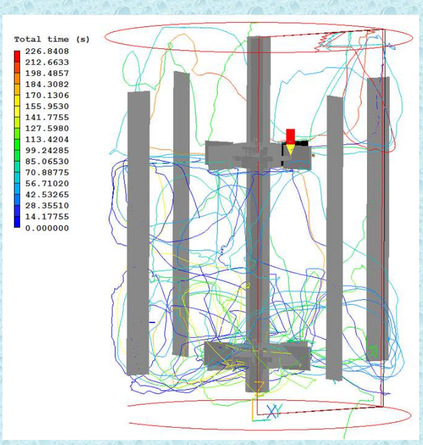

***Figure 9**. Particle tracking in CFD (simulation)*

Manifold-Based Inference for A Supervised Gaussian Process Classifier

Anis Fradi[1,3], Chafik Samir[1,3], and Anne-Françoise Yao[2,3]

[1]CNRS-LIMOS (UMR 6158) & [2]CNRS-LMBP (UMR 6620)

[3]University of Clermont Auvergne, France

Introduction

What?

- A regularization approach, called weighted ridge logistic.
- Two Bayesian approaches, called manifold Laplace approximation (MLA) and manifold expectation propagation (MEP).

Why?

- High dimensionality poses statistical challenges and renders many traditional classification algorithms impractical to use.

How?

- A modified version of ridge logistic, with the advantage of reducing the search space of regularization parameter, which is more efficient for computational time.
- A novel approach having the advantage of learning data into new feature space under some constraints (reduce non-linearity, increase separability) in a Bayesian context.

Discussion and conclusion

- The effectiveness of the proposed approaches has been proved within an application to image classification that contains some defected boxes among correct ones.
- From various conducted tests, we demonstrated that the results are enhanced by both proposed approaches regarding the baseline approach (logistic regression).
- The proposed based on manifold Gaussian process classifier achieve high accuracy.
- The MEP has more predictive power and generalization capability than MLA.
- The difference between MEP and MLA is caused almost exclusively by approximation errors in MLA.

Perspectives

- Estimation of model's hyper-parameters by variational and Bayesian methods.

Regularization approach

- **Summary:** The idea consists of considering the weighted sum between the unstructed log-likelihood of logistic regression and l^2-norm of unknown parameters β.
- **Details:**

Formulation How to find the maximum likelihood estimate (MLE) ?

$$\beta^{\lambda,*} = \arg\max_{\beta} \left\{ l^{\lambda}(\beta) = \frac{(1-\lambda)}{2} l(\beta) - \frac{\lambda}{2} ||\beta||_2^2 \right\} \quad ; \quad 0 < \lambda < 1$$

Description of data $\{\mathbb{X}, \mathbb{Y}\} = \{(x_i, y_i)\}_{i=1}^{N}$, where $y_i \in \{0, 1\}$ and $x_i \in \mathbb{R}^p$

Variational methods: Newton/gradient

$$\beta^{k+1} \approx \frac{(1-\lambda)}{2}(-\nabla^2 l^{\lambda}(\beta^k))^{-1}(\nabla^2 l(\beta^k)\beta^k + \nabla l(\beta^k))$$

- **Problems:** $\dim(\beta) = p + 1 >> N \Longrightarrow$ dimensionality reduction.
  $\beta^{\lambda,*}$ can be a local maximum $\Longrightarrow$ Bayesian inference gives more candidates through the prior.

Bayesian approaches

- **Summary:** The idea is to learn the Gaussian processes classifier (GPc) in a feature space to get the proposed manifold Gaussian processes classifier (MGPc)
- **Details:**

A MGPc $G : \mathcal{H} \to \mathbb{R}$ is equivalent to a GPc $f = G \circ M : \mathbb{R}^p \to \mathbb{R}$ with a covariance function $\tilde{c}$ such that $\tilde{c}(x, x') = c(M(x), M(x'))$. M is a deterministic and parametrized function obtained by an unsupervised way, that maps the input space $\mathbb{R}^p$ into the feature space $\mathcal{H} \subseteq \mathbb{R}^m$ ($m << p$).

Formulation How to find an explicit form to the posterior proportionality ?

$$\mathbb{P}(\mathbf{G}|\mathbb{Z}, \mathbb{Y}) \propto \mathbb{P}(\mathbf{G}|\mathbb{Z}) \times \prod_{i=1}^{N} \mathbb{P}(y_i|G_i) \quad ; \quad \mathbf{G} = G(\mathbb{Z})$$

Description of data $\{\mathbb{Z} = M(\mathbb{X}), \mathbb{Y}\} = \{(z_i, y_i)\}_{i=1}^{N}$, where $y_i \in \{-1, 1\}$ and $z_i \in \mathcal{H}$

Approximation methods MLA **&** MEP

MLA: Employing a Gaussian approximation to the true posterior from the second order Taylor expansion around the MAP estimator.

MEP: Replacing the individual likelihoods by unnormalized Gaussians and minimizing the Kullback-Leiber divergence iteratively between the true posterior and its approximation.

An illustration of key steps to classify a test input ($y^* = -1$)

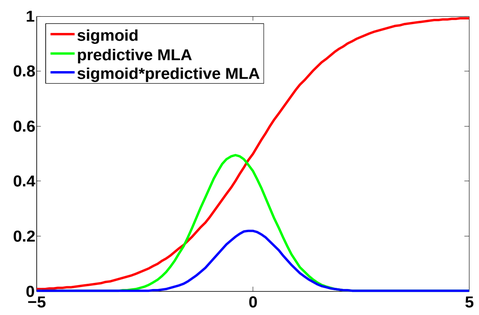

(MLA)

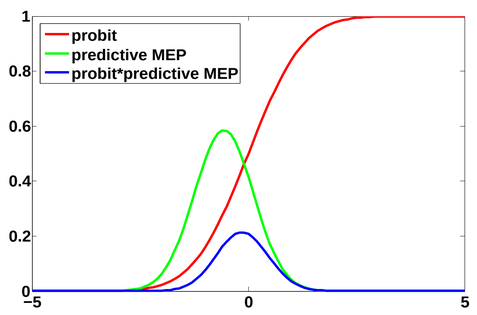

(MEP)

Comment: Approximate predictor of class "1": $\bar{\pi}_* = \mathbf{0.41}$ for MLA **&** $\bar{\pi}_* = \mathbf{0.33}$ for MEP

Boxes with different representations

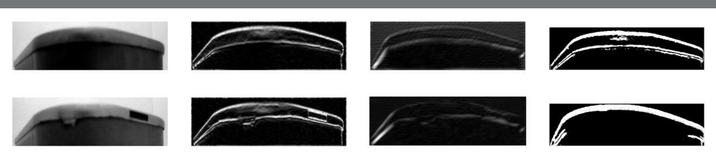

Non-defective (top) and defective (bottom) boxes (original, gradient, binarization, Gabor)

Results: Logistic regression

Error rates \ features	gradient	Gabor	binarization
FP	**20%**	**51%**	**53%**
FN	**27%**	**47%**	**43%**
CE	**25%**	**48%**	**45%**

Results: Bayesian approaches

Error rates \ methods	MLA	MEP
FP	**11%**	**8.5%**
FN	**19%**	**10%**
CE	**17%**	**9.5%**

Results: Weighted ridge logistic

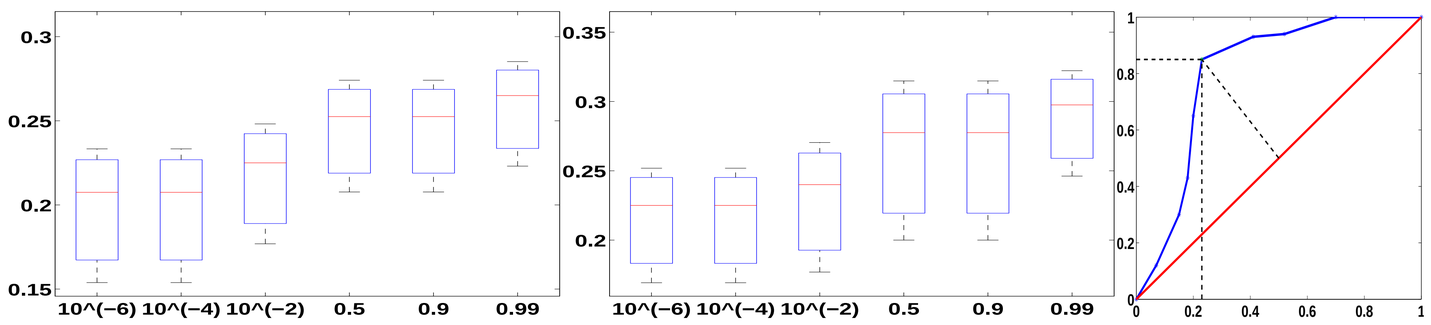

Errors as a function of regularization parameters (FN=upper values, FP=lower values and CE=values in the middle) obtained by: Newton (left) and gradient (middle). ROC curve (right)

Results: Figure

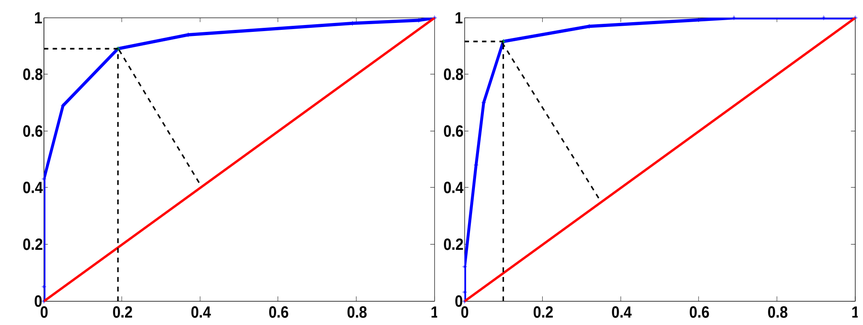

ROC curves for Bayesian approaches: MLA (left) and MEP (right)

Anis.FRADI@etu.uca.fr chafik.samir@uca.fr Anne.YAO@uca.fr

Functional regression to explain the evolution of livestock farms' performances

Ecole doctorale Sciences Pour l'Ingénieur

Anne de la Foye[1], Chafik Samir[2], Anne-Françoise Yao[3], Patrick Veysset[1]

[1]INRA UMRH, [2] UCA-LIMOS, [3] UCA-LMBP

Introduction

French beef farmers have extended their holdings (area and herd) for 30 years whereas their income per worker stagnate (Veysset & al 2014) and their technical efficiency decrease (Veysset & al 2017).

What we observe on 38 holdings from the center of France surveyed between 1992 and 2016 (see figures) :

What factors explain the holdings' performances stagnation or decrease ?

Holding size

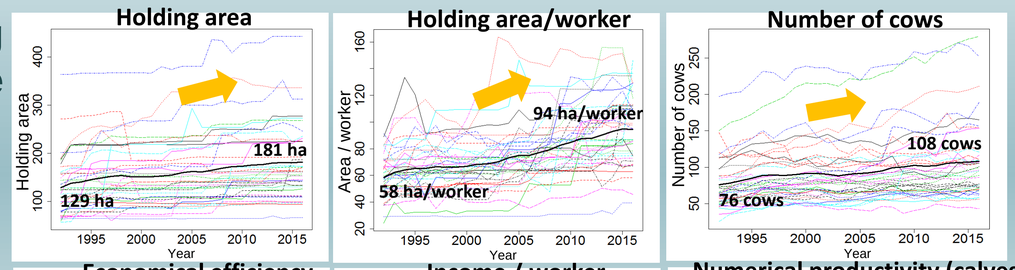

Holding performances

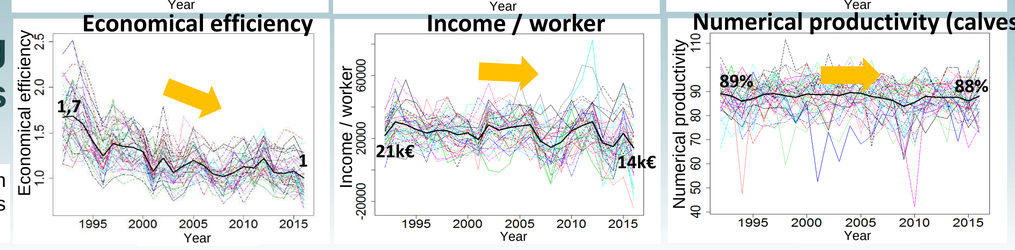

Objectives

Application

Explain the holdings' performances evolution

with the most relevant structural technical or economical static or dynamic characteristics

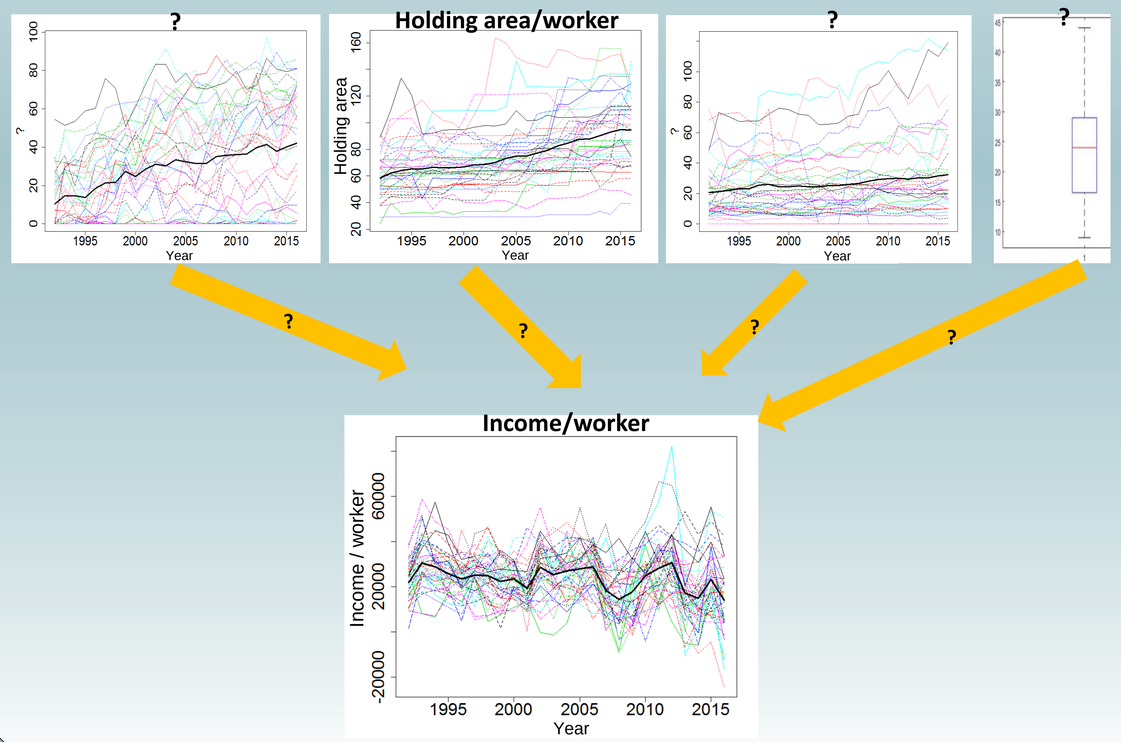

Modelling

1. **Interpret regression coefficients β(t,s)** in equation

$$Y_i(s) = \int_t \beta(t,s)X_i(t)dt + \varepsilon(s)$$

$\forall\, s \in \{1992, \dots 2016\},\ \ i \in \{1, \dots 38\}$ with

- i : holding index
- Y_i : performance evolution for holding i (income/worker) → functional response
- X_i : evolution of a characteristic for holding h (area/worker) → functional predictor

so that the least squares criteria be penalized while maximizing covariance :

$$\max_{\substack{w,\|w\|=1 \\ c,\|c\|=1}} cov^2\left(\int_t X(t)w(t)dt, \int_t Y(t)c(t)dt\right)$$

with c(t) and w(t) the model's PLS components

2. **Extend to a model with several functional or scalar predictors**

3. **Define criteria for the selection of the best model**

Bibliography

Veysset, P., Benoit, M., Laignel, G., Bébin, D., Roulenc, M., & Lherm, M. (2014). Analyse et déterminants de l'évolution des performances d'élevages bovins et ovins allaitants en zones défavorisées de 1990 à 2012. *Productions Animales*, 27(1), 49–64.

Veysset, P., Lherm, M., Roulenc, M., Troquier, C., & Bébin, D. (2015). Productivity and technical efficiency of suckler beef production systems: Trends for the period 1990 to 2012. *Animal*, 9(12), 2050–2059.

Veysset, P., Lherm, M., Boussemart, J. & Natier, P. (2017). Formation et répartition des gains de productivité en élevage bovin viande. Qui sont les gagnants et les perdants entre 1980 et 2015 ?. *Économie rurale*, 361,(5), 71-91.

Benatia, D., Carrasco, M., & Florens, J.-P. (2017). Functional linear regression with functional response. *Journal of Econometrics*, 201(2), 269–291. https://doi.org/10.1016/J.JECONOM.2017.08.008

Hall, P., & Horowitz, J. L. (2007). Methodology and convergence rates for functional linear regression. *The Annals of Statistics*, 35(1), 70–91.

Preda, C., & Saporta, G. (2005). PLS regression on a stochastic process. *Computational Statistics and Data Analysis*, 48(1), 149–158.

Yao, F., Müller, H.-G., & Wang, J.-L. (2005). Functional linear regression analysis for longitudinal data. *The Annals of Statistics*, 33(6), 2873–2903.

Dynamical effects of filtering structures on the mitigation of lake eutrophication

Auguste Caen[1], Delphine Latour[2 3], Jean-Denis Mathias[1]

1 UR LISC, Laboratoire d'Ingénierie pour les Systèmes Complexes, IRSTEA - Clermont Ferrand
2 Université Clermont Auvergne, Laboratoire Microorganismes: Génome et Environnement, BP 10448, Clermont-Ferrand, France
3 CNRS, UMR 6023, Laboratoire Microorganismes: Génome et Environnement, BP 80026, Aubière, France

Ecole doctorale Sciences Pour l'Ingénieur

Introduction

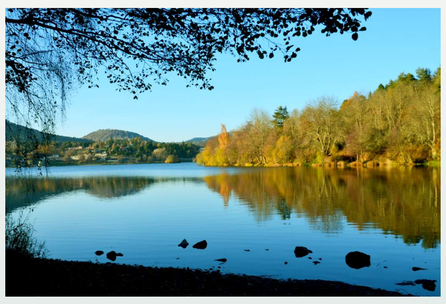

Oligotrophic lake

Eutrophic lake

Mitigation of lake eutrophication currently lies in the development of infrastructures upstream from lakes, that limit nutrient inputs, such as wetlands or sedimentation ponds. Because of their filter effect on the water passing through them, we call such structures "filtering structures". Here we examine the effects of several filtering structures on the phosphorus dynamics in a downstream lake. We adapt a dynamical model of the phosphorus quantity in a lake to study three kinds of structure according to their effect on the phosphorus: a buffer effect, a fixed trapping effect, and a varying trapping effect. These models enable us to understand the filtering structure effects on a downstream lake: we show the inertia effects of a structure with a buffer effect, and we study the cleaning of a filtering structure as a way to control phosphorus levels, and so maintain a lake in an oligotrophic state.

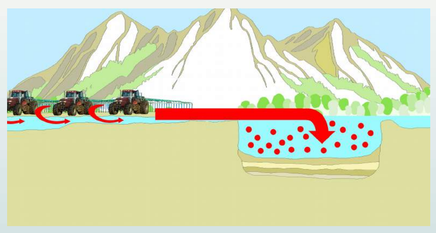

Without filtering structure

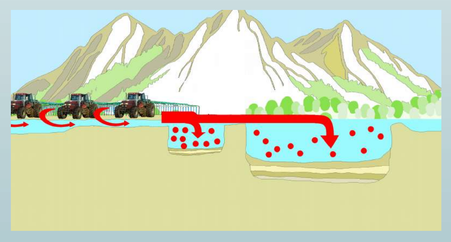

With a filtering structure

Methods

I) A dynamical Model of the Phosphorus quantity in the lake water body (*Carpenter 1999*)

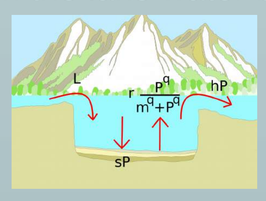

$$\frac{dP(t)}{dt} = L(t) - hP(t) - sP(t) + r\frac{P(t)^q}{m^q + P(t)^q}$$

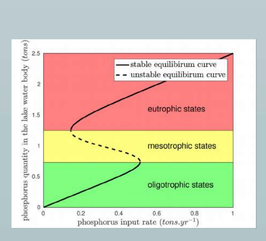

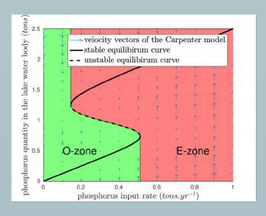

II) Three filtering structures

B-structure

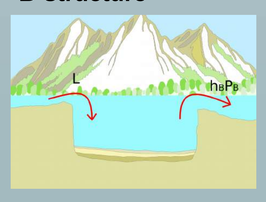

A buffer effect :

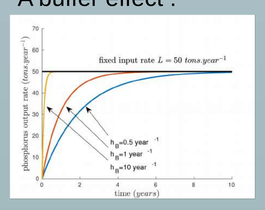

$$\frac{dP_B(t)}{dt} = L(t) - h_B P_B(t)$$

FT-structure

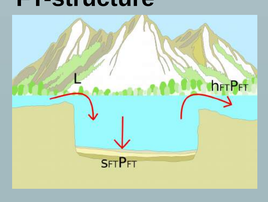

A fixed trapping effect :

$$h_{FT} P_{FT}^{eq} = \frac{h_{FT}}{s_{FT} + h_{FT}} L < L$$

$$\frac{dP_{FT}(t)}{dt} = L(t) - h_{FT} P(t) - s_{FT} P(t)$$

VT-structure

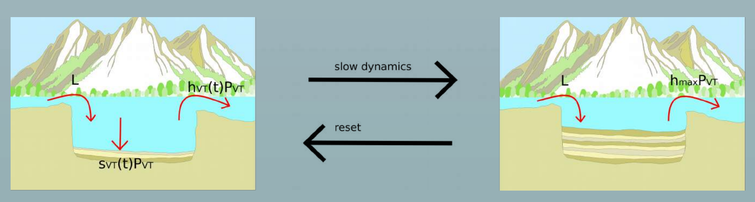

A varying trapping effect : $\frac{dP_{VT}(t)}{dt} = L(t) - (s_{VT}(t) + h_{VT}(t))\,P_{VT}(t)$

with

for $t = 0 : h_{VT}(0) = h_i$ and $s_{VT}(0) = s_i$

for $t = \infty : h_{VT}(\infty) = h_{max}$ and $s_{VT}(\infty) = 0$

III) Conclusion

The filter effect of a filtering structure depends on its parameter values.

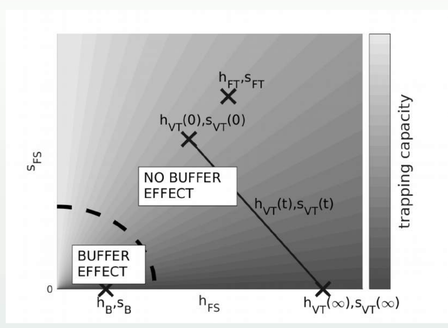

Results

I) Effect of a B-structure on a downstream lake

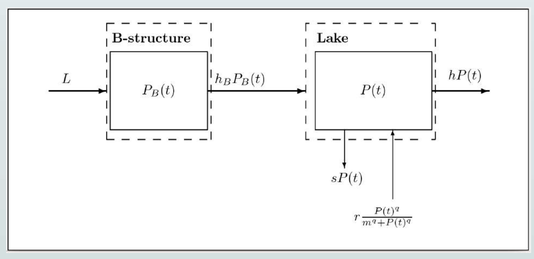

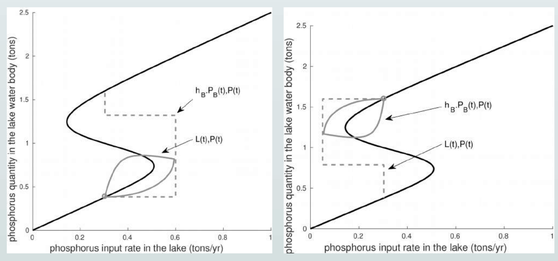

II) Effect of a FT-structure on a downstream lake

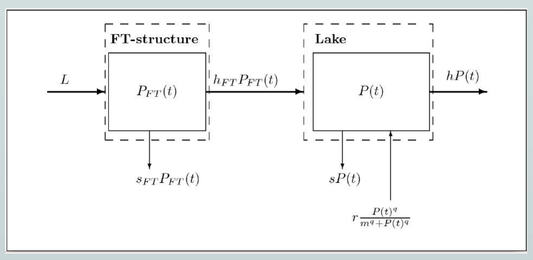

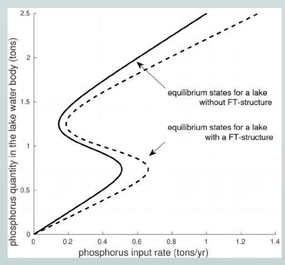

III) Effect of a VT-structure on a downstream lake

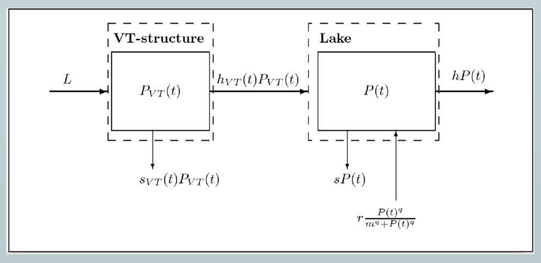

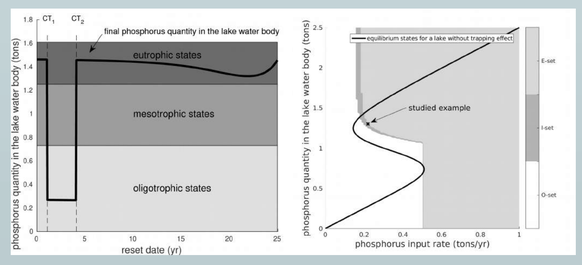

Conclusions

The B-structure increases the downstream lake inertia.

The FT-structure decreases the input phosphorus rate in the downstream lake.

The VT-structure allows to control the input phosphorus rate in the downstream lake.

We thank the Région Auvergne, France, for its financial support. This work was supported by a contrat Plan Etat Région from the Région Auvergne, France: CPER 2015-2020 -- ConnecSens.

Bibliography

Carpenter, S. R., Ludwig, D., & Brock, W. A. (1999). Management of eutrophication for lakes subject to potentially irreversible change. Ecological applications, 9(3), 751-771.

Optimisation of vehicles' reliability and maintainability

Basile Haté[1,2], Aurélie Talon[1], Nicolas Gayton[1], Caroline Ramus-Serment[2]
[1] Université Clermont Auvergne, Polytech, Institut Pascal, SIGMA Clermont, 63000 Clermont-Ferrand, France
[2] PSA Group, Belchamp Technical Centre, 25420 Voujeaucourt, France

Ecole doctorale Sciences Pour l'Ingénieur

Journée des écoles doctorales – 14th june 2018

Background

Aims

Optimise PSA vehicles' reliability and maintainability

Design (PSA)	Post-sale (PSA)	Post-sale (Customer)
How could feedback data and data from driving tests help improve components reliability before car's commercialisation?	*How could data from driving test and first customers' data optimise vehicles' maintenance?*	*How could on-board measurement unit give the maintenance needs to the customer?*

Design process of a car

Preliminary studies	Design and development			Vehicles' commercialisation
	Original concept	On-road testing	Vehicle's modification based on the on-road testing	

Vehicle in development — ***Vehicle in circulation***

Methods

		Issue	Data	Method	Results
1	Selection of the components to take into account	*Which are the less reliable components?* *Which are the most urgent cases?*	BTA and NAVIG data from vehicles in circulation	Statistical treatment	*List of parts to take into account*
2	Identification of components that are reliable or modifiable	*How and when quantify or qualify the indicators for each component?* *How to interpolate between two discrete values?*	Based on other vehicles: - Now : BTA unit - After 2020 : BSRF unit Based on the same car: - SPARTE Database, during validation phase - BTA unit, when customer drives	Group of methods to deal with qualitative and quantitative datas in small or high quantity + Integrate uncertainties	*Performance indicator* *Proposal of a first curve + updated curve* *Time*
3	Elaboration of a maintenance strategy	*When replace which component?* *Which strategy adopt : do nothing, replace one or more parts, plan some replacement?*	Influence of a failure on the other parts Direct and indirect maintenance costs Residual performance	Test and simulation of various maintenance strategies + Sensitivity analysis	Maintenance strategies New maintenance policy Prototype of customer interaction

Results

PSA databases :
- Identification completed
- Links established
- Description completed
- Classification in progress

Data treatment methods :
- Identificationcompleted
- Description in progress
- Comparison in progress

First year objectives :
- Understand databases and treatment methods,
- Select the most adapted « data ↔ method » couples

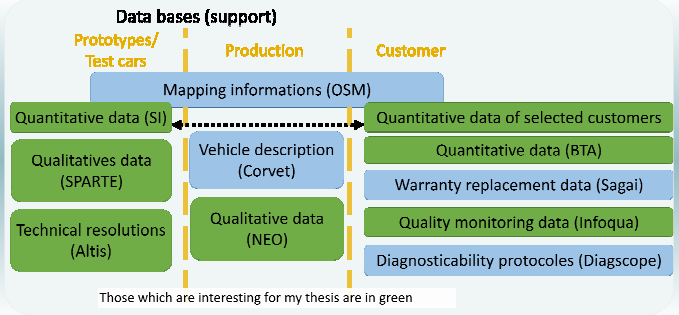

Conclusion

Databases are known and understood
Data treatment methods are identified, descriptions are in progress

Perspectives

Use the acquired knowledge to develop the methodology of optimisation of vehicles' reliability and maintainability

Bibliographie

Sikorska, J. Z. et al. (2011). *Prognostic modelling options for remaining useful life estimation by industry*. Mechanical Systems and Signal Processing 25, 1803-1836.
Lee, J. et al. (2014). *PHM design for rotary machinery systems—Reviews, methodology and applications*. Mechanical Systems and Signal Processing 42, 314-334

Modeling and simulation of 2D materials based plasmonic structures for sensor applications

M. Ben Rhouma[1,2], K. Edee[1], M. Antezza[2,3]

Ecole doctorale Sciences Pour l'Ingénieur

[1]Université Clermont Auvergne, Institut Pascal, BP 10448, F-63000 Clermont-Ferrand, France
[2]Laboratoire Charles Coulomb - UMR 5221 CNRS, University of Montpellier, Montpellier, France
[3]Institut Universitaire de France, 1 Rue Descartes, Paris, France

Maha.BEN_RHOUMA@uca.fr

Motivations and objectives

Graphene ➡ 2 D honeycomb carbon crystal [1]

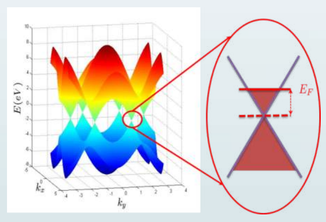

Unique electronic band structure : Linear Dirac spectrum

⬇

Unusual optical conductivity ➡ Particular and attractive optical properties :

- TM Graphene surface plasmons : low loss , high confinement
- TE Graphene surface plasmons : very difficult to excite in practice
- Electrically tunable conductivity

⇒ Various plasmonic applications in the IR and the THz regions of the EM spectrum [2,3]

Antennas, Absorbers, Modulators → Sensors

Objectives

Develop theoretical and numerical methods in order to study graphene based plasmonic structures for sensor applications

Physical System and Methods

The generic structure

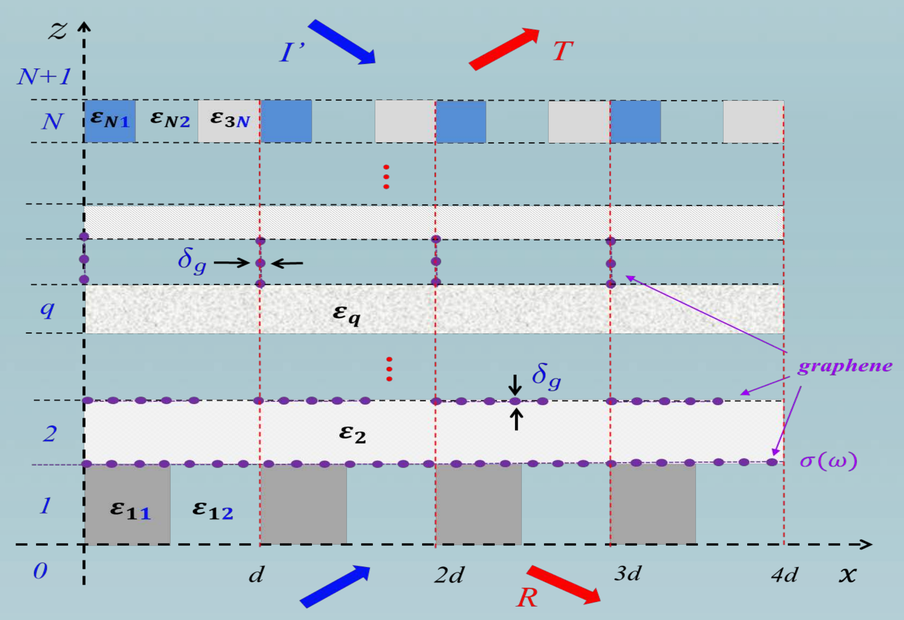

The Fourier Modal Method : FMM

In each medium (q), the fields can be expressed as:

$$U_{qy}(x,z) = \sum U_{nq}(z) e^{i\alpha_n x} \quad \forall \quad q \in \{0, ..., N+1\}$$

$$U_{qy}(x,y) = \begin{cases} E_{qy}(x,z) & \text{TE polarization} \\ H_{qy}(x,z) & \text{TM polarization} \end{cases}$$

The General solution :

$$\mathcal{U}_q(z) = P_q(e^{D_q(z-z_{q-1})} a_q + e^{-D_q(z-z_q)} b_q)$$

Boundary conditions ➡ S-matrix Algorithm $\begin{pmatrix} R \\ T \end{pmatrix} = S \begin{pmatrix} I \\ I' \end{pmatrix}$

Codes validations

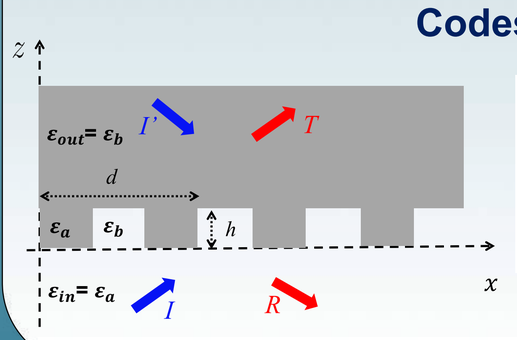

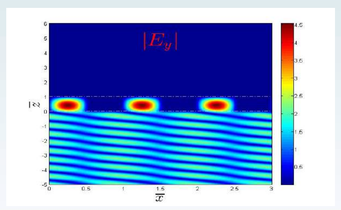

TE Polarization

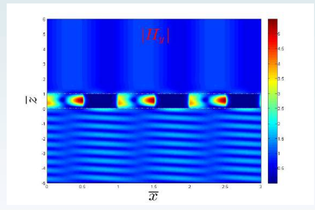

TM Polarization

FMMASR (Adaptive Spatial Resolution)

Stretched coordinates ➡ $x = f(u)$

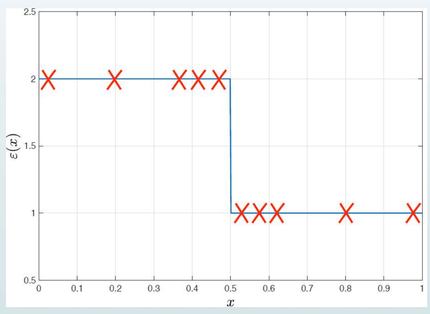

High Resolution @ Discontinuity Points

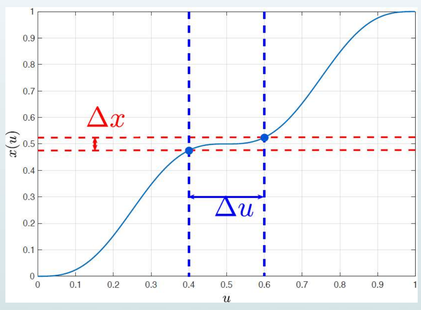

Results

Horizontal Strips

Absorption

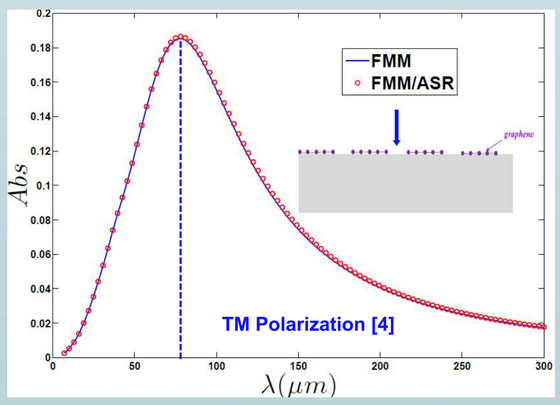

Convergence

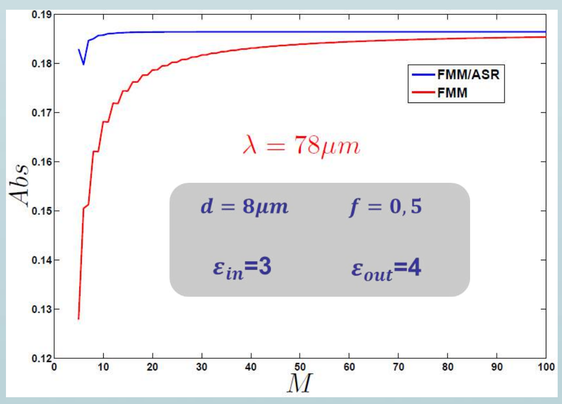

Vertical Strips

Absorption

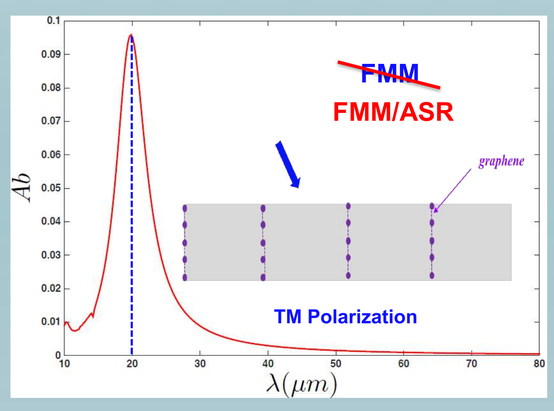

Convergence

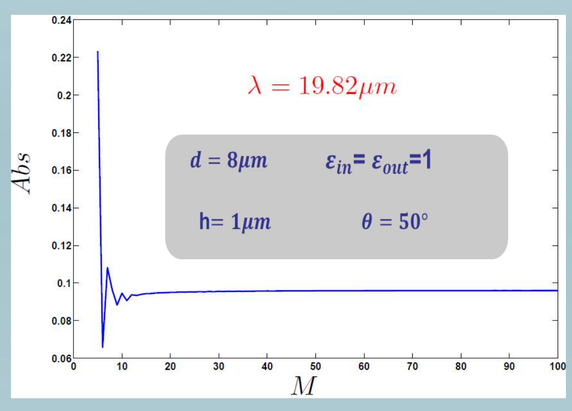

Map of the magnetic field

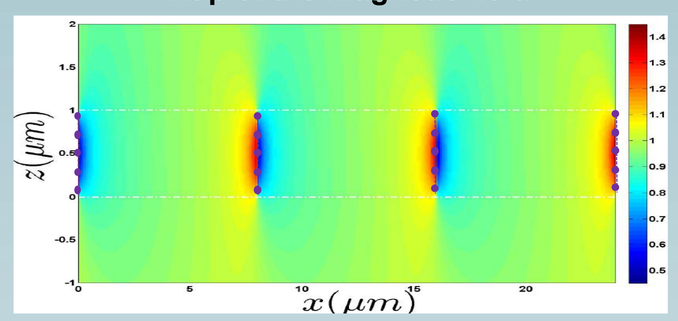

Conclusions

The former objective of the PhD work is achieved: the construction of general versatile and efficient codes for the modeling and simulation of graphene based nano-devices. Furthermore, we discovered a problem with the FMM in the case of pathological vertical gratings and proposed an efficient solution through the use of the ASR concept. We are now ready to begin the next step consisting on the exploration of graphene plasmonic devices.

Bibliography

1. A. K. Geim et al, Nat. Mater. 6, 183–191 (2007).
2. D. Rodrigo et al, Science 349, 165–168 (2015).
3. Tony Low and Phaedon Avouris, ACS Nano 8, 2, 1086-1101 (2014)
4. A. Nikitin et al, Phys. Rev. B 85, 081405 (2012)

Life cycle assessment of Bioethanol

Bhawna SHARMA, Christian LARROCHE, Claude Gilles DUSSAP

*** University Clermont Auvergne, Institute Pascal, 63000, Clermont-Ferrand, France.**

Introduction

Liquid biofuels are widely acclaimed replacement to fossil fuels to minimize the dependence on fossil fuels and improves the energy security to promote economic development. The first generation biofuels can be produced from sugar and starch based feed- stocks such as sugarcane, corn, potato, cassava. Due to the use of food or feed grains appears unsustainable as the process requires cultivable land and generates conflicts between industrial and food/feed use of feed-stocks. Therefore, it cannot be successfully become a viable fuel source. The production of second generation bioethanol which is produced from ligno-cellulosic biomass, not used for food, is gaining momentum as it does not compete with food or feed(1). Ligno-cellulosic biomass (rice straw, corn cob, wheat straw, sugarcane bagasse, cotton stalk) are best alternative as these are abundant, renewable and relatively cheap. The area of research mainly focus on the energy balance, greenhouse gas emission and other impact categories and also the production cost to discuss their potential environmental as well as socioeconomic impacts.
.

Objective

- To study and design the ethanol production processes.
- To predict the GHG emission from ethanol production processes.

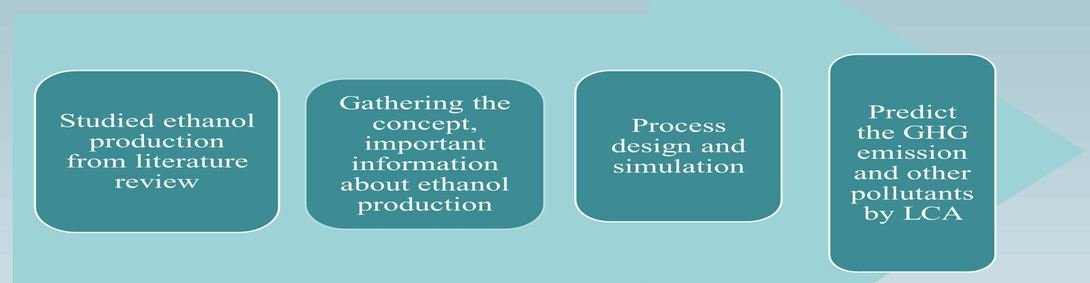

Methods

Bioethanol production from the biochemical conversion pathway-

1- Pre-treatment of lignocellulosic biomass-

- To destroy the structure of cellulosic biomass cell wall.
- Make cellulose more accessible to the subsequent process of hydrolysis.

2- Hydrolysis –

- Hydrolysis is used to convert cellulose and hemi-cellulose to glucose and xylose.
- The temperature is about 50º C for hydrolysis.
- Cellulase and xylanase are used as an enzyme.

3-Fermentation

- Fermentation is used to convert simple sugars into ethanol.
- *Saccharomyces cerevisiae* is mainly used as a yeast.
- Temperature is about 30-37ºC.

4- Ethanol purification

- Extractive distillation is used.
- Mostly Ethylene glycol is used as a solvent.

❑ Each step is simulate by the chemical simulator **PROSIMPLUS.**
❑ The primary objective of simulation is to generate the mass and energy balances from which the requirements for raw-materials, consumables, utilities and energy needs are calculated.

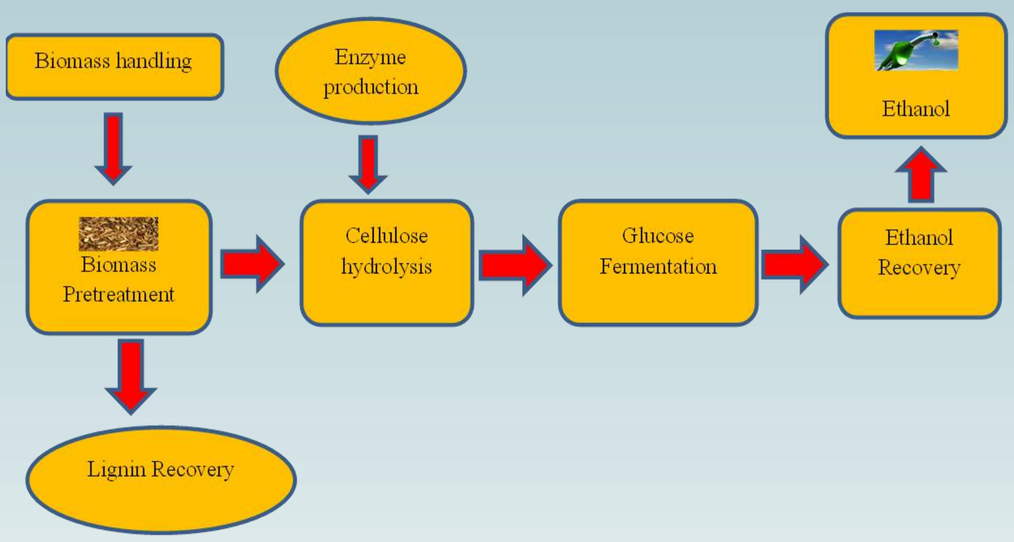

Results

❑ Simple distillation of Ethanol-water mixture is carried out by the **PROSIMPLUS** by a **McCabe-Thiele method** with a flow rate of distillate with 15.7 kg/s and feed stage is 7 whereas number of stage is 25.

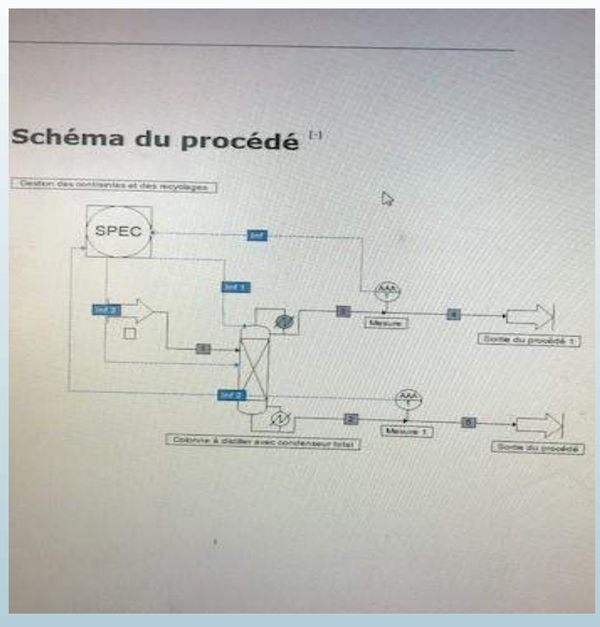

Conclusions

SCOPE OF THE FUTURE WORK-

- ❖ PROSIMPLUS is used to simulate all the processes.
- ❖ Woody biomass is used as a main raw material.
- ❖ LCA of woody biomass through the biochemical conversion pathway will be carried out.

Bibliography

1. **Jeswani, H. K., Falano, T., & Azapagic, A. (2015).Life cycle environmental sustainability of lignocellulosic ethanol produced in integrated thermo-chemical biorefineries. *Biofuels, Bioproducts and Biorefining*, *9*(6), 661-676.**

Study of the behavior of unsaturated fine-grained soils under cyclic loading - Application to the development of a methodology for diagnosis and maintenance of the Trans-Gabon Railway subgrade.

Bilal YOKA KHAIL, Pierre BREUL and Mathilde MORVAN

Université Clermont Auvergne

Context

The repeated moving of trains induces cyclic loading on the railway subgrade soil which, in certain situations (high axle load, adverse environmental context, failure of the drainage system), can lead to a state of failure of the track (photo 1). In the case of the Trans-Gabon Railway line, subgrade instability problems are recorded due to the severe environmental context (high rainfall) and the presence of evolving subgrade soils.
At present, the behavior under cyclic loading, in unsaturated condition, of railway subgrade with fine-grained soils is still poorly mastered.

Figure 1:Derailment of a mineral train in Gabon

Objectives

- To propose a diagnostic methodology to evaluate the in-situ mechanical resistance and the amplitude of plastic strain of the railway subgrade soil, according to the water conditions and the amplitude of cyclic loading applied
- To Estimate, from in-situ measurements, the characteristics of the subgrade soil (water content, dry density) in order to feed the plastic strain prediction model.

Methods

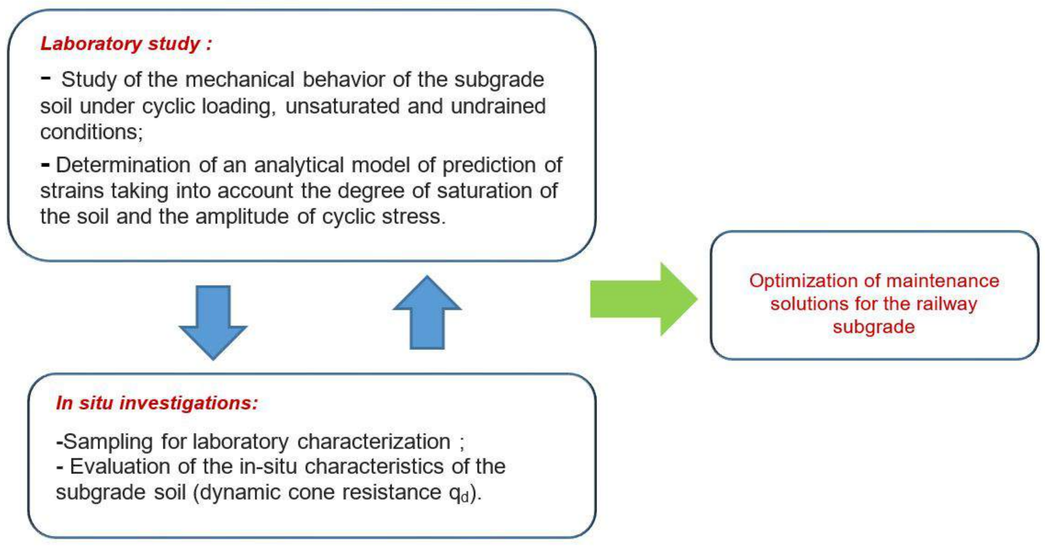

Figure 2:General methodology

Mathematical model

The analytical model for the prediction of the strains that we propose to determine will have to take into account the amplitude of the cyclic loading. (Δq_{max}) and the degree of saturation of the soil (S_r). The model gives the plastic axial strain (ε_a^p) such as [3] :

$$\varepsilon_a^p(N, S_r, \Delta q_{max}) = t(S_r, \Delta q_{max}).f(N)$$

Where f_N is the axial plastic strain according to the number of cycles of the load application to the axle (N) and $t(S_r, \Delta q_{max})$ is the axial plastic strain depending on the amplitude of loading and the soil moisture status.

Materials

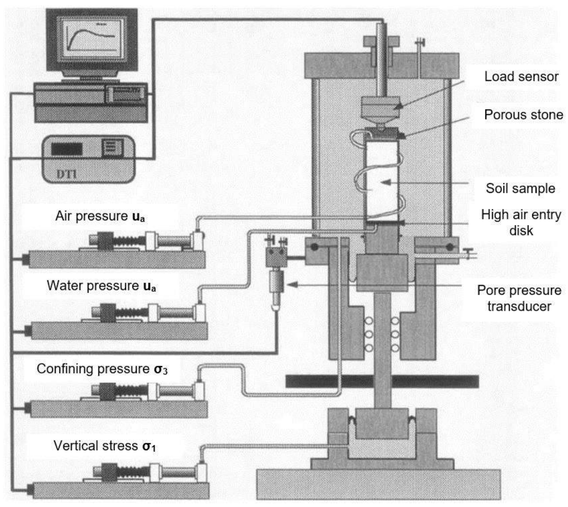

Figure 3:Modified Bishop and Wesley (1975) triaxial cell [1]

Figure 4:Dynamic penetrometer [2]

Studied sites

For this study, we are interested in two areas of the Trans-Gabon Railway line on which recurring problems of instability of the subgrade are often listed. These areas are located on the sites of a geological formation formed during the Lower Cretaceous (Neocomian to Barremian) age, mainly marls, argillites and sandstones. The soil in the two study areas is identified as pelitic alteritis.

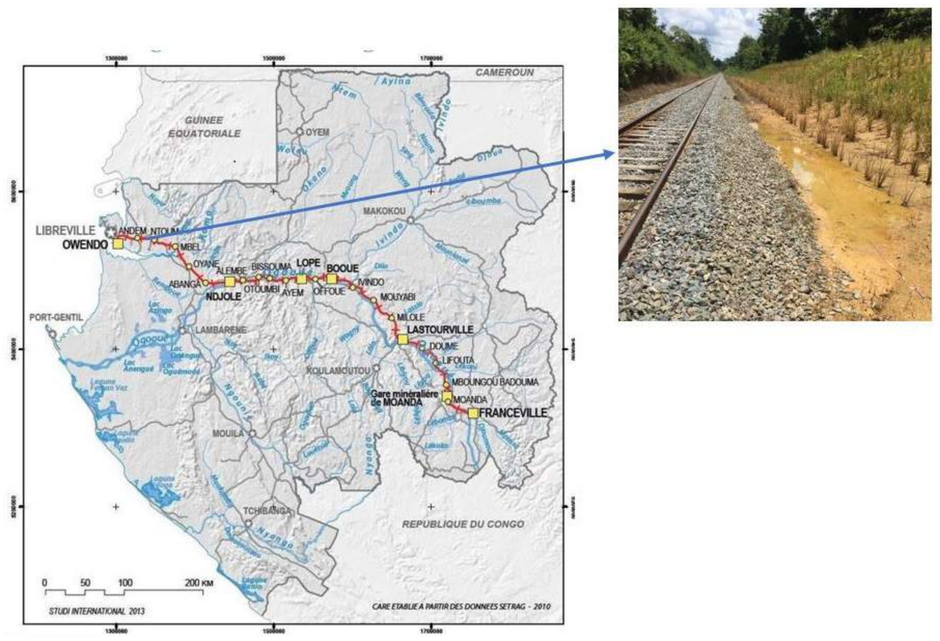

Figure 5:Location of study areas

Expected results

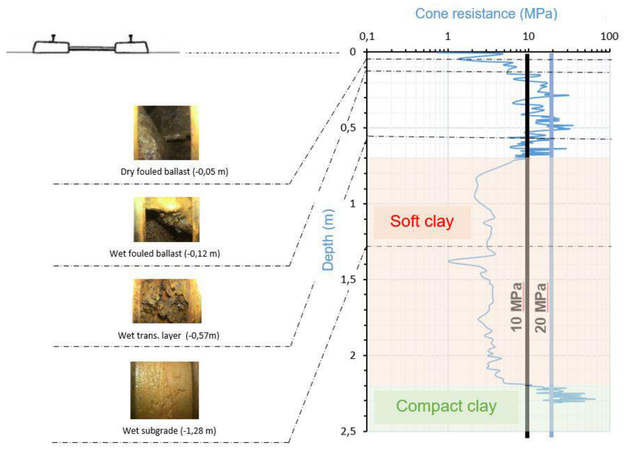

Figure 6:Penetrometric (PANDA 2) and geoendoscopic test coupling performed on the Trans-Gabon Railway line [2]

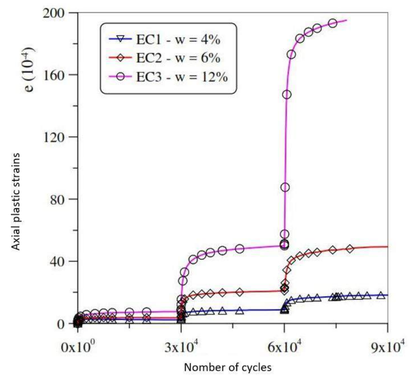

Figure 7:Development of the axial plastic strain with the number of cycles application [3]

conclusion and perspectives

This study should allow us to :

- To provide input data to feed the soil bank database on A3 and A4 class materials (according to the french GTR 92 classification (NF P 11-300) ;
- To produce a model of prediction of plastic strains taking into account the variation of the hydric state, valid for railway subgrade in fine-grained materials

References

[1] F. Geiser.
Comportement mécanique d'un limon non saturé étude expérimentale et modélisation constitutive.
page 311, 1999.

[2] Y. Haddani, P. Breul, G. Saussine, M. A. Benz Navarrete, F. Ranvier, and R. Gourvès.
Trackbed mechanical and physical characterization using panda/ geoendoscopy coupling.
Procedia Engineering, 143:1201 – 1209, 2016.

[3] V. Trinh.
Comportement hydromécanique de matériaux constitutifs de plateformes ferroviaires anciennes.
PhD thesis, Université Paris-Est, 2011.

Acknowledgements

- The authors wants to thank the Doctoral School of Sciences for the Engineer and the Clermont Auvergne University.

MODÈLE DE CONNAISSANCE D'UN PHOTO-RÉACTEUR D'ÉTUDE POUR LA PRODUCTION D'HYDROGÈNE SOLAIRE

Caroline SUPPLIS, Jérémi DAUCHET, Victor GATTEPAILLE, Fabrice GROS, Matthieu ROUDET, Jean-François CORNET

Université Clermont Auvergne, CNRS, Sigma Clermont, Institut Pascal, UMR 6602, F-63000 Clermont-Ferrand, France

Ecole doctorale Sciences Pour l'Ingénieur

Introduction

- Production de vecteurs énergétiques propres, sûres et efficaces

PRODUCTION DE CARBURANTS SOLAIRES

- Energie solaire par nature fluctuante :
  - Stockage sous forme chimique : Hydrogène (H_2).
  - Apport d'énergie à un photocatalyseur pour oxyder l'eau et reduire H^+ en H_2.

- Actuellement deux principaux verrous :
  - En chimie : Développement de photocatalyseurs efficaces et peu coûteux,
  - **En SPI : Conception et optimisation des photo-procédés.**

- Le rayonnement est le phènomène limitant les photo-procédés [1] :
  - Optimisation du rayonnement,
  - Augmentation de la cinétique de production d'H_2,
  - Augmentation des performances énergétiques.

ETUDE DE L'INTERRACTION PHOTONS/MATIÈRE

Banc expérimental

Présentation du photoréacteur

Un photo-réacteur étanche a été utilisé pour la production photo-catalytique d'H_2.
- Densité de flux de photons contrôlée à l'entrée du réacteur par un panneau de LED
- Mesure de $<r_{H_2}>$ par capteur de pression de haute précision et modèle associé.

Le banc expérimental permet d'acquérir des courbes de pression en fonction du temps. Une relation entre $<r_{H_2}>$ et la variation de la pression en fonction du temps dP/dt a été obtenue à partir d'un bilan massique sur l'H_2 dans la phase liquide et gaz [2,3].

Capteur de pression permettant d'obtenir la vitesse de production d'H_2

$$r_{H_2} = \left(\frac{V_G}{V_L RT} + \frac{1}{H_{H_2}}\right)\frac{dP}{dt}$$

PHOTONS ENTRANT PAR L'AVANT DANS LE PHOTOREACTEUR

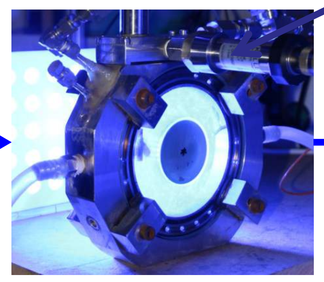

PHOTONS SORTANT PAR L'ARRIÉRE DU PHOTOREACTEUR

Système photocatalytique pour la production d'H_2

$$2S^{2-} + 2H_2O \xrightarrow{h\nu,\ CdS} S_2^{2-} + 2OH^- + \mathbf{H_2}$$

$$SO_3^{2-} + H_2O \xrightarrow{h\nu,\ CdS} SO_4^{2-} + \mathbf{H_2}$$

Des particules de sulfure de cadmium (CdS) sont utilisées comme modèle de photo-catalyseur sous rayonnement visible en présence de donneurs sacrificiels permettant de produire de l'H_2.

Modèle multi-échelle

La démarche consiste à décrire les principales étapes liées au transfert de rayonnement qui gouverne le procédé à plusieurs échelles ainsi que son couplage thermocinétique avec les vitesses de réaction.

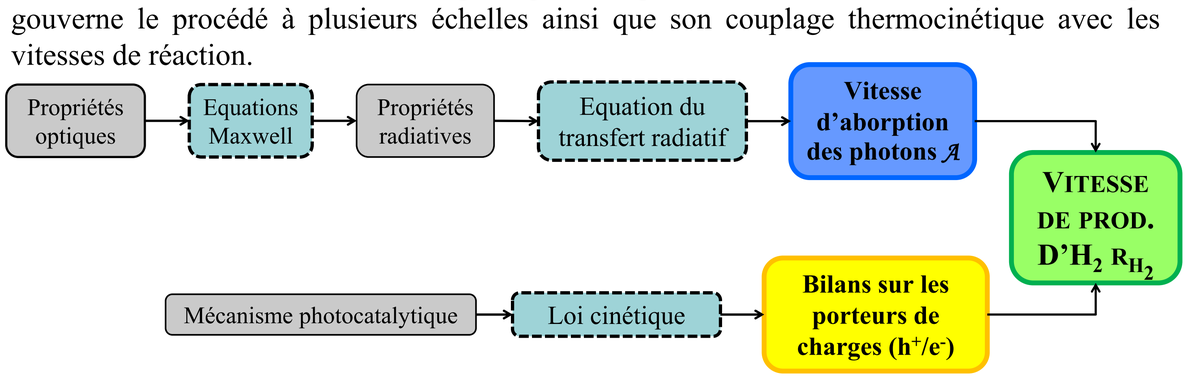

Elle suit une progression depuis l'échelle microscopique, par l'étude des interactions des photons avec les particules de catalyseur, en passant par l'échelle mésoscopique en déterminant le champ de rayonnement et la quantité de photons absorbés localement, jusqu'à l'échelle macroscopique, c'est-à-dire l'échelle du procédé, en déterminant de façon prédictive, les vitesses de réaction moyennes ainsi que l'efficacité thermodynamique du réacteur.

$$r_{H_2}(\mathbf{x}) = C_{cat}\phi\beta\sqrt{\frac{2\rho_{max}\beta}{\mathcal{A}(\mathbf{x})}}\mathcal{A}(\mathbf{x}) = \Phi(\mathcal{A}(\mathbf{x}))\mathcal{A}(\mathbf{x})$$

- Φ rendement quantique global de la réaction,
- C_{cat} concentration en catalyseur (connue),
- ϕ rendement quantique stœchiométrique (connu),
- ρ_{max} rendement maximum de conversion de l'énergie lumineuse en énergie physico-chimique (connu),
- β rapport des constantes cinétiques intervenant dans la réaction catalytique (inconnu)

Résultats

Propriétés optiques

La première étape de notre chaine méthodologique est la détermination des propriétés optiques de CdS que l'on trouve facilement dans la littérature.

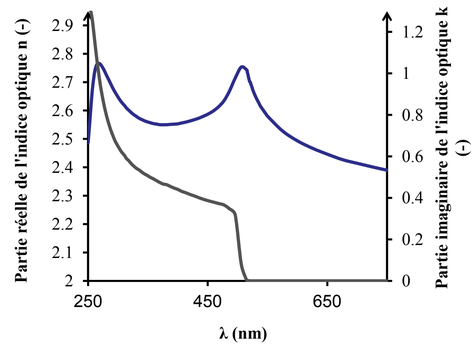

Indices optiques des particules de CdS

Propriétés radiatives

Les propriétés radiatives des particules de CdS ont été calculées grâce aux équations de Maxwell. On obtient ainsi : Le coefficient d'absorption E_a, le coefficient de diffusion E_d et la fonction de phase p.

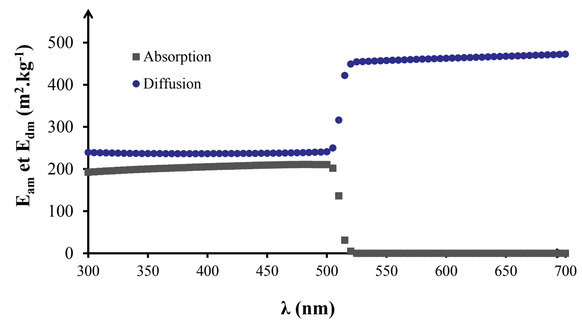

Propriétés radiatives des particules de CdS

Analyse du transfert radiatif

L'ETR a été résolue rigoureusement par la méthode de Monte Carlo. La vitesse d'absorption locale $\mathcal{A}(\mathbf{x})$ du rayonnement est ainsi déterminée en fonction de la densité de flux incidente. La diffusion des photons par les bulles d'hydrogène a été prise en compte. En intégrant sur le volume du réacteur, il est possible d'obtenir la vitesse d'absorption moyenne $<\mathcal{A}> = \frac{1}{V}\iiint_V \mathcal{A}\,dV$.

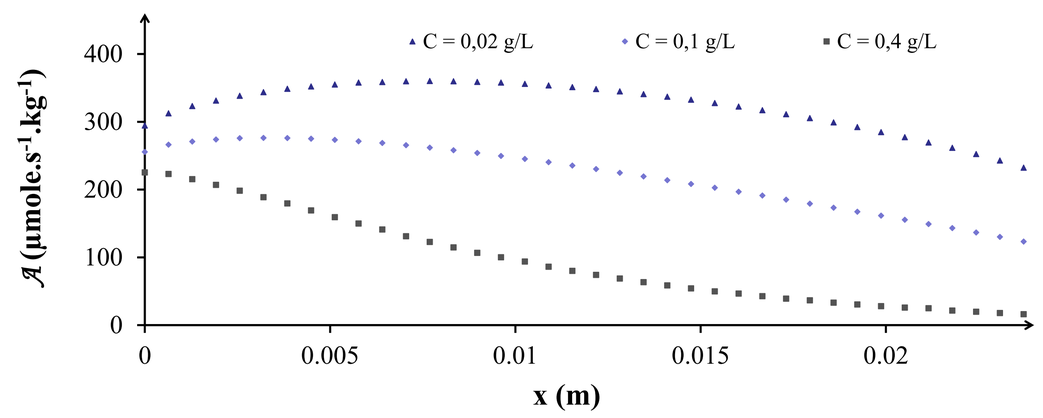

Champ local d'absorption des photons

Validation du modèle

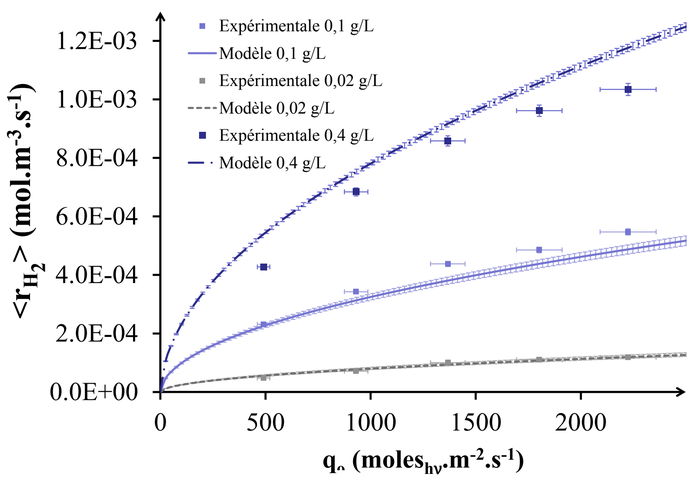

Vitesse de production d'H_2

- Intégration de la vitesse locale de production d'hydrogène sur le volume du réacteur pour obtenir une valeur moyenne théorique de $<r_{H_2}> = \frac{1}{V}\iiint_V r_{H_2}\,dV$.
- Tracé des données expérimentales et théoriques pour 0.02 g/L, 0.1 g/L et 0.4 g/L en CdS,
- Le seul paramètre inconnu β (agrégeant les constantes cinétiques) a été identifié sur une concentration en CdS (0,02 g/L) et utilisé de façon prédictive sur les deux autres concentrations (0,1 et 0,4 g/L).

Conclusions

- A partir des indices de réfraction du CdS (issus de la littérature), les propriétés radiatives (diffusion, absorption) des particules ainsi que celles des bulles d'hydrogène ont été calculées et validées. Elles permettent d'obtenir le champ de rayonnement $\mathcal{A}(\mathbf{x})$ par résolution de l'ETR,
- Au moyen de la loi de couplage non linéaire établie, les vitesses volumétriques locales de production d'hydrogène ont été calculées débouchant sur l'estimation de la vitesse volumétrique moyenne en accord avec les données expérimentales.

Bibliographie

[1] A. Cassano et al. Ind. Eng. Chem. Res., 1995, 2155-2201
[2] G. Dahi et al. Chemical Engineering and Processing 98 (2015) 174–186
[3] C. Supplis et al. Int. J. Hydrog. Energy, 43(17), 8221-8231, 2018.

Structural Reliability Analysis based on an automatic selection of Surrogate Models

Chahrazed AMRANE, Pierre BEAUREPAIRE, Cécile MATTRAND, Nicolas GAYTON and Jean-Marc BOURINET

Universite Clermont Auvergne, CNRS, SIGMA Clermont, Institut Pascal,F-63000 ClermontFerrand, France

Objectives

1. Estimation of the structure's **failure probability** using **surrogate models**.
2. Development of numerical methods for the automatic selection for surrogate that best fits the limit state function by using an **evolutionary algorithm**.
3. Determination of the surrogate associated weights when ensemble of surrogates are selected to approach the limit state function.

Introduction

- **Structural reliability analysis** is a challenging task as it is a very time-consuming computation. It consists of evaluating the **failure probability**, which requires a very complex and multi-variable integration based on the limit state function. In engineering problems, the limit state function estimation involves complex and time-consuming finite element analyses. Consequently, **surrogate models** are usually used instead since they can reduce the computational cost. Various surrogate models exist, such as the polynomial chaos expansion (PC), response surface method, Kriging model etc. exists with different tunning. The choice of the most suitable one for a given problem is not obvious. In this work, we are interested in developing an automatic selection procedure based on an **evolutionary algorithm**. It should determine the optimal surrogate to any problem. Furthermore, there are situations where none of the meta-models is the best choice and distinguishing between those surrogates in not an evidence. Using **ensembles of surrogates**, in this case, should be a reasonable solution.

Definitions

- Surrogate models
  - Surrogate models are mathematical models used to approach computationally expensive simulations.They have to be as accurate as possible.

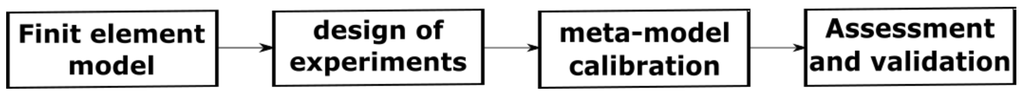

Figure 1:Process of calibrating a meta-model

- Evolutionary Algorithms
  - Evolutionary algorithms are population based heuristic optimization algorithms inspired by biological evolution.

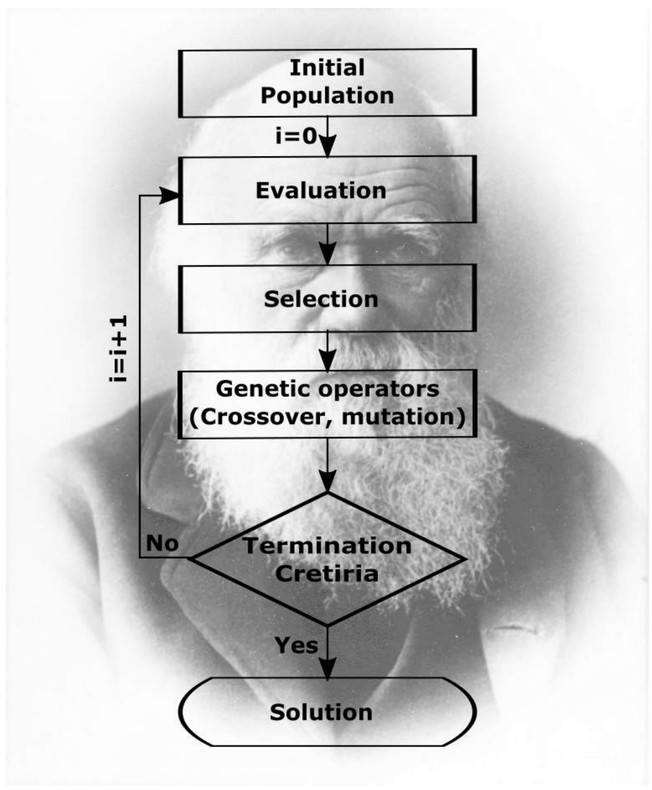

Figure 2:Flowchart of Evolutionary Algorithms

State of the art

In the literature, this problem is generally studied using different approaches:

- Gorissen and al (2009) proposed in [1] an evolutionary algorithm to perform surrogate model selection. But they emphasize the existence of so much parameters to tune and the dependence on the genetic operators.
- Shi and al (2012) introduced in [2] a selection method under data uncertainty in the context of large scale optimization.

State of the art: Continuation

- Zhou and Jiang, 2016 tackled the meta-model selection in [3] by using a stepwise regression.
- Ben Salem and Tomaso (2017) developed in [4] a new selection criteria used in a genetic aggregation method.

Methods

- Structural Reliability Analysis based on surrogates
  - The failure probability of the structure is $P_f = \int_{g(x)\leqslant 0} f_X(x)dx$.

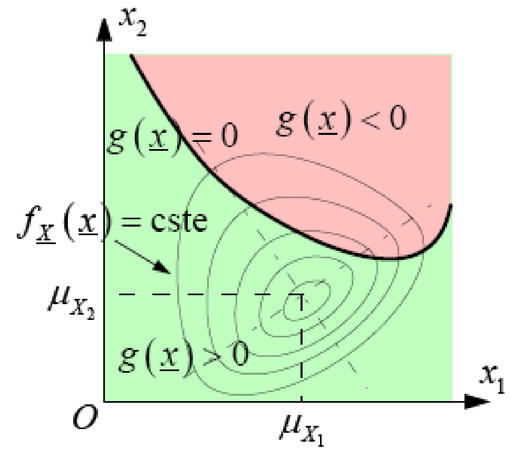

Figure 3:Performance Function g(x)

  - The estimation of P_f is done either by approximation (FORM/SORM) or simulation (MCS, IS, etc.).

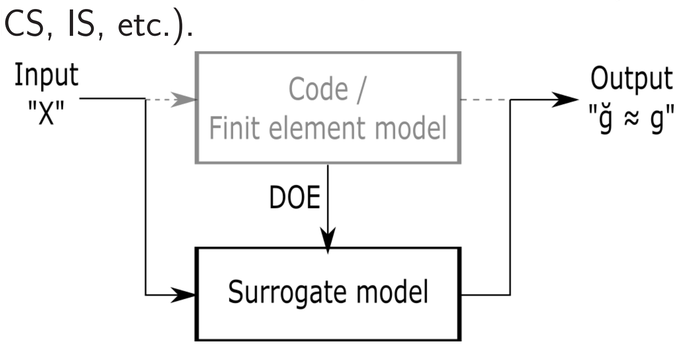

Figure 4:Using a surrogate model

- Meta-models automatic selection using an Evolutionary Algorithm
  - The individuals are the different optimized surrogate models.
  - The fitness function is the selection criteria.
  - The optimized meta-model settings are the genetic informations of the individuals.
  - The aggregation of meta-models occurs if the genetic operators are applied to the settings of two different types.

$$\hat{G}(x) = \sum_{i=1}^{p} w_i \hat{g}_i(x)$$

Challenges and perspectives

- Proposing a **new relevant surrogate model selection algorithm** using an **evolutionary algorithm**.
- Tunning the evolutionary algorithm parameters.
- Choosing an appropriate **criteria of selection**.
- Optimizing the surrogate associated **weights** in case ensembles are created.
- Assessing the **level of confidence** of the selected surrogate prediction.

References

[1] Dirk Gorissen, Tom Dhaene, and Filip De Turck.
Evolutionary model type selection for global surrogate modeling.
Journal of Machine Learning Research, 10(Sep):2039–2078, 2009.

[2] Lei Shi, RJ Yang, and Ping Zhu.
A method for selecting surrogate models in crashworthiness optimization.
Structural and Multidisciplinary Optimization, 46(2):159–170, 2012.

[3] XiaoJian Zhou and Ting Jiang.
Metamodel selection based on stepwise regression.
Structural and Multidisciplinary Optimization, 54(3):641–657, 2016.

[4] Malek Ben Salem and Lionel Tomaso.
Automatic selection for general surrogate models.
In *12th World Congress of Structural and Multidisciplinary Optimisation*, 2017.

chahrazed.amrane@sigma-clermont.fr

Design of a cable driven parallel robot for additive manufacturing

Damien GUENERS

Supervised by Chedli BOUZGARROU, Hélène CHANAL

Université Clermont Auvergne, SIGMA Clermont, CNRS, UMR 6602, Institut Pascal, BP 10448, F 63171 AUBIERE

Ecole doctorale Sciences Pour l'Ingénieur

Introduction

Cable driven parallel robots are robots for which the fixed base and the mobile platform are connected by cables. There are no guiding elements except those of the pulleys used to wind and unwrap the cables.

The **main advantages** of this technology are:

- **reduction of the moving masses** resulting in a large acceleration capacity of the moving platform;
- **reconfigurability and modularity**: the robot can be reconfigured easily by changing the anchor points of the actuators and adapting its geometric control model;
- **reduction of the production costs**.

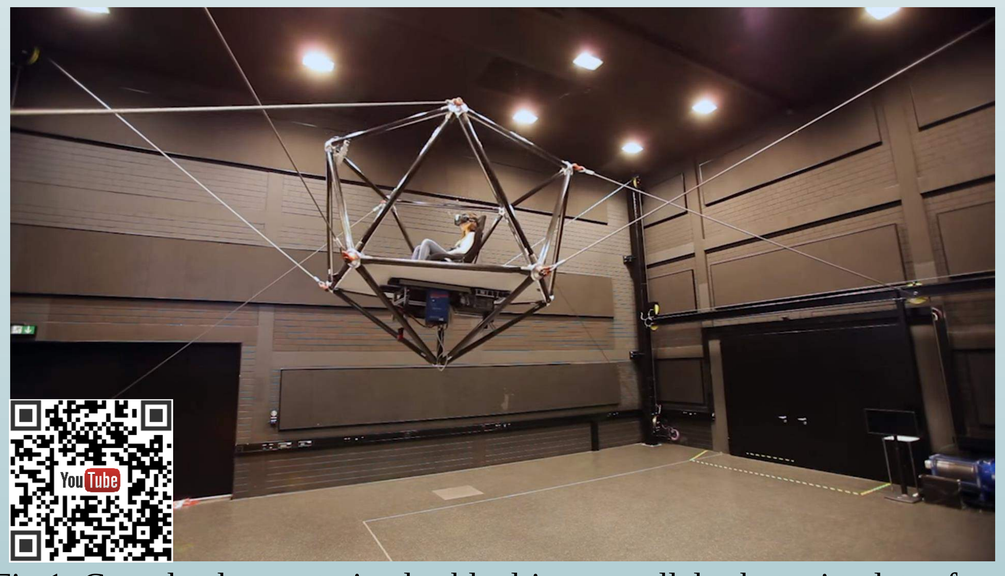

Fig 1: Completely constrained cable driven parallel robots simulator from Max Plank Institute [2]

Additive manufacturing is a manufacturing process by adding material. As opposed to subtractive manufacturing commonly used in the industry to machine parts by removing material from a crude. The vast majority of these solutions use a Cartesian robot, a horizontal plane 2D motion for the movement of the head and a linear 1D movement for the support table, which corresponds to 3 degrees of freedom(DoF) machines.

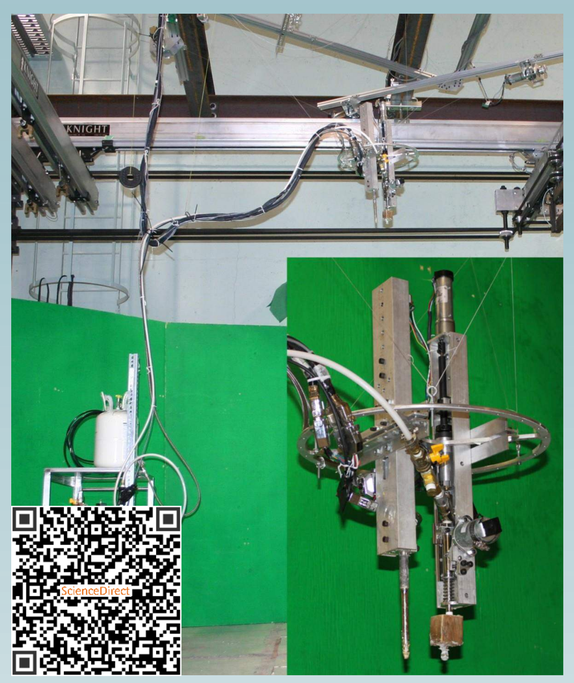

Fig 2: Suspended cable driven parallel robots for large-scale 3D printing from University of Laval [3]

The manufacturing process which need more than 3 DoF are **Fused Deposition Modeling** and **electron-beam melting**. This will enable more complex parts to be produced. This can decrease the manufacturing cost by using less material and a less expensive architecture. But this can also increase the production speed, and propose a modular architecture to adapt to the size of the part. These different approaches to innovation can be satisfied by a cable architecture.

The use of cable robots for additive production in a short term is conceivable. Unlike a use for subtractive production, where the mechanical stresses are stronger, and the rigidity of the cable solutions being too weak.

Problematics

- Design of a high dynamic cable robot for accurate position control for large-scale printing;
- Dimensional synthesis maximizing the workspace and the rigidity of the robot.

Objectives

- **Preliminary design:**
  Structural synthesis, geometric and kinematic-static of a 6 DoF cable robot having a guaranteed level of rigidity in a workspace optimized in terms of accessibility in position and orientation.
- **Modeling:**
  Dynamic modeling of the robot taking into account the elasticity of the cables and the behavior of the drive chain. Static and dynamic performance evaluation by model simulation.
- **Design:**
  Realization of a demonstrator and evaluation of its static and dynamic performances by experimental characterization.
- **Model adjustment and design optimization.**

Kinematics

The inverse kinematics model can be easily defined by the equation [4]:

$$l_i = \left\| \overrightarrow{A_i B_i}\big|_O \right\|_2 = \left\| -\overrightarrow{OA_i}\big|_O + \overrightarrow{OC}\big|_O + R_C \overrightarrow{CB_i}\big|_C \right\|_2$$

Where:

- l_i is the length of the i^{th} cable.
- $\overrightarrow{OC}\big|_O$ is the position vector of the effector on the origin frame;
- R_C is the rotation matrix from the origin frame to the effector frame which contains the orientation of the effector;
- $\overrightarrow{CB_i}\big|_C$ is the fixed vector of the attachment point B_i on the effector frame;
- $\overrightarrow{OA_i}\big|_O$ is the fixed vector of the attachment point A_i on the origin frame;

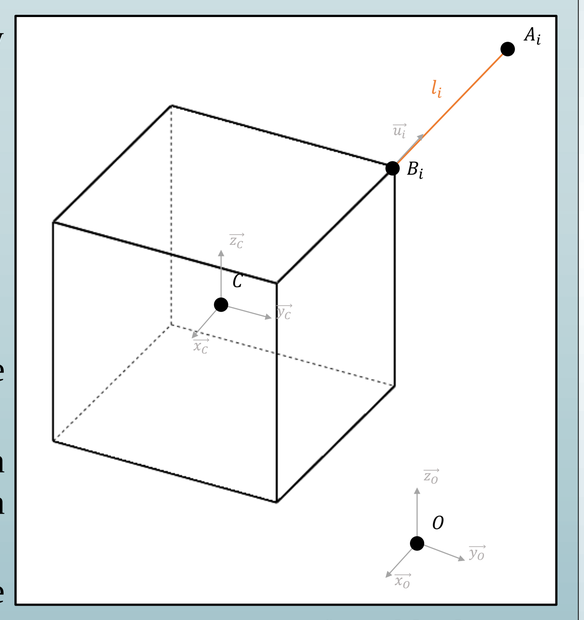

Fig 3: Kinematics of a cable driven parallel robot

Prospect

The prospect is to **analyze the dynamic behavior of the robot**. To this end we need to implemented a dynamic model with elastic wire **by using Lagrange equations**. There are 6+n generalized coordinates $x_C, y_C, z_C, \psi, \theta, \varphi, q_1, \dots, q_n$. n multiplicator of Lagrange are introduced with n holonomic constraints :

$$f_i(x_C, y_C, z_C, \psi, \theta, \varphi, q_i) = \overbrace{R_{reduc}(q_i - q_0) + l_0}^{l_i} - \left\| -\overrightarrow{OA_i}\big|_O + \overrightarrow{OC}\big|_O + R_C \overrightarrow{CB_i}\big|_C \right\|_2$$

The Lagrange equations of the dynamics can be defined by 6+n equations for a robot with 6 DoF and n wires:

$$\mathcal{L}_{p_i}: \frac{d}{dt}\frac{\partial T}{\partial \dot{p_i}} - \frac{\partial T}{\partial p_i} = P_{p_i} + \sum_{k=1}^{n} \lambda_k \frac{\partial f_k}{\partial p_i}$$

Where p_i is the generalized coordinate,T is the kinetic energy of the robot, P_{p_i} is the generalized force, λ_k is a Lagrange multiplicator, R_{reduc} is the reduction ratio between the cable length and the drum angle, q_0 is the drum angle at 0 and l_0 is the wire length at 0.

Bibliography

1. **C. Gosselin, "Cable-driven parallel mechanisms: state of the art and perspectives,"** ***Mech. Eng. Rev.*****, vol. 1, no. 1, pp. DSM0004-DSM0004, 2014.**
2. **P. Miermeister *et al.*, "The CableRobot simulator large scale motion platform based on Cable Robot technology," in *IEEE International Conference on Intelligent Robots and Systems*, 2016, vol. 2016–Novem, pp. 3024–3029.**
3. **E. Barnett and C. Gosselin, "Large-scale 3D printing with a cable-suspended robot,"** ***Addit. Manuf.*****, vol. 7, pp. 27–44, 2015.**
4. **T. Bruckmann, L. Mikelsons, T. Brandt, M. Hiller, and D. Schramm, "Wire Robots Part I: Kinematics, Analysis & Design,"** ***Parallel Manip. New Dev.*****, vol. 1, no. April 2008, 2008.**

Cette thèse est subventionnée par la Région Auvergne-Rhône-Alpes dans le cadre du programme Pack Ambition Recherche 2017 – Projet CABFAB

Contribution to EMC predictive modeling of electronic systems at frequencies above GHz.

Ecole doctorale Sciences Pour l'Ingénieur

E.Tefouet, Reseach supervisor F .Paladian

CLERMONT AUVERGNE UNIVERSITY

Introduction

The characterization of electronic systems, in particular in conducted emission, represents nowadays a theme pregnant with electromagnetic compatibility for frequencies higher than GHz. In order to have a predictive tool allowing the best modeling of all the electromagnetic couplings (conduction and radiation) occurring at the level of the different sub-parts of the system, the objective of the thesis is to develop a model under LTSpice for the determination of the voltages generated by it.

These systems include shielded cables whose role is crucial to the studied frequencies and characterize by their transfer impedance or their shielding effectiveness.

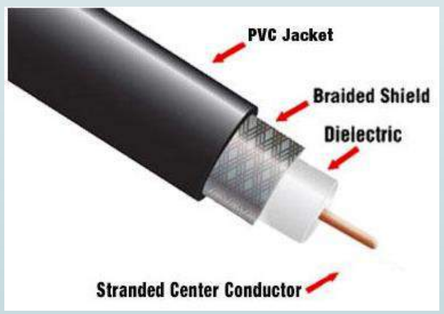

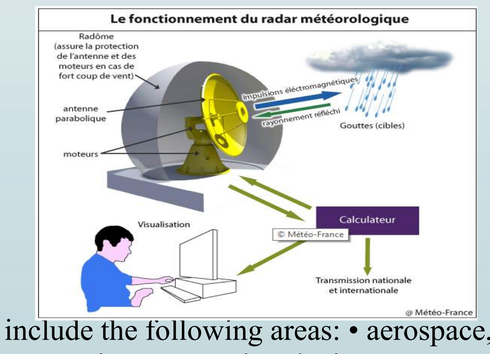

The applications of coaxial cables are diverse and include the following areas: • aerospace, • telecommunications, • radio / television, • cameras, • various measuring devices, • computer, • medical: scanners, ultrasound, • military: radars, measurements…

Methods

Different experimental techniques have been developed to evaluate the immunity of cables against electromagnetic interference. Among the best known, can be mentioned BCI method (Bulk Current Injection) or Triaxial or Quadriaxial banks, the principles implemented requiring extensive control of the various elements of the set up measurement and giving rise to frequency limitations.

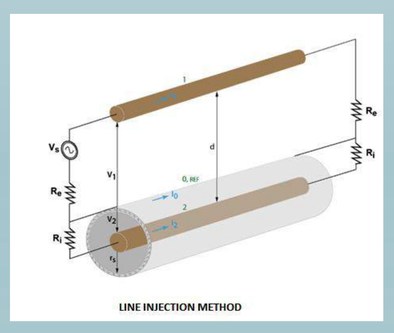

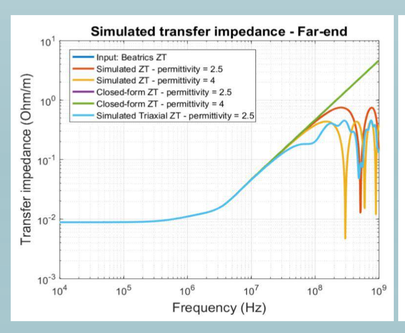

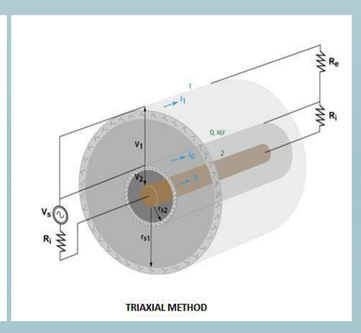

For these different reasons, it is advisable to move towards measurements in Reverberant Chamber with Mode Mixing (RC) allowing to generate a statistically homogeneous and isotropic electromagnetic field, of random polarization. This structure makes it possible to reproduce a real electromagnetic environment at high frequencies (above 150 MHz for the Institut Pascal Pascal RC).

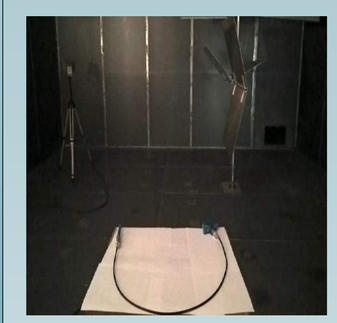

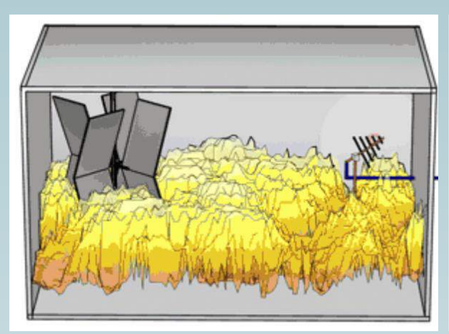

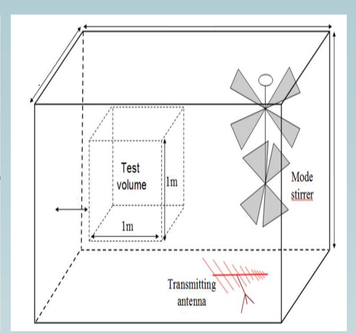

It should be noted that for the cable transfer impedance measurement benches previously mentioned, the shielding is subjected to a TEM wave. Screening effectiveness measurements of RG58 type cable samples will be carried out using several methods and the results obtained will be validated by comparison with theoretical data (obtained from transmission line theory and MS CST).

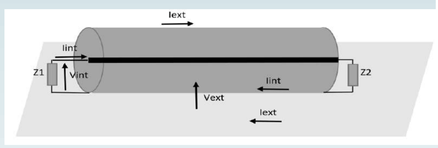

$$(Z_T)_{dB} = log\left|\frac{2Z_{c-int}(1e^{+\gamma_{int}L} - \rho_0\rho_L e^{-\gamma_{int}L})}{(1-\rho_L)(1-e^{-\gamma_{int}L})(e^{+\gamma_{int}L} - \rho_0)(1-e^{-\gamma_{int}L})}\right| - SE_{dB}$$

Improvements to the methods available in the literature will be proposed as part of the thesis.

Results

Several measurements were performed in the IP laboratory RC, on the RG58 cable samples, and then compared to the results obtained by CST simulations.

The RC measurements of the power received on a shielded ($S21_B$) and unshielded ($S21_{NB}$) cable make it possible to determine the shielding effectiveness SE as:

$$\mathrm{SE} = 10log_{10}\left(\frac{S21_{NB}}{S21_B}\right)$$

With the Triaxial and injection line method simulations, we get the currents flowing in the core (I_c) and the braid (I_o) of the cable to calculate the shielding effectiveness as:

$$SE(z) = 20log_{10}\frac{I_c(z)}{I_0(z)}$$

The following illustrations show how differents are the results according to the method.

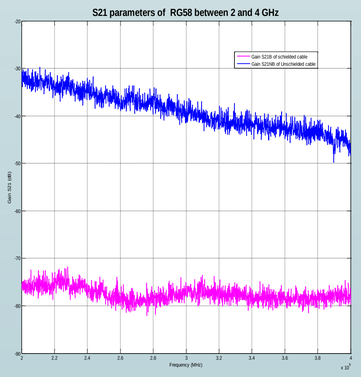

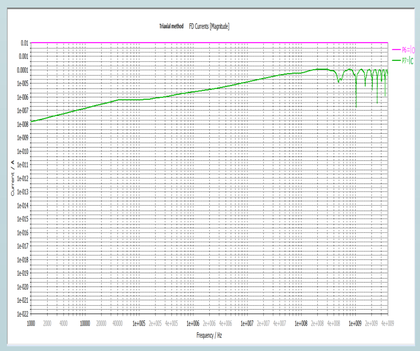

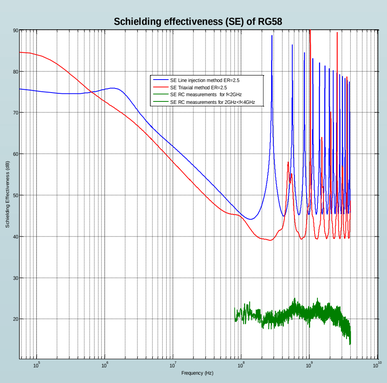

Several elements could justify this dispersion, we propose to see on the illustrations below, the impact of the non-taking into account of the type of connector, in the evaluation of the shielding effectiveness.

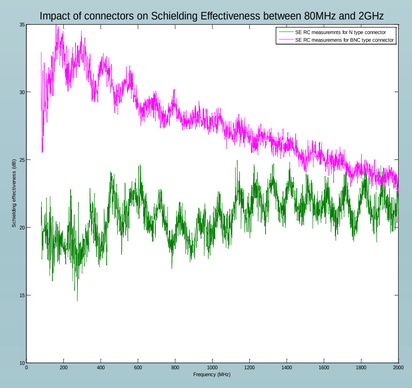

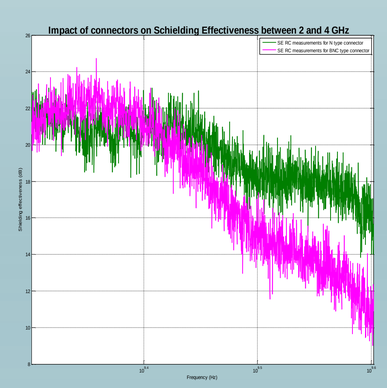

Conclusions

The Triaxial method and the injection line method do not take into account the influence of the connectors and the geometrical braiding structure, which could justify the difference in the evaluation results of the shielding effectiveness achieved compared to the shielding effectiveness measured in RC.

In the modeling of systems at frequencies above GHz, we would take account of the characterization of the geometrical discontinuities of the wired systems and the grounding at high frequencies.

Different numerical approaches including the so-called "full-wave" methods based on the numerical resolution of the Maxwell equations, and methods based on the theory of TLT transmission lines. Their influence must imperatively be considered in the numerical simulation of electronic systems at frequencies above GHz, the second part of the thesis will be devoted to the development of models reproducing the electromagnetic behavior of these elements.

Bibliography

1. **T. Kley, *Optimized single-braided cable shields*, IEEE Transactions on Electromagnetic Compatibility, Vol. 35, 1–9, 1993.**
2. **S. A. Schelkunoff, *The electromagnetic theory of coaxial transmission lines and cylindrical shields*, Bell System Technical Journal, Vol. 13, 532–579, 1934.**
3. **J.H.G.J. Lansink Rotgerink, H. Schippers and J. Verpoorte, *Multi-conductor transmission line modelling of transfer impedance measurement methods*, EMC Europe 2017, Angers.**
4. **V. M. Primiani,, F. Moglie, A.P. Pastore, *Modeling of the Reverberation Chamber Method for Determining the Shielding Properties of a Coaxial Cable*, IEEE Transactions on Electromagnetic Compatibility, Vol. 50, 246–251, 2008.**

Reflectometry for the SHM of existing 2D and 3D structures

Fatme MUSTAPHA[1] ,Jaume BENOIT[1], Pierre BONNET[2]

[1] *CEA, LIST, Laboratoire de Fiabilisation et d'Intégration des Capteurs Nano-Innov, Bât. 862-PC172, 91191 Gif-sur-Yvette Cedex, France*
[2] *Université Clermont Auvergne, CNRS, SIGMA Clermont, Institut Pascal, Clermont-Ferrand, France*

Ecole doctorale Sciences Pour l'Ingénieur

Introduction

Structural health monitoring (SHM) is the process of implementing a damage detection and characterization strategy for engineering structures[1].

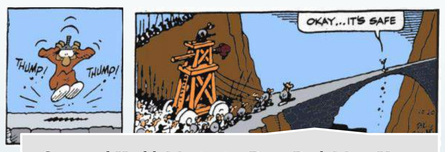

Structural Health Monitoring Dates Back Many Years

Human Casualties


Fires


Aircraft crashes


Bridge collapse

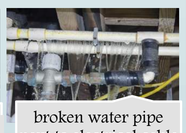
broken water pipe next to electrical cable

Monitoring of structures affected by external factors

Overcome accessibility limitations, complex geometries, depth of hidden damage

SHM

Greater vigilance in key areas

Minimize human factors with automated data analysis

Economical Losses


Property damage


Schedule delivery delay

Mission aborting


Damage in power plant

Steps of SHM [2]

- Determination of damage existence
- Determination of damage's geometric location
- Quantification of damage severity
- Prediction of remaining life of the structure

Benefits of SHM [3]

Near-Term

- Elimination of costly & potentially damaging structural disassembly
- Reduced operating and maintenance costs
- Reduction of inspection time
- Overcome accessibility & depth of flaw impediments
- Early flaw detection to enhance safety and allow for less drastic and less costly repairs
- Minimized human factors concerns due to automated, uniform deployment of SHM sensors (improved sensitivity)

Long-Term

- Optimized structural efficiency
- Substitution of condition-based maintenance for current time-based maintenance practices

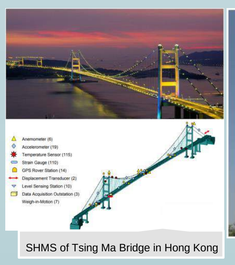
SHMS of Tsing Ma Bridge in Hong Kong


SHMS of Canton Tower in Guangzhou

Methods

How to do SHM in practice ? [4]

Visual inspection

- Base on human senses
- Subjective/Non-quantitative

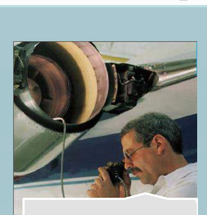
Visual inspection


Distributed Sensor Networks for Structural Health Monitoring


Thermal infrared test

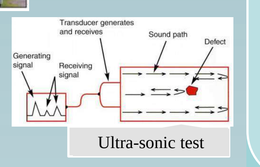

Ultra-sonic test

Vibration based SHM

- Based on the premise that damage will alter the dynamic properties of the structure, e.g. structural response, frequencies, mode shapes, damping or modal strain energy change
- By measuring the structural response by means of sensors strategically placed on the structure, and intelligently analyzing these measured responses, it is possible to identify damage occurrence (most of sensors can be wirelessly connected)

Static based SHM

- Based on the premise that damage will alter the static properties of the structure e.g. displacements, rotations
- Considerable static deflection requires large amount of static force

Non-Destructive Evaluation(NDE)

- Various technologies for different purposes
- The effectiveness of such inspections depends upon the accessibility of the structural location to be examined

Reflectometry methods

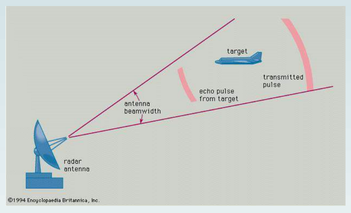

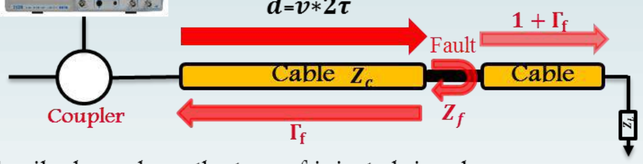

Based on the principle of radar

Family depends on the type of injected signal (TDR, STDR, SSTDR, NDR, FDR)

Advantages of reflectometry

- Good performance : detection, localization and characterization
- Easy integration

Disadvantages of reflectometry

- In some methods an expensive directional coupler must be used to separate the incident and reflected signals
- The types of the faults cannot be exactly distinguished

Problematic

- Existing SHM approaches tend to be highly labor intensive and costly
- Efficient results were obtained by Appling the reflectometry to structures in 1D (complex wire networks)
- Reflectometry was recently limitedly applied to higher order structures (2D and 3D)
- In other methods we need access to the whole structure

The idea is to be able to diagnose a defect when it appears or, better still, predict the appearance of it at the first warning signs.

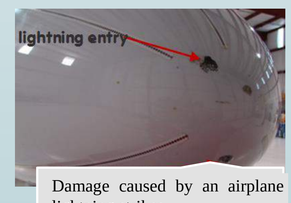

Damage caused by an airplane lightning strikes.

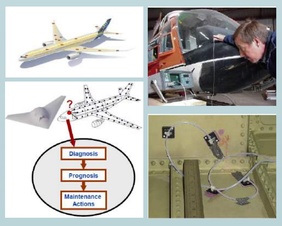

The development of new signal processing algorithms

The optimization of frequencies and/or waveforms

Stages of our work

State of the Art: Bibliographic study

Review and test reflectometry on 1D (wire network) structure (*)

Modeling in search of a case that interests the industry : Using CST, create and test 2D and 3D structures (airplanes, pipes..) using several methods

Adapt Reflectometry from 1D to 2D study and establish numerical module

Validate the research part and do the experimental part

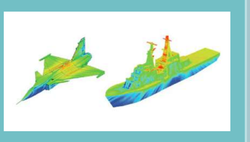

Results

(*) Accepted International conference paper
M. KAFAL, F. MUSTAPHA, J. BENOIT, W. BEN HASSEN, «A Non Destructive Reflectometry Based Method for the Location and Characterization of Incipient Faults in Complex Unknown Wire Networks », IEEE AUTOTESTCON 2018.

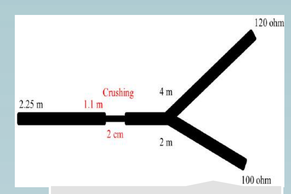

Original Tested Unknown Faulty Network

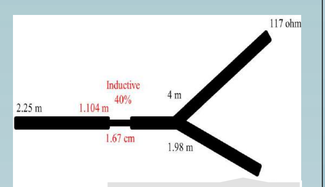

Reconstructed Faulty Network

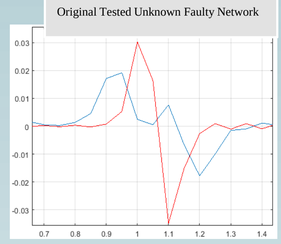

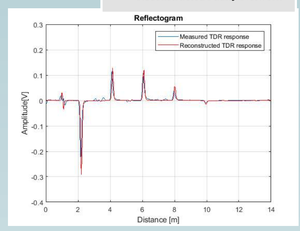

Soft defect detection , location and characterization by solving the inverse problem of the measured reflectometry response by using optimization algorithms

Bibliography

[1] J. Ko and Y. Ni, "Technology developments in structural health monitoring of large-scale bridges, Engineering structures", vol. 27, pp. 1715- 1725, 2005.
[2] Daniel BALAGEAS, " Introduction to Structural Health Monitoring" 2006.
[3] Dennis Roach,S Neidigk " Structural Health Monitoring for Aircraft: Viable Inspection Tool or Passing Fancy? " 2011.
[4] K. Roy and S. Mukhopadhyay, "Workshop onStructural Health Monitoring". June, 2016.
[5] Mukhopadhyay, Subhas Chandra, ed. New developments in sensing technology for structural health monitoring. Vol. 96. Springer Science & Business Media, 2011.

Relief map design tool for visually impaired people

UNIVERSITÉ Clermont Auvergne
Ecole Doctorale Sciences Pour l'Ingénieur

IGN INSTITUT NATIONAL DE L'INFORMATION GÉOGRAPHIQUE ET FORESTIÈRE

Fillières-Riveau Gauthier

In collaboration with the IGN institute

LIMOS

Introduction

This research project, called ACTIVmap, is aimed at developing a tactile maps design tool for visually impaired people. Nowadays, the adapted map are made by redrawing manually the roads, buildings and everything that needs to be represented using a traditional map or aerial photograph (Géoportial, Google Earth...) as support. This is a time consuming process and does not permit a real adaptation to the handicap.

The need of research and technical orientations are motivated by the specific constraints of the target audience and the know-how of professionals of the visually impaired support (adapter-transcriber, locomotion instructor ...) and are the result of the collaboration between them and teams of researchers to covers the fields of cartography, computing and assistance to the visually impaired.

In order to realise the set of tools, we have to first identify and classify the constrains, due to the specificities of the visual impair but also by the exploration of new conception and fabrication approach.

After that, we brought professionals to participate to guide our choices and methods by their know-how. This invitation to participation was made through a map collection campaign adapted to the visually impaired public.

Finally, the results of this call for participation allow us to focus our research on the main needs in cartographic adaptation by taking into account the expertise of professionals in the field of assistance to the visually impaired.

Works

To identify and classify the constrains a scientific watch and analysis of studies conducted on visual impairment highlighted the need to exchange with experts in the field. Indeed a lack of norms and standards allowing to frame the realization of relief map for visually impaired encouraged us to exchange with these professionals and people suffering from blindness in order to better understand this handicap and the associated problems.

So, we organize a map collection campaign to made a set of samples that describe and illustrate the experts practices in map conception and adaptation. This involve that we spend time communicating and exposing our project to adaptation professional communities, and putting tools in place to enable them to participate. This was done through a website (https://activmap.limos.fr/) with an upload platform on a dedicated page explaining our request and offering a consent form for intellectual property rights (use, publication, sharing...).

In parallel we work on a prove of concept relief map done by 3D printing to explore a other way to fabric and a new representation mode of the map elements (roads, building…) with multiple elevation that offering the possibility to present more information (classic methods use textures variation and blind people can only differentiate 3 to 5 of these texture template on the same document).

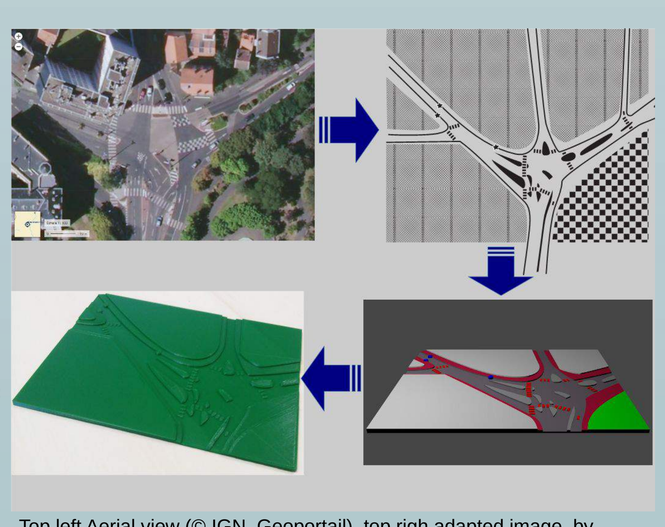

Top left Aerial view (© IGN, Geoportail), top righ adapted image by MARTIN Durga (© CRDV), bottom left 3D model and bottom right the printed model made by ourselves

The involvement of a mapping organization allows us to take advantage of their knowledge on cartographic generalization, not used today for this purpose, which would simplify the geometric shapes representing the map elements, in order to simplify tactile reading and mental space representation by the visually impaired.

First Results

The participation campaign for the acquisition of adapted maps allow us to collect 113 maps. The results of the maps obtained are as follows:

Map scale	Number of map (%)	Comments
Building	1 (0,88%)	From building plan
Crossroads / junction	5 (4,42%)	From aerial view, floor and sidewalk markings shown
Square / block	12 (10,62%)	From aerial view (Geoportal...), some marked buildings (town hall...)
Street map / city centre map	65 (57,52%)	From aerial view or clasic plan, some buildings marked (town hall, church...)
city	14 (12,39%)	From plan, representation by zone (built area...)
Large scale	16 (14,16%)	very variable, mainly for the teaching of geography secondary school / high school

Use case	Number of map (%)	Comments
Locomotion / trip	50 (44,25%)	for mental representation and space's understand
teaching	15 (13,27%)	similar to the maps used in the history course, sometimes the layout is simplified and the map split when the information is numerous
Culture and tourist itinerary	43 (38,05%)	for understanding the place or following a route or a visit (can generally be related to a neighbourhood plan with points of tourist interest and / or highlighting a path to follow)
Transport	5 (4,42%)	only the route of the means of transport and the main stops are shown and not the urban environment

Prospects

Works carried out is the first step necessary for the realisation of the project. They made it possible to make choices as to the restriction of the field of application towards the plans of type plan of district / town centre, and, to direct the research. The experts' knowledge gathering and exchanges around the project led them to participate in the project and guide us in the development and implementation of tools to help them in their work.

The next steps identified will aim to facilitate tactile reading and to facilitate the mental representation of the space of visually impaired people, in particular by introducing and adapting mapping generalization methods to the constraints of the targeted disability. And in another way, we need to continue the work on the exploration of fabrication methods as 3D printing to bring new approaches and solutions for relief document's support.

The first reactions to 3D-printed maps look promising, but we are also waiting for more detailed feedback on the use of 3D-printed maps, experimented in the field by instructors in locomotion at the "Centre de Rééducation pour Déficient Visuel" (CRDV) in Clermont-Ferrand.

Bibliography

1. **Sander M.S., Bournot M.C., Lelièvre F., Tallec A., 2005 -** ***Les personnes ayant un handicap visuel – les apports de l'enquête Handicaps-Incapacités-Dépendance*****, études et résultats n°416, Direction de la recherche des études de l'évaluation et des statistique (DREES), France, 12p.**
2. **Hennig S., Zobl F., Wasserburger W., 2017 -** ***Accessible Web Maps for Visually Impaired Users: Recommendations and Example Solutions*****, Cartographic Perspectives volume 0 number 88,**
3. **Fillières-Riveau G., Favreau J.M., Barra V., Touya G, forthcoming publication –** ***Conception de carte en relief pour les personnes déficientes visuelles*****, EUGEO 2018, Presses universitaire Blaise Pascal (PUBP), France, 12p.**

Application of decision making to assure sustainable design and manufacturing

Getasew TADDESE*, Prof. Emmanuel DUC**, Dr. Severine DURIEUX**

*****Université Clermont Auvergne, CNRS, SIGMA Clermont, Institut Pascal, F-63000 Clermont–Ferrand, France***

****School of Mechanical & Industrial Engineering, Addis Ababa University, P.O.BOX 385, Addis Ababa, Ethiopia***

Ecole doctorale Sciences Pour l'Ingénieur

Introduction

Sustainable design and manufacturing is a complex system where various performance indicators must be considered to fully achieve it. Industries such as aerospace, automotive and health, are facing challenges of balancing priorities between economic, environmental and social factors. So far, various researchers tried to address sustainability aspect of traditional manufacturing processes and design aspect by developing frameworks and strategies, but none were comprehensive in addressing all dimensions of sustainability. An increased awareness of people in considering impacts of product on the environment (pollution and resource consumption on the ecosystem), human health (safety and risk) and value (durability, less maintenance and high performing product with minimized overall cost) is currently compelling industries to seek for assuring sustainability by taking balanced consideration of all dimensions to keep them highly competent and reputable in the current market system.

Thus, this study identifies complete list of decision variables and performance indicators for additive manufacturing (AM) and propose a comprehensive multicriteria decision making framework to fully address sustainability during the design and manufacturing of a part. Furthermore, proper validation and implementation is required after identifying performance indicators and possible interactions between them. Through this whole process, modular (energy/material/cost) models will also be adapted and developed which can independently be utilized for partial evaluation as required by users or industries.

Methods

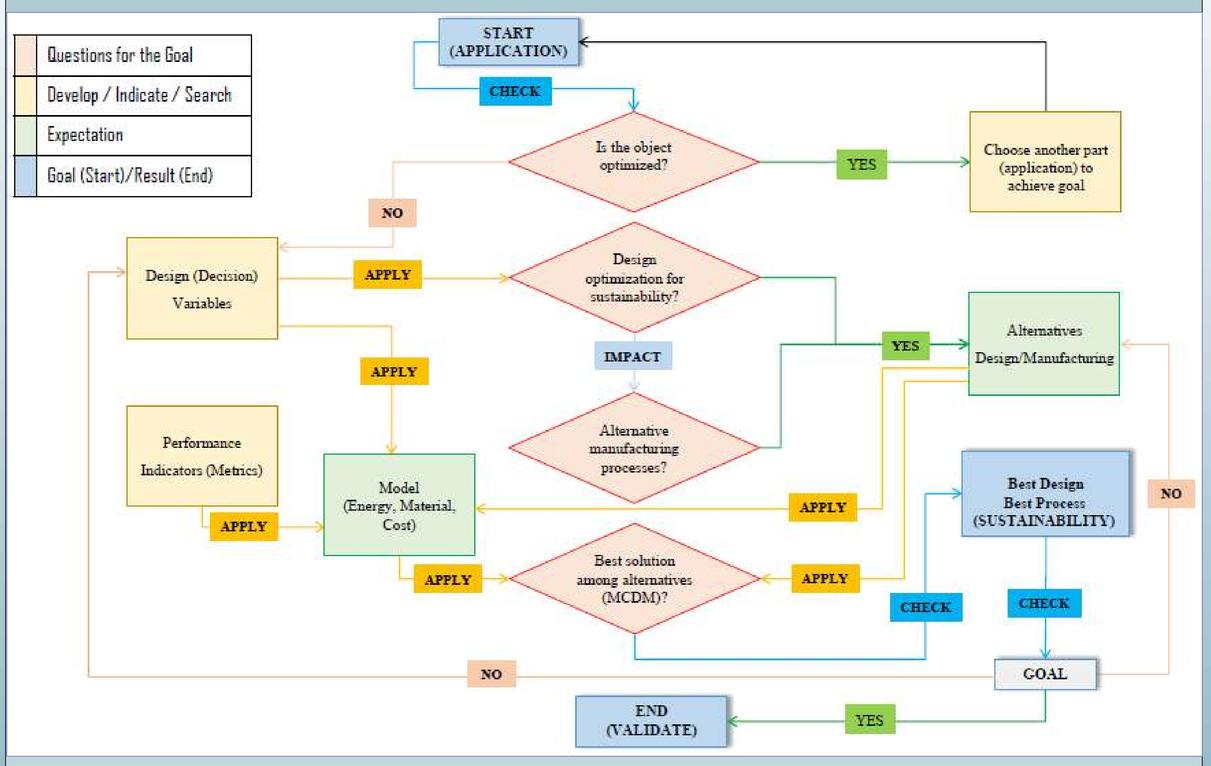

Figure 1: General framework

Simplified outline of the methodology:

- Identify and evaluate existing and proposed AM process.
- Description of the new AM solution using set of decision variables.
- Identify set of performance indicators according to functionality and sustainable manufacturing.
- Propose a comparison methodology.
- Modeling of the Additive Manufacturing Process.
- Analyze sustainability based on the identified Performance Indicators.
- Compare sets of new AM solutions with the existing solutions.
- Application: validation of the solution using a part from a real industry application (aerospace or automotive)

Results (expected)

The expected major results of the study are:

- Identification and development of complete list of decision variables and performance indicators (sample indicated in Fig. 2).
- Develop a comprehensive MCDA tool for AM processes towards assuring sustainable manufacturing.
- Modeling of possible alternatives formed from each of the PI's listed on the fourth row.
- A MCDA to select the best alternative among models.

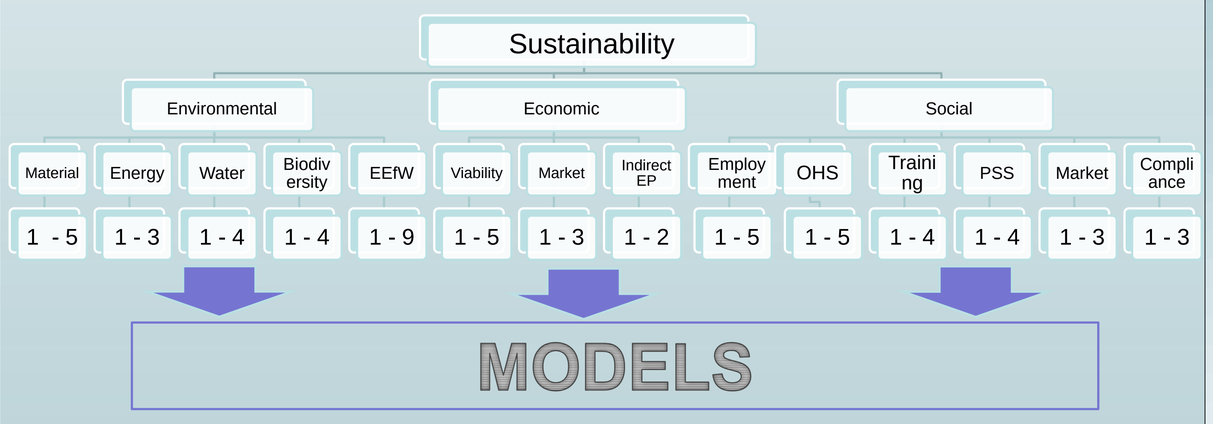

Figure 2: MCDA framework (Sample)

Remark:

Additional row as row 5 (not indicated on the figure 2) will contain possible alternatives which are utilized by researchers to develop models.

Conclusions (expected)

- Additive Manufacturing as new way to improve sustainability performance of part and process.
- Role and impact of additive manufacturing for sustainability of design and manufacturing of high value products.
- A new frame work for assuring sustainability during the design and manufacturing of part which considered complete list of performance indicators for all dimensions of sustainability.

Bibliography (selected)

Ahmad, S., Wong, K.Y., Tseng, M.L., Wong, W.P., 2018. Sustainable product design and development: A review of tools, applications and research prospects. Resour. Conserv. Recycl. 132, 49–61. https://doi.org/10.1016/j.resconrec.2018.01.020

Haapala, K.R., Zhao, F., Camelio, J., Sutherland, J.W., Skerlos, S.J., Dornfeld, D.A., Jawahir, I.S., Clarens, A.F., Rickli, J.L., 2013. A review of engineering research in sustainable manufacturing. J. Manuf. Sci. Eng. 135, 041013

Jin, M., Tang, R., Ji, Y., Liu, F., Gao, L., Huisingh, D., 2017. Impact of advanced manufacturing on sustainability: An overview of the special volume on advanced manufacturing for sustainability and low fossil carbon emissions. J. Clean. Prod. 161, 69–74. https://doi.org/10.1016/j.jclepro.2017.05.101.

Shao, G., Brodsky, A., Shin, S.-J., Kim, D.B., 2017. Decision guidance methodology for sustainable manufacturing using process analytics formalism. J. Intell. Manuf. 28, 455–472. https://doi.org/10.1007/s10845-014-0995-3

Sossou, G., Demoly, F., Montavon, G., Gomes, S., 2018. An additive manufacturing oriented design approach to mechanical assemblies. J. Comput. Des. Eng. 5, 3–18. https://doi.org/10.1016/j.jcde.2017.11.005

Yuan, C., Zhai, Q., Dornfeld, D., 2012. A three dimensional system approach for environmentally sustainable manufacturing. CIRP Ann. 61, 39–42. https://doi.org/10.1016/j.cirp.2012.03.105

About Getasew TADDESE:

He is a senior Lecturer at the School of Mechanical and Industrial Engineering, Addis Ababa University, Ethiopia. He got BSc degree in Mechanical Engineering from Mekelle University in Ethiopia and MSc degree in Materials Engineering and Nanotechnology from Politecnico di Milano, Italy and double MSc degrees in Environmental Assessment and Integrated Management from L'Istituto Universitario di Studi Superiori di Pavia, Italy and Tongji University, Shanghai, China.

Currently, he is working on his first year PhD study at Sigma Clermont as a result of collaboration established as Ethio-France PhD program between the Ethiopian Ministry of Education, the French Embassy in Addis Ababa and Campus France.

Hardware architecture and protocols for wireless sensor networks suitable for environmental monitoring

UNIVERSITÉ Clermont Auvergne

LIMOS

PhD student : Guereguin Der S. SIDIBE

Dicector : Pr. Michel MISSON

Advisor : Dr. Marie Françoise SERVAJEAN

I. Introduction

- **Wireless sensor networks (WSN)** are widely used in environmental monitoring (Fig1)
- **Advantages :** easy to deploy, auto configurable and many applications areas (eg : environment, militry, industry..)
- **Technologies used :** PHY & MAC protocols layer (IEEE 802.15.4, LoRa, Sigfox) Network layer (Zigbee, LoRaWAN...)
- **Disadvantages :** Ressouce constrained (memory, battery..) Dfficult to maintain

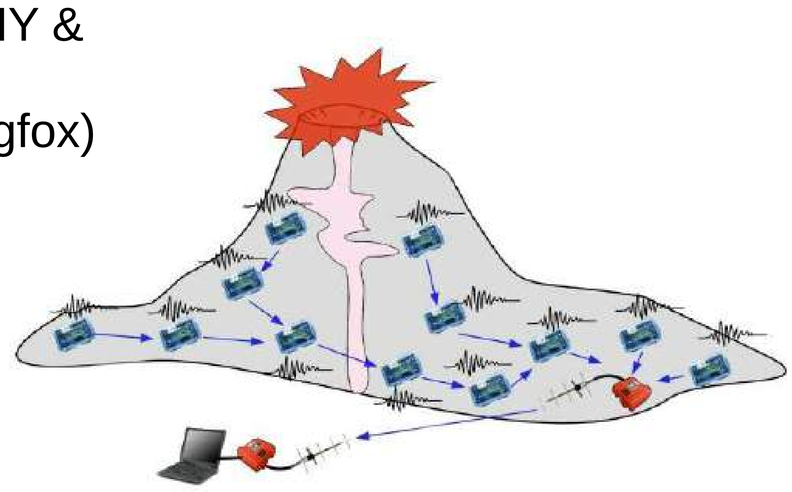

Fig1 : Volcan monitoring with WSN

II. Problematic & Objectives

- Emerging solutions in data collection area prioritize long range transmission in the expense of data rate (eg: 27 kps for loRa)
- How to statisfy applications that need long transmission range and high data rate ?

Combine switched beam antennas (Fig2) with WSN low layers (IEEE 802.15.4)
-reach long distance provided by the antenna
-250 kps data rate

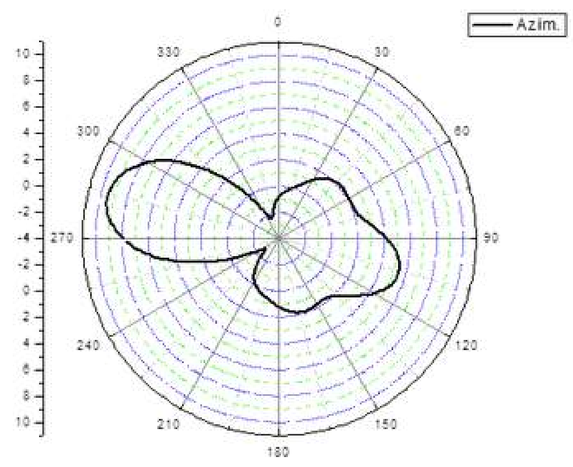

Fig2 : Switched beam antenna radiation pattern

III. Approach

- In data collection the trend is to retain star topologies (LoRa : Fig4)
- **Our approach :** Equip the sink in a star topoly (Fig3 sink is the node 1) with a switched beam antenna

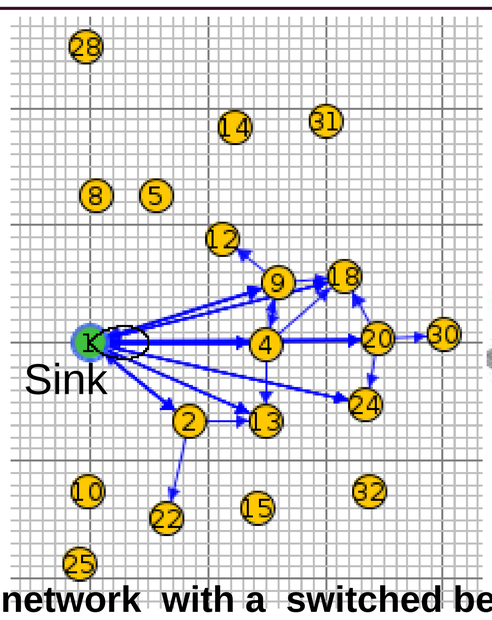

Fig3 :Star network with a switched beam antenna in the sink

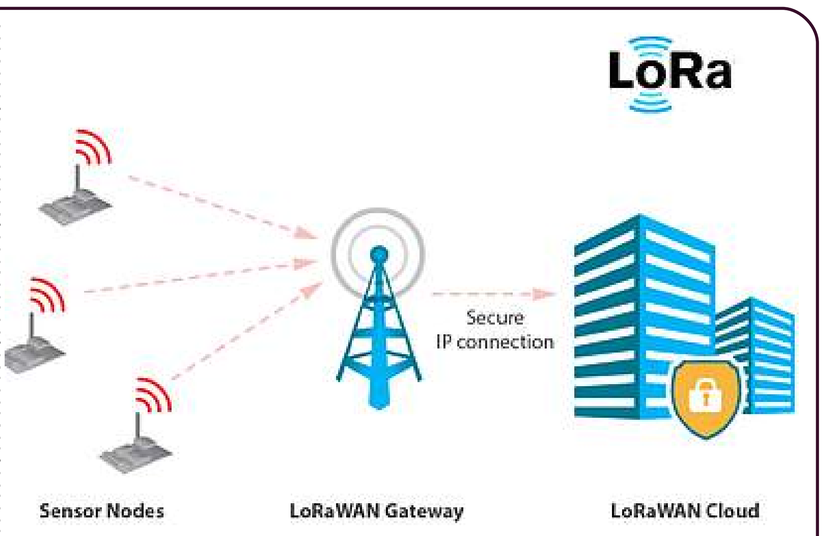

Fig4 : LoRa network

III. Perspectives

- Optimize the neighbor dsicorvery phase
- Optimize the beam switching scheme to inquire nodes

A simulation approach for configuring manufacturing systems in changing environment

Hani POURVAZIRI

LIMOS, Université Clermont Auvergne, SIGMA-Clermont, France

Ecole doctorale Sciences Pour l'Ingénieur

Introduction

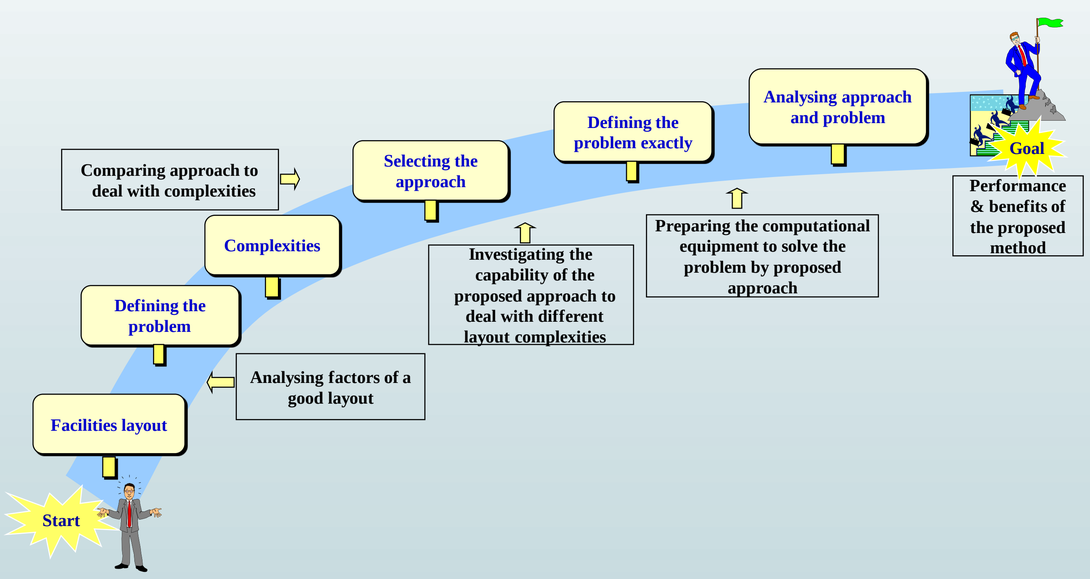

Facility layout: The arrangement of everything within and around buildings.
factory, hospital, office, we focus on **manufacturing system (factory)**

Basic Objective

- **Facilitate a smooth flow of work, material, and information through the system**

Supporting objectives

- **Facilitate product or service quality**
- **Use workers and space efficiently**
- **Avoid bottlenecks**
- **Minimize material handling costs**
- **Eliminate unnecessary movement of workers or material**
- **Minimize production time or customer service time**
- **Design for safety and security**
- **Facilitate communication and interaction between workers, between workers and their supervisors, or between workers and customers**
- **Facilitate the entry, exit, and placement of material, products, or people**
- **Encourage proper maintenance activities**
- **Provide a visual control of operations or activities**
- **Provide flexibility to adapt to changing conditions**
- **Maximize customer satisfaction**
- **Improve employee morale**
- **Improve customer/client interaction**

Methods and complexities

Complexities in facility layout

Facility layout approaches

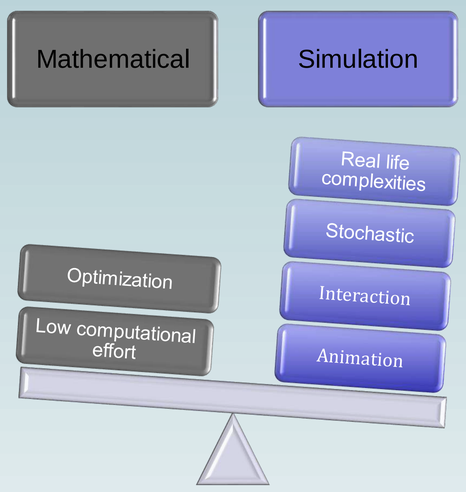

How can we enhance simulation to be able to do

Optimization **and reduce its** **computational effort** **?**

Optimization ?

Simulation optimization (SO) refers to the optimization of an objective function subject to constraints, both of which can be evaluated through a stochastic simulation.

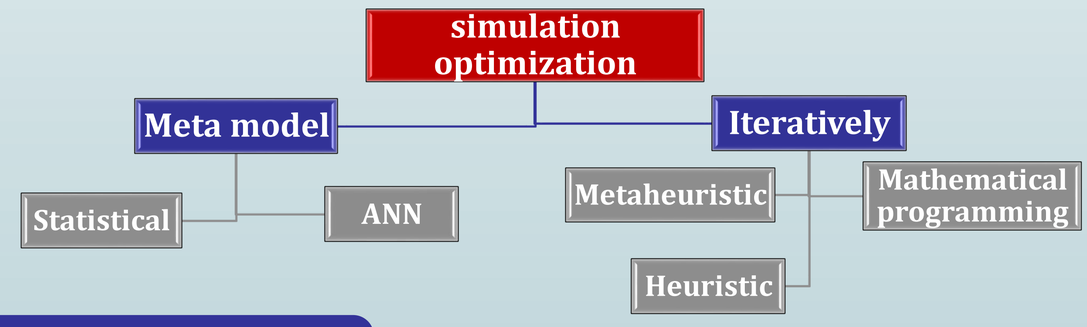

Meta model

- Different type of system configurations are generated in simulation model and run
- 1) Statistical techniques like regression, 2) Artificial neural network technique

Iteratively

- Simulation is called during optimization execution procedures
- 1)Meta heuristic algorithm, 2) Heuristic algorithm, 3) Mathematical programing

computational effort ?

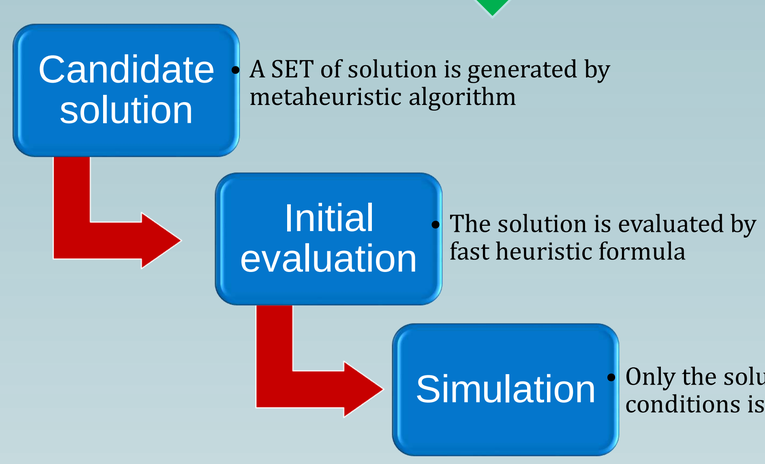

Conclusion

The proposed approach, by solving the weakness of simulation, is able to analyse complex facility layout problems. The optimum layout will be applicable for real manufacturing system specially those are dealing with uncertainty.

Bibliography

Tompkins, J.A., White, Y.A., Bozer, E.H., Frazelle, J.M.A., Tanchoco, J. (1996). Facilities Planning. Wiley, New York.
Drira, A., Pierreval, H., Hajri-Gabouj, S. (2007). Facility layout problems: a survey. Ann. Rev. Control 31, 255–267,
Pourvaziri, H., Pierreval H., 2017, Dynamic facility layout problem based on open queuing network theory, European Journal of Operational Research, 259, (2) 538-553.

Description of hepatic HCC lesions using persistent homology

Ecole doctorale Sciences Pour l'Ingénieur

Hawa MOHAMED ALI, Antoine VACAVANT, Manuel GRAND-BROCHIER

INTRODUCTION

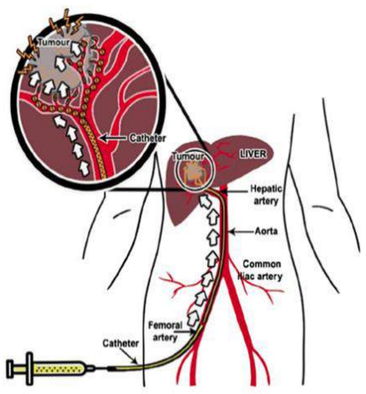

- Our research group focuses on the computer evaluation of tumoral response
- For hepatic diseases, in particular HCC (HepatoCellular Carcinoma)
  - 5th cause of cancer in the World (500,000 new cases / year)
  - 3rd cause of death by cancer in the World

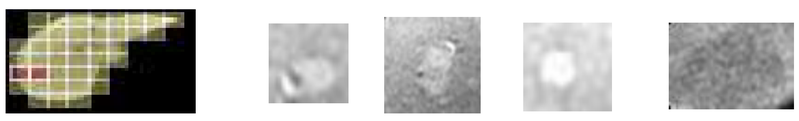

METHOD : PERSISTENT HOMOLOGY (PH)

- A popular tool in topological data analysis.
- Algebraic tool for discerning topological features (holes, graph) of data.

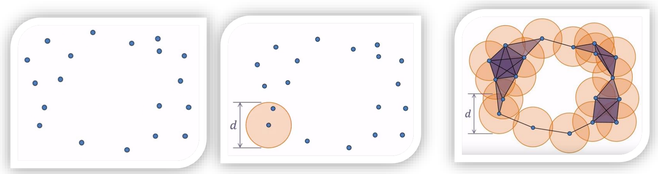

- Persistent

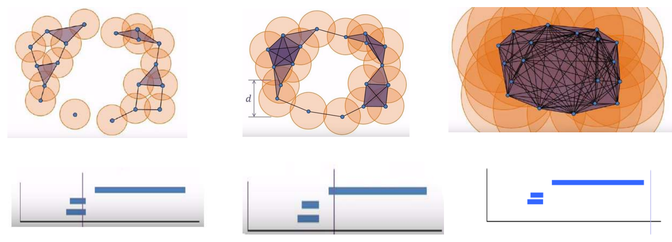

- Shape analysis : holes representation using thickness, breadth [Aldo et al., 2016].

- Shape analysis : topological invariant [Anne Collins et al., 2004].

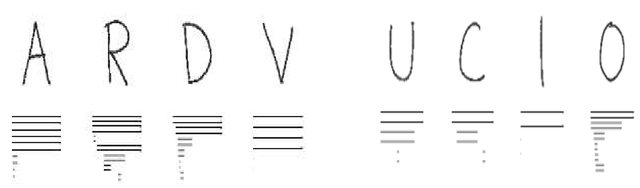

APPLICATION TO MEDICAL IMAGE PROCESSING

- Framework for hepatic lesions [Adcock et al.,2014]

Image I

$$I = \begin{bmatrix} 0.1 & 0.12 & 0.13 & 0.14 & 0.15 \\ 0.16 & 11 & 10 & 12 & 0.17 \\ 0.18 & 13 & 14 & 15 & 0.19 \\ 0.2 & 9 & 16 & 17 & 0.21 \\ 0.22 & 0.23 & 0.24 & 0.25 & 0.26 \end{bmatrix} \qquad BW = \begin{bmatrix} 0 & 0 & 0 & 0 & 0 \\ 0 & 1 & 1 & 1 & 0 \\ 0 & 1 & 1 & 1 & 0 \\ 0 & 1 & 1 & 1 & 0 \\ 0 & 0 & 0 & 0 & 0 \end{bmatrix}$$

- the distance from the lesion border to each pixel
- pixel intensity (ranked in ascending order)
- Barcode
- metric $\delta(I, J) = |I \cup J - I \cap J|$

$$distance = \begin{bmatrix} 0 & 0 & 0 & 0 & 0 \\ 0 & 1 & 1 & 1 & 0 \\ 0 & 1 & 2 & 1 & 0 \\ 0 & 1 & 1 & 1 & 0 \\ 0 & 0 & 0 & 0 & 0 \end{bmatrix}$$

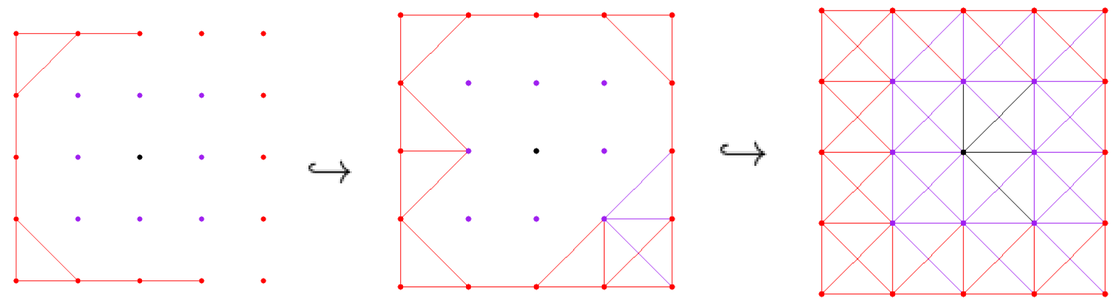

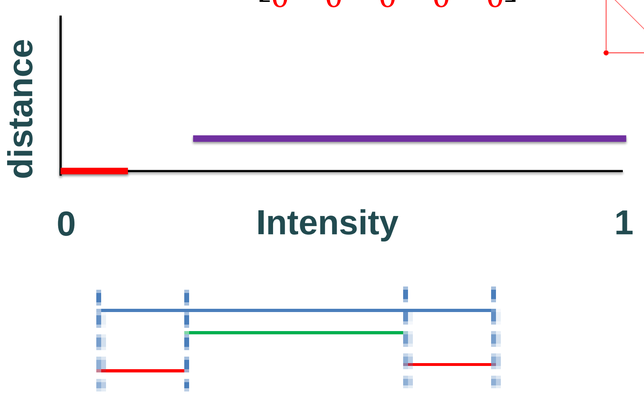

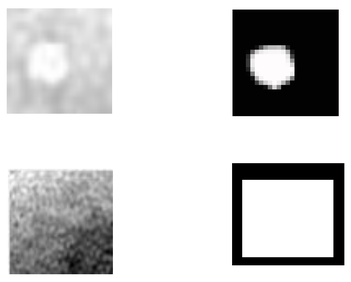

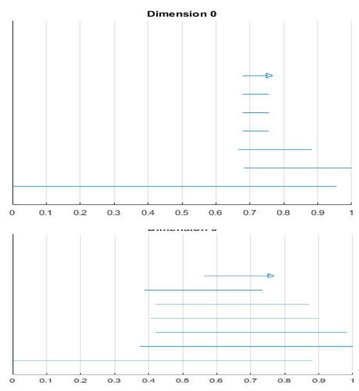

RESULTS

- Database : 10 000 patchs of healthy tissu / 100 patchs of lesion.
- Persistence for lésion

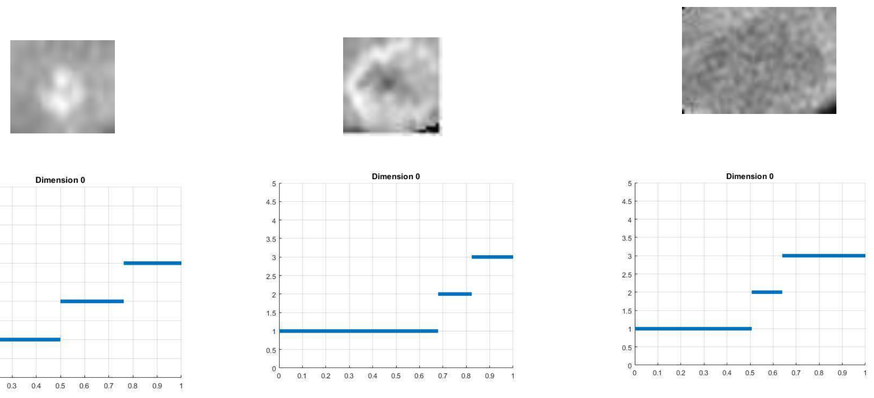

- Persistence for healthy tissu

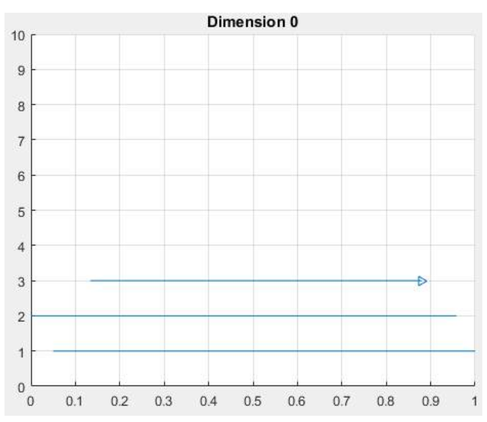

CONCLUSION

- This framework may be complementary to the standard techniques currently in use.
- Extract topological features to compute the persistence can improve the result.
- Useful for segmentation of tumor.
- This framework is flexible enough to be used in a variety of contexts.

BIBLIOGRAPHY

[1] A. Adcock, D. Rubin, G. Carlson Classification of Hepatic Lesions Using the Matching Metric. Computer Vision and Image Understanding, 121:36–42, 2014.
[2] A. Collins, A. Zomorodian, G. Carlsson, L. Guibas, A barcode shape descriptor for curve point cloud data, Comput. Graph. 28 (2004) 881–894.
[3] Aldo Gonzalez-Lorenzo, Alexandra Bac, Jean-Luc Mari, Pedro Real. Two Measures for the Homology Groups of Binary Volumes, International Conference on Discrete Geometry for Computer Imagery (DGCI 2016), Apr 2016, Nantes, France. Lecture Notes in Computer Science, 9647, pp.154-165, 2016

The inpainting technique using the EM algorithm

M. Jacqueline Atoche Bravo, Vincent Barra and Eladio Ocaña

Instituto de Matemática y Ciencias Afines - IMCA and Université Clermont Auvergne-ISIMA

Objectives

1. Restore a damaged area in visually plausible form using information outside the damaged domain.
2. Use the EM algorithm for to find the classes in each neighborhood (patch) and together with the color information to obtain a better description of the patches.

Introduction

- In the last years, different works have been present to cope with the problem of the reconstruction of missing data. One of the techniques used for the reconstruction of an image is the "inpainting" technique, whose objective is to restore a damaged area in visually plausible form using information outside the damaged domain. The proposed criterion for the search of the most similar patch includes the sum square error (SSE) both for the brightness of pixels as well as for the classes (modes) found in the image.

Problem Formulation

- Let us consider a image $I(x, y)$ with dimension of $M \times N$ pixels and partly damaged.
- I can be divided in two parts: a *target region* Ω, that represents the missing pixels and a *source region* Φ, from which the most similar patch is extracted for the reconstruction of Ω.

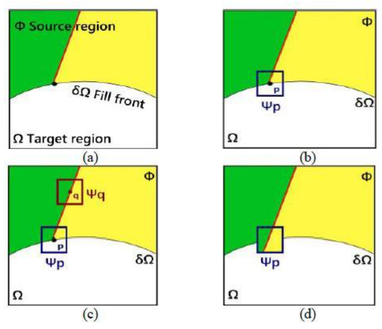

Figure 1: Inpainting

- To each pixel $p(x, y) \in \partial\Omega$ we assign an inpainting priority value $P(p)$ defined by:

$$P(p) = C(p).D(p) \tag{1}$$

where $C(p)$ and $D(p)$ represent the *confidence* and *data* terms respectively.

Methods

- To determine the classes within the image, we use the expectation-maximization (EM) algorithm.
  - Let $\tilde{X} = \{x(u, v) : x(u, v) \in I\}$ as incomplete data where the missing part is Z,
  - Suppose that L is the number of pixels in $\tilde{X}$, the missing part can be evaluated as a set of L labels $Z = \{z^{(1)}, z^{(2)}, \ldots, z^{(L)}\}$.

$$z^{(i)} = [z_1^{(i)}, z_2^{(i)}, \ldots, z_M^{(i)}]$$

  such that $z_r^{(i)} = 1$ ($r \in \{1, 2, \ldots, M\}$) if the $i-$th pixel x^i of $\tilde{X}$ belongs to the $r-$th data ω_r, and $z_r^{(i)} = 0$ otherwise.
  - The complete log-likelihood function is given by

$$\ell(\Psi|\Theta) = \log p(\Psi|\Theta) = \sum_{i=1}^{L}\sum_{r=1}^{M} z_r^{(i)} \ln[P_r p(x^i|\theta_r)] \tag{2}$$

  where $\theta_r = [\mu_r, \sigma_r]$, and $P_r = P(\omega_r)$.
  - **E-step**: Compute $z_r^{(i)}$ given the parameter estimates from the previous M-step

$$z_r^{(i)} = \frac{P_r.N(x^i|\mu_r, \sigma_r)}{\sum_{j=1}^{M} P_j.N(x^i|\mu_j, \sigma_j)} \tag{3}$$

  - **M-step**: Obtain new parameter estimates (denoted by the prime)

$$P_r' = \frac{1}{L}\sum_{i=1}^{L} z_r^{(i)} \tag{4}$$

$$\mu_r' = \frac{\sum_{i=1}^{L} z_r^{(i)} x^i}{\sum_{i=1}^{L} z_r^{(i)}} \tag{5}$$

$$\sigma_r' = \sqrt{\frac{\sum_{i=1}^{L} z_r^{(i)} (x^i - \mu_r')}{\sum_{i=1}^{L} z_r^{(i)}}} \tag{6}$$

  - We can assign to each pixel x^i of $\tilde{X}$ the optimal class label:

$$\hat{\omega} = \arg\max_{\omega_r \in \Omega}\{P(\omega_r|x_i)\} \tag{7}$$

Mathematical Section

- The proposed criterion for the search of the most similar patch includes the sum square error (SSE):

$$\Psi_{\hat{q}} = \min_{\Psi_q \in \Phi} d(\Psi_{\hat{p}}, \Psi_q) \tag{8}$$

  where $d(\Psi_{\hat{p}}, \Psi_q) = SSE(\Psi_{\hat{p}}, \Psi_q) + SSE(class(\Psi_{\hat{p}}), class(\Psi_q))$
- The second criterion for the search is to use SSE for the classes (modes). We use equation (8) to find K similar patches.
  - In the patch $\Psi_{\hat{p}}$, we can distinguish two regions A of the known pixels and B of missing pixels. For each patch N_k, we make the same division of the area.
  - Given a pixel vector $x = [x_1, x_2, \ldots, x_K]$, such that $x_j \in N_j$ represents the pixel value in the jth neighborhood. The linear predictor can be expressed as $y = f[x] = \sum_{j=1}^{K} \alpha_j.x_j$
  - To find the alpha values:

$$\begin{bmatrix} x_1^1 & x_2^1 & \ldots & x_K^1 \\ x_1^2 & x_2^2 & \ldots & x_K^2 \\ \vdots & \vdots & \ddots & \vdots \\ x_1^R & x_2^R & \ldots & x_K^R \end{bmatrix} \cdot \begin{bmatrix} \alpha_1 \\ \alpha_2 \\ \vdots \\ \alpha_K \end{bmatrix} = \begin{bmatrix} y_1 \\ y_2 \\ \vdots \\ y_R \end{bmatrix} \Leftrightarrow \underline{P}.\underline{\alpha} = \underline{Y} \tag{9}$$

  -

$$\alpha^* = (\underline{P}^t.\underline{P})^{(-1)}.\underline{P}^t.\underline{Y} \tag{10}$$

  The reconstruction phase of each missing data in $\Psi_{\hat{p}}$, consist in predict y by means of the linear predictor 9.

Results: Figure

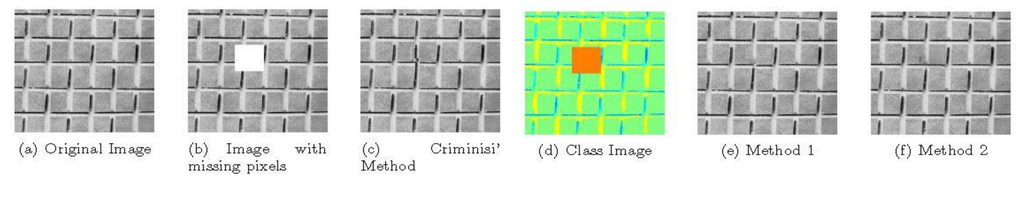

Figure 2: Test Image: Texture

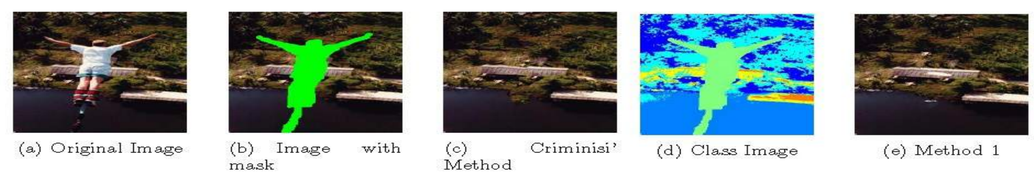

Figure 3: Test Image

Results: Table

- For quantify the reconstruction accuracy, we use the root-mean-square error (RMSE):

	Criminisi' Method	Method 1	Method 2
Texture 1	2.1180	1.7337	2.0889

Table 1: RMSE

Conclusion

- Combining the classes found in each neighborhood (patch) with the color information allows us to obtain a better description of the patches.
- Our experiments show a better reconstruction of the images, and they are visually almost equal to their original image.

References

[1] L. Lorenzi, F. Melgani, and G. Mercier.
Inpainting strategies for reconstruction of missing data in vhr images.
IEEE Geoscience and Remote Sensing., 2011.

[2] F. Melgani.
Contextual reconstruction of cloud-contaminated multitemporal multispectral images.
IEEE Transactions on Geoscience and Remote Sensing., 44(2):442–455, 2006.

Acknowledgments

- Partially subsidized by Cienciactiva CG 176-2015

jacqui0790@gmail.com

Design and optimization of a robot for Al/CFRP/Ti orbital stacking drilling

Jean-Baptiste GUYON

supervised by Hélène CHANAL, Benoît BLAYSAT & Benjamin BOUDON

Université Clermont Auvergne, CNRS, SIGMA Clermont, Institut Pascal

Introduction

- My thesis topic is part of the project *European and Chinese Platform for Stacked Aero-Structure Drilling Process and Equipment* (or ECSASDPE) whose final objective is the creation of a robot dedicated to high quality Al/CFRP/Ti stacking drilling on complete aeronautical structural elements such as a wing or a fuselage section.
- The machine thus designed will improve the quality of the holes, the speed at which these holes are drilled and reduce inconvenience for technicians.

Context

- Machined materials:
  A stack of glued Aluminium,Carbon Fiber Resin Polymer and Titanium:
  - ▷ Aluminium: easily machinable material;
  - ▷ Carbon Fiber Resin Polymer: easily machinable but also easily damaged;
  - ▷ Titanium: hard material and bad temperature dissipator. [1]

  ↪ Best way to machin is Orbital Drilling

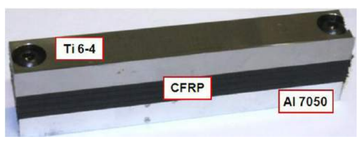

Figure 1:Al/CFRP/Ti Stack

- Tool cinematic:
  2 main process design:
  - ▷ Conventional Orbital Drilling (COD): Rotation & revolution of the tool.
  - ▷ Tilted Orbital Drilling (TOD): Rotation, revolution & tilting of the tool. [2]

  ↪ Specific cinematic for Orbital Drilling

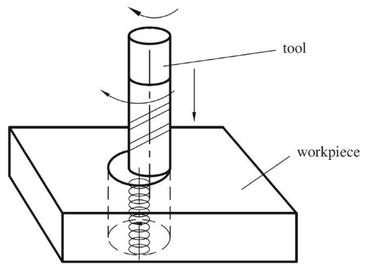

Figure 2:Orbital drilling concept

- Cutting forces modelisation: [3]
  - ▷ $dF_i = K_{ic} \cdot h \cdot \partial a_p + K_{ie} \cdot \partial S$
    $i = \{t, r, a\}$

  ↪ Low effort for Orbital Drilling

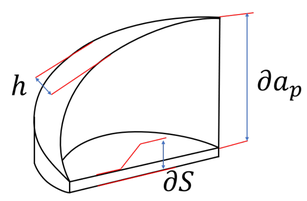

Figure 3:Chip definition

- Drilled holes quality:
  - ▷ Geometry of the hole.[4]
  - ▷ Roughness of the hole.[4]
  - ▷ Burr at interfaces.[4]
  - ▷ No ruins of the CFRP.[5]

  ↪ Several quality items to check

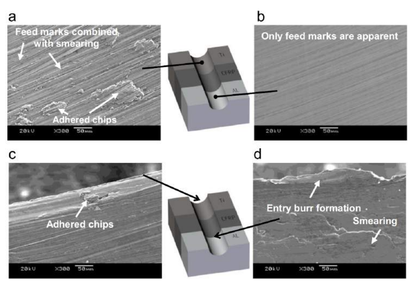

Figure 4:Hole micrography

Methodology

1. Modelise the Tripteor X7 in explicit formulation & identificate structure parameters.
2. Apply the model to other Exechon type machines.
3. Determine an optimised architecture for Parallel Kinematic Machine to do orbital drilling.

Parallel Kinematics Machine (PKM)

- Presentations of PKM [6] :
  - ▷ Advantages of PKM: stiffness & high deplacement rate.
  - ▷ Difficulties of PKM: complex command & low deplacement range.
- Tripteor X7 specifications (overconstrained PKM):
  - ▷ 3 controled linear parameters
  - ▷ 2 controled angular parameters
  - ▷ 6 end-effector position parameters
  - ▷ 13 intermediary angular parameters

Tripteor X7

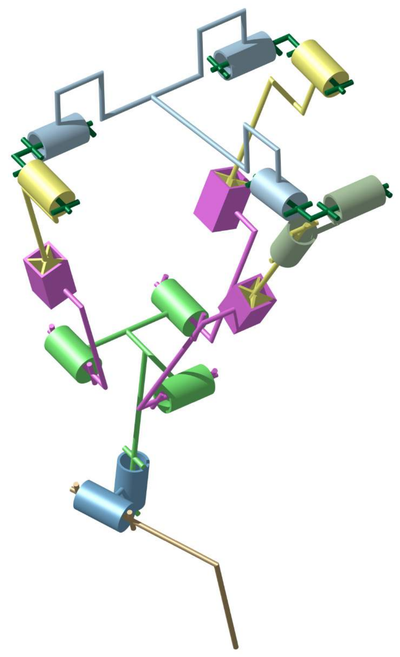

Figure 5:Kinematic schemes of the Tripteor X7

Figure 6:Worplace of the Tripteor X7

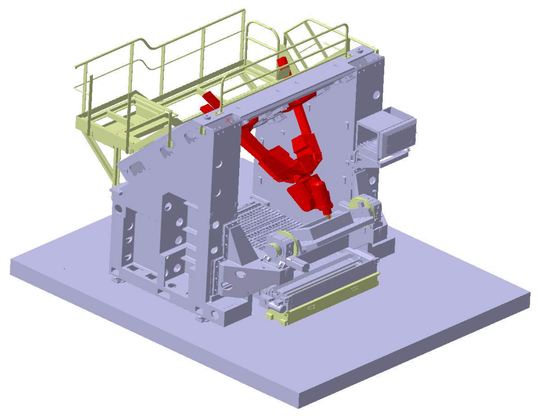

Figure 7:CAD of the Tripteor X7

Parallel Kinematics Machine (suite)

- Vector and angular closure:

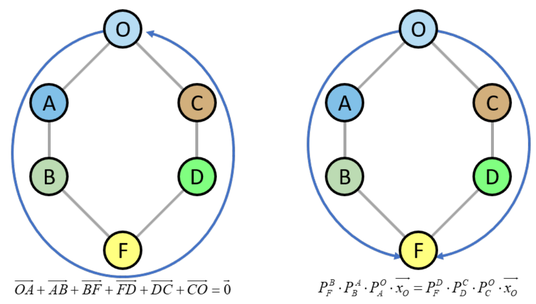

Figure 8:closure method

- 2-time PKM definition:
  1. Parallel structure closure ⇒ Constraint equation:
     $\overrightarrow{X}_{platform} = f(Q_i) \quad i \in \{1, 2, 3\}$
  2. Full structure closure ⇒ Constraint equation:
     $\overrightarrow{X}_{tool} = f(Q_i) \quad i \in \{1, 2, 3, 4, 5\}$

  ↪ Total of 12 3D equations.

Conclusion

- At the moment, the explicit formulation of the explicit geometrical modelisation is about to be completed.

References

[1] Nuno Filipe Morais Neto.
Orbital drilling of titanium alloys for aeronautics applications. experimental studies.
2017.

[2] Qiang Wang, Yongbo Wu, Teruo Bitou, Mitsuyoshi Nomura, and Tatsuya Fujii.
Proposal of a tilted helical milling technique for high quality hole drilling of cfrp: kinetic analysis of hole formation and material removal.
The International Journal of Advanced Manufacturing Technology, Sep 2017.

[3] Haiyan Wang, Xuda Qin, Chengzu Ren, and Qi Wang.
Prediction of cutting forces in helical milling process.
The International Journal of Advanced Manufacturing Technology, 58(9):849–859, Feb 2012.

[4] I.S. Shyha, S.L. Soo, D.K. Aspinwall, S. Bradley, R. Perry, P. Harden, and S. Dawson.
Hole quality assessment following drilling of metallic-composite stacks.
International Journal of Machine Tools and Manufacture, 51(7):569 – 578, 2011.

[5] E. Brinksmeier, S. Fangmann, and R. Rentsch.
Drilling of composites and resulting surface integrity.
CIRP Annals - Manufacturing Technology, 60(1):57 – 60, 2011.

[6] M. Weck and D. Staimer.
Parallel kinematic machine tools – current state and future potentials.
CIRP Annals, 51(2):671–683, 2002.

j-baptiste.guyon@uca.fr

Studying and modeling electric arc under the effect of high magnetic field

ALMURR Jessica, ROCHETTE David

Université de Clermont-Auvergne, Laboratoire de Physique de Clermont, Socomec.

Ecole doctorale Sciences Pour l'Ingénieur

Introduction

Owing to the fact that DC circuits become more in demand, researches have been focused lately on developing DC low voltage switches. In order to do that, it is necessary to have detailed knowledge about DC breaking technique. The latest consists on creating an electric arc between the electrodes of the switch while they are opening, and increasing its voltage so that the arc's potential is greater than the supplied voltage.

Because of the very complicated processes, the developers have been relying mostly on experimental investigations so far. On the other hand, the increasing performance of computers allows simulating more and more details of the switching arc.
In this work, we are going to present an experimental set-up where the displacement of an electrical arc between two parallel arc runners is studied with high-speed imaging, voltage, current pressure and magnetic measurements. In parallel, a two-dimensional (2-D) simulation model is described, which is based on the differential equations for fluid and electromagnetic physics, the so-called MHD equations.

Methods

DC breaking concept for a RL circuit

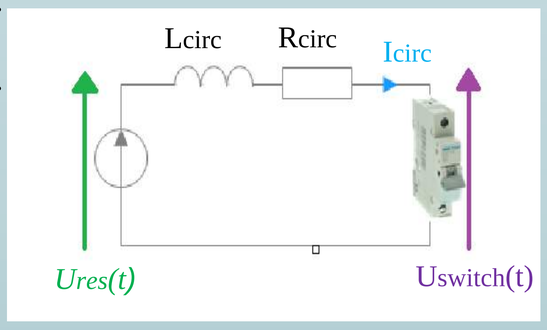

$$Ures(t) = Rcirc*Icirc + Lcirc\frac{dIcirc}{dt} + Uswitch$$

$$\frac{dIcirc}{dt} = -\frac{Rcirc}{Lcirc}Icirc + \left(\frac{Ures - Uswitch}{Lcirc}\right)$$

$$Uswitch(t) = r*Icirc + Uarc$$

$$\frac{dIcirc}{dt} < 0$$
To interrupt the current

$$Ures - Uswitch < 0$$
$$Uarc > Ures$$
We have to increase the arc voltage

Experimental settings for a simple arc chamber

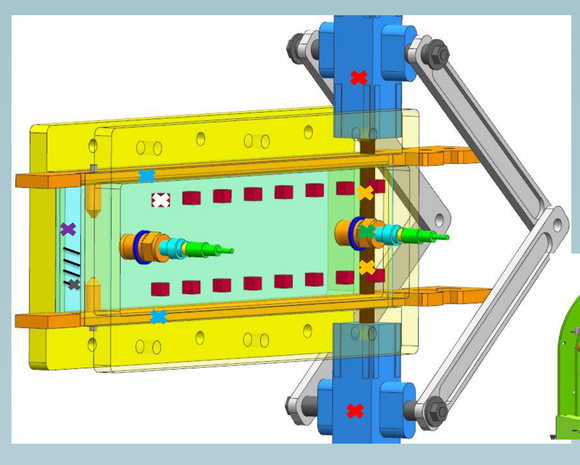

- Potentiometer
- Hall effet sensor
- Copper rails
- Pressure sensor
- High speed camera
- Copper moving contacts
- Helmholtz coil
- Splitter plates

2D time dependent electric air arc model

Energy Balance

- Joules heating J^2/Γ
- Radiation $4\pi\varepsilon_N$
- Electron anthalpy $\frac{5}{2e}K_B TJ$
- Conduction $-\lambda\nabla T$

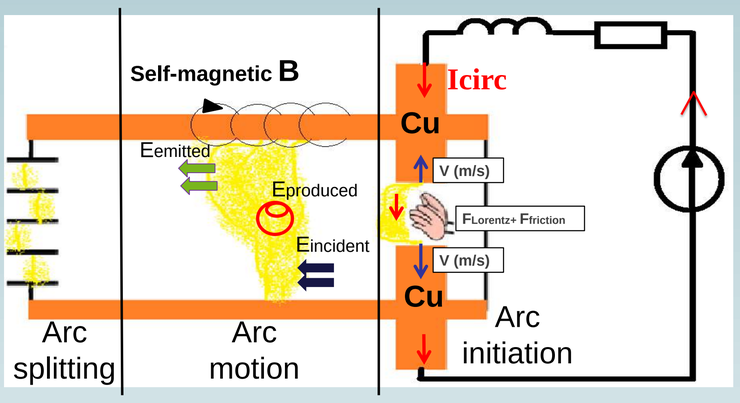

The system of magneto-hydro-dynamic MHD equations in the local thermal equilibrium approximation

- $\frac{\partial\rho}{\partial t} + \nabla(\rho\mathbf{v}) = 0$
- $\rho\frac{\partial \boldsymbol{v}}{\partial t} + \rho(\mathbf{v}.\nabla)\mathbf{v} = \nabla[-\mathbf{PI} + \mu(\nabla\boldsymbol{v} + (\nabla\boldsymbol{v})^T) - \frac{2}{3}\mu(\nabla.\boldsymbol{v})I] + \mathbf{j}\times\boldsymbol{B}$
- $\rho c_p\frac{\partial T}{\partial t} + \rho c_p(\mathbf{v}.\nabla)\mathbf{v} = -\nabla.(\lambda\nabla T) + \left[\mu(\nabla\boldsymbol{u} + (\nabla\boldsymbol{u})^T) - \frac{2}{3}\mu(\nabla.\boldsymbol{u})I\right] + \mathbf{J}^2/\Gamma - 4\pi\varepsilon_N + \frac{5}{2e}K_B TJ$
- $\mathbf{E} = -\nabla.\varphi$
- $\boldsymbol{j} = -\sigma\nabla\varphi$
- $\nabla\times\boldsymbol{H} = \boldsymbol{J}$

Results

For a first approximation, a 2D time dependent model, for an air electric arc is choosen. A simplified geometry of the dimension 30x12mm is used. The copper rails are of 30 mm length and 3 mm width, the gap between them is 6 mm. The contacts open with a velocity of 10 m/s. The temperature distribution is presented which shows the shape of the arc during 0,15 ms.

Temperature distribution in the arc chamber **(Kelvin)**

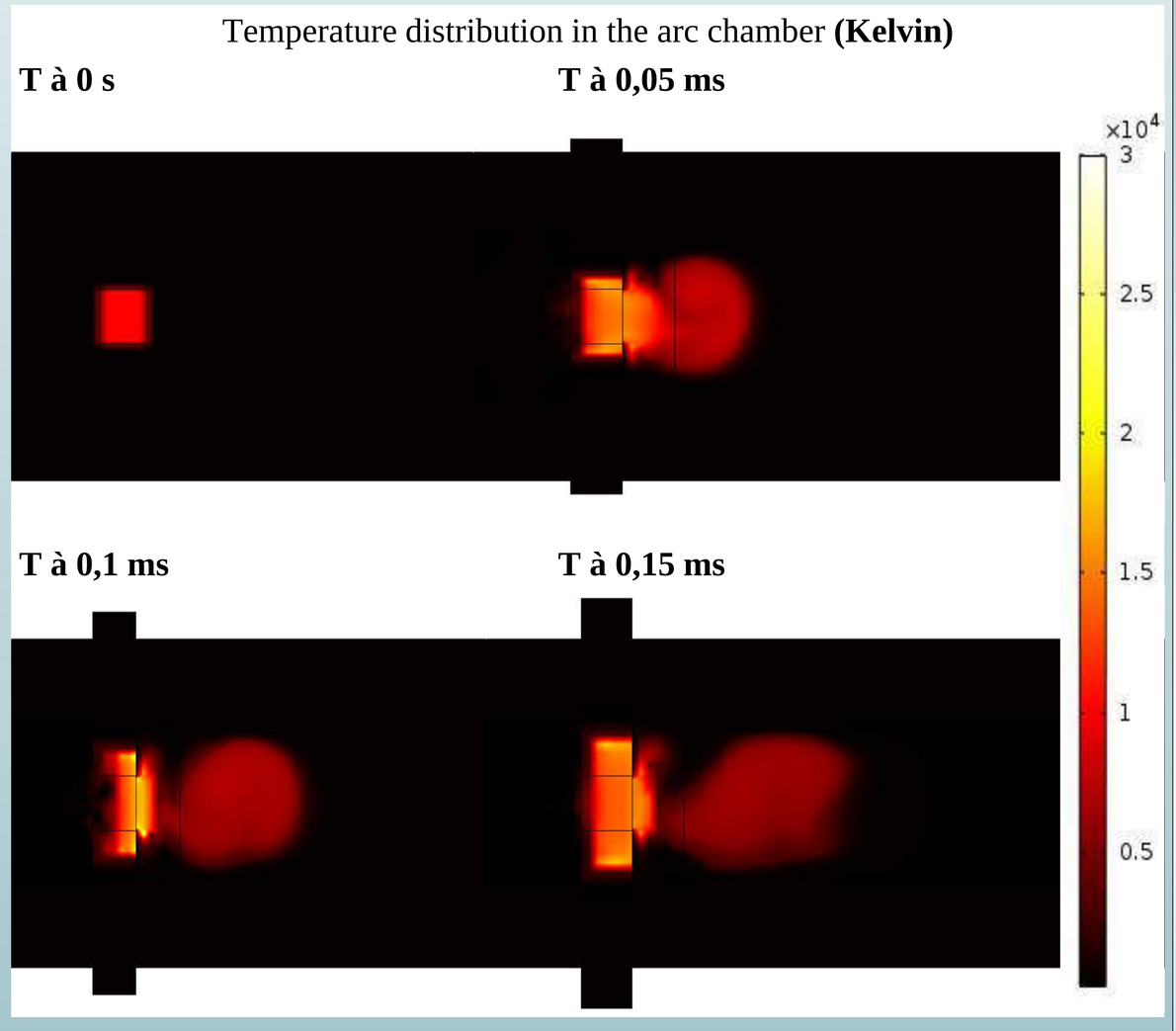

The air arc in switches typically exists near atmospheric pressure; its temperature is usually of the order of 10 kK. So as initial condition a rectangle surface between the moving contacts with 10kK temperature is taken (T=0s) . The results show the arc elongation with the moving contacts after 0,05 ms, and its propagation in the chamber to the splitter plates during the time.

Conclusions

A 2-D model for the simulation of the electric arc has been presented. It takes into account the gas-dynamic as well as the electromagnetic processes. With this model it is possible to simulate the motion of the arc in a simple arc chamber. First results of temperature distribution at different time steps have been presented. The elongation of the electric arc when the contacts open can be observed.
Moreover, an experimental set-up is presented. It is designed for both validation of the model and explanation of the measurements.
Furthermore, the results of an improved simulations as a 3-D models will be compared to those given by the experimental set-up in order to validate the model.

Bibliography

1. Yi Wu, Mingzhe Rong, *Numerical Analysis of the Effect of the Chamber Width and Outlet Area on the Motion of an Air Arc Plasma*, 2008
2. Mingzhe Rong, Yi Wu, Qian YANG, *Simulation on Arc Movement under Effect of Quenching Chamber Configuration and Magnetic Field for Low-Voltage Circuit Breaker*, 2005
3. Frank Karetta and Manfred Lindmayer, *Simulation of the Gasdynamic and Electromagnetic Processes in Low Voltage Switching Arcs*, 1998
4. Manfred Lindmayer, Joachim Paulke, *Arc motion and pressure formation in low voltage switchgear*, 1996

Deep Learning For Fraud Detection

Kergann Le Cornec[1], *AlexandreFabre*[2], *PascalLafourcade*[1], *VincentBarra*[1]

Université Clermont Auvergne, CNRS, ENSMSE, LIMOS,F-63000 CLERMONT-FERRAND, France[1], *Coffreo*[2]

ICPR Fraud Detection Contest

- Identify which **receipt** is frauded.
- Small dataset of **600 Images** (470 genuine, 130 frauded).

Idea

- **Dividing** the image into smaller frames to increase the dataset.
- We used **linear methods for data augmentation** (rotation,flip).
- Detecting important information using **Image Manipulation**.
- Feed those important information to a **Deep Learning Network**.
- **Train** the network to detect if the image is **tampered** or **genuine**.

Local Binary Patterns

$$\begin{pmatrix} 15 & 200 & 115 \\ 27 & 70 & 24 \\ 213 & 5 & 60 \end{pmatrix} \longrightarrow \begin{pmatrix} 1 & 0 & 0 \\ 1 & x & 1 \\ 0 & 1 & 1 \end{pmatrix} \mathcal{P} \begin{pmatrix} 2^0 & 2^1 & 2^2 \\ 2^3 & x & 2^4 \\ 2^5 & 2^6 & 2^7 \end{pmatrix} \longrightarrow \begin{pmatrix} 15 & 200 & 115 \\ 27 & 217 & 24 \\ 213 & 5 & 60 \end{pmatrix}$$

We first compare the reference pixel (here the pixel with the value 70) to each of his neighboor, if the neighboor is greater we replace it by a 0 and if it is lower or equal we replace it by a 1. We use $\mathcal{P}$ for the ponderation operator, to transform the matrix into a binary number, $(11011001)_2 = 217$.

Discrete Wavelet Transform

$$x_{n,i} = \{70\ 56\ 61\ 49\} \rightarrow \{x_{n-1,i}, d - 1_{n,i}\} = \{63\ 55\ 7\ 6\}$$

The transformation replaces the sequence with its pairwise average $x_{n-1,i}$ and difference $d_{n-1,i}$ defined as:

$$x_{n-1,i} = \frac{x_{n,2i}+x_{n,2i+1}}{2}, d_{n-1,i} = \frac{x_{n,2i}-x_{n,2i+1}}{2}$$

We extend the one-dimensional Wavelet transform in two dimensions.

$$\begin{bmatrix} 70 & 56 & 61 & 49 \\ 52 & 46 & 39 & 43 \\ 63 & 45 & 46 & 54 \\ 53 & 39 & 40 & 44 \end{bmatrix} \rightarrow \begin{bmatrix} 63 & 55 & 7 & 6 \\ 49 & 41 & 3 & -2 \\ 54 & 50 & 9 & -4 \\ 46 & 42 & 7 & -2 \end{bmatrix} \rightarrow \begin{bmatrix} 56 & 48 & 5 & 2 \\ 50 & 46 & 8 & -3 \\ 7 & 7 & 2 & 4 \\ 4 & 4 & 1 & -1 \end{bmatrix}$$

We first apply one dimensional Haar-wavelet in each row and then on each column.

Error Level Analysis

To find the tampered parts, we first apply **JPEG compression** with the quality loss of **90%**, then we calculate the difference between the first image and the compressed one.

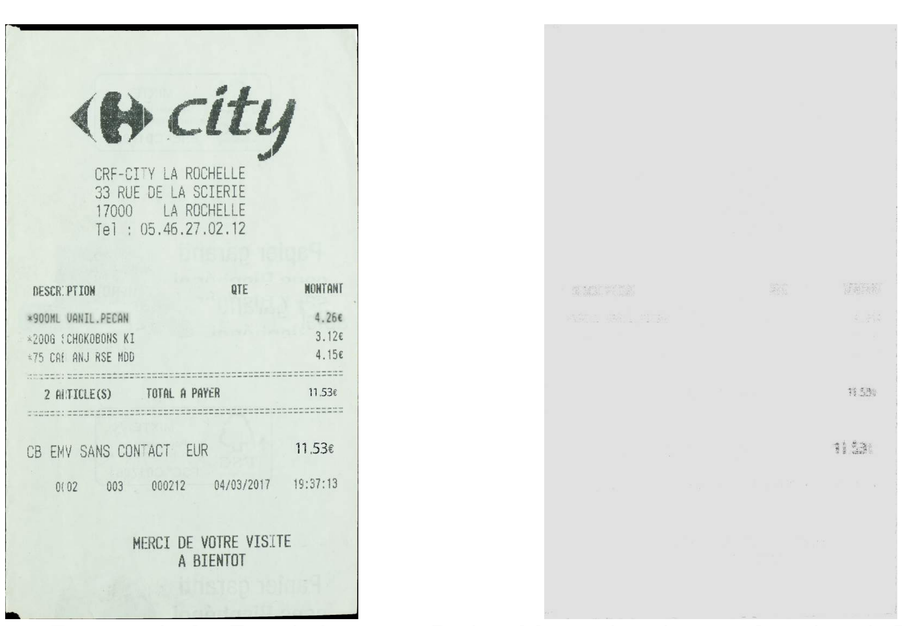

Figure 1:Left: Frauded image. Right: Manipulated areas found with ELA

This technique is based on the idea that tampered areas can act differently to JPEG compression than the rest of the image.

Finetune Deep Learning Models

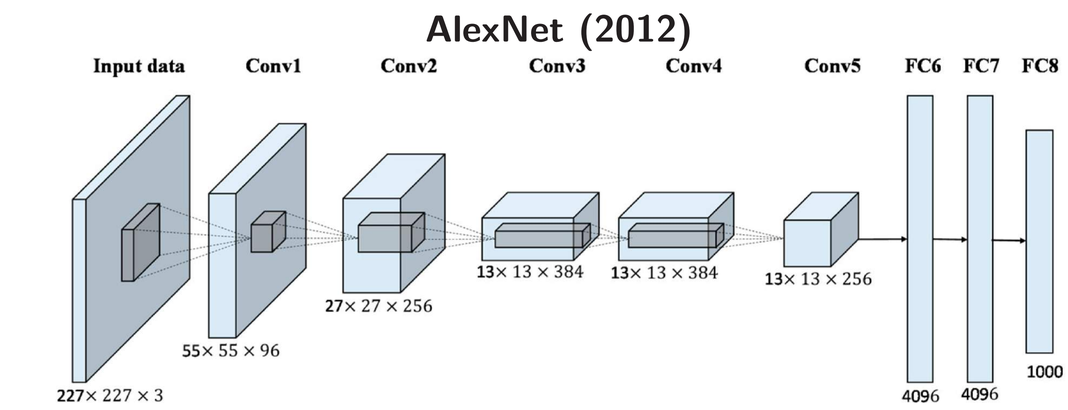

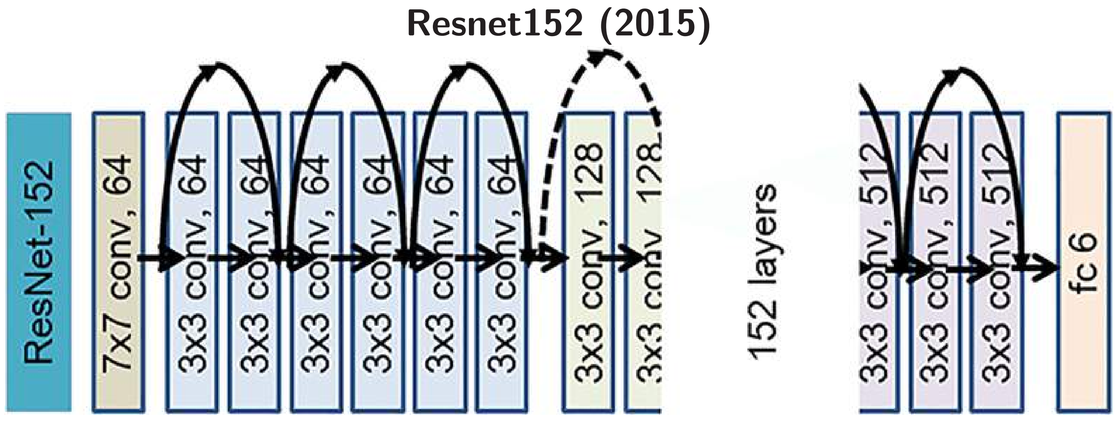

Results

All learning were done with a graphic card **Titan X Pascal** on the framework **Tensorflow**, 24 hours were needed to fully train our best network.

Network	Combined Methods	Accuracy
AlexNet	RGB	62%
AlexNet	ELA+PCA+LBP	65%
AlexNet	ELA+Wavelet+LBP	74%
AlexNet	ELA+Wavelet+GrayScale	76%
AlexNet	ELA+Wavelet+GrayScale+Fraud Creation	85%
ResNet152	RGB	63%
ResNet152	ELA+PCA+LBP	65%
ResNet152	ELA+Wavelet+LBP	75%
ResNet152	ELA+Wavelet+GrayScale	80%
ResNet152	ELA+Wavelet+GrayScale+Fraud Creation	91%

Conclusion

- Achieved more than **90 %** accuracy.
- Easily **adaptable** to any types of images (bills, document).
- Creating different types of image manipulation might improve our model's **reliability**.

Acknowledgments

- Thanks to Alexandre Fabre with whom I worked on this project and to coffreo making this collaboration possible.
- Advice given by Vincent Barra and Pascal Lafourcade has been a great help.

References

[1] Alex Krizhevsky, Ilya Sutskeve, and Geoffrey E. Hinton.
ImageNet Classification with Deep Convolutional Neural Network.
2012.

[2] Kaiming He, Xiangyu Zhang, Shaoqing Ren, and Jian Sun.
Deep Residual Learning for Image Recognition.
2015.

[3] H.MahaleaMouad, M.H.AlibPravin, L.YannawarcAshok, and T.Gaikwadd.
Image inconsistency detection using local binary pattern (lbp).
2017.

[4] Lubhavni Sharma and Parminder Singh.
Digital Image Forgery Detection using Wavelet Decomposition and Edge Detection.
2015.

kelecornec@isima.fr

Theoretical and experimental modeling of the energy and environmental behavior of bio-based building materials

Maroua BENHALED[1], Salah-Eddine OULDBOUKHITINE[1], Sofiane AMZIANE[2]

[1] IUT de Montluçon, Université Clermont Auvergne, Institut Pascal BP 10448, F-63000 Clermont-Ferrand

[2] Université Clermont Auvergne, Institut Pascal BP 10448, F-63000 Clermont-Ferrand

Environmental cirumstances

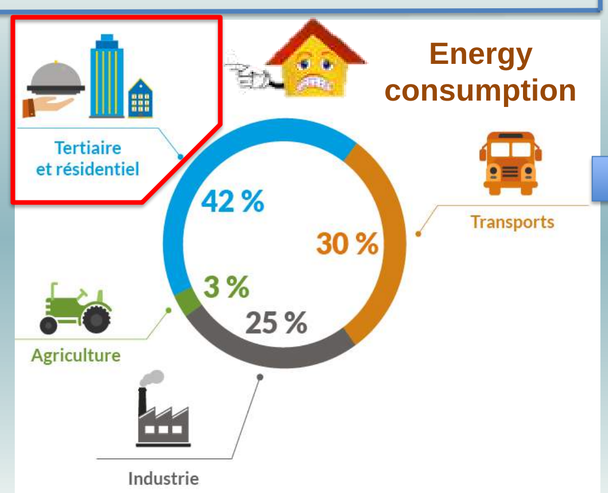

Source: Ministry of the Environment, Energy and the Sea

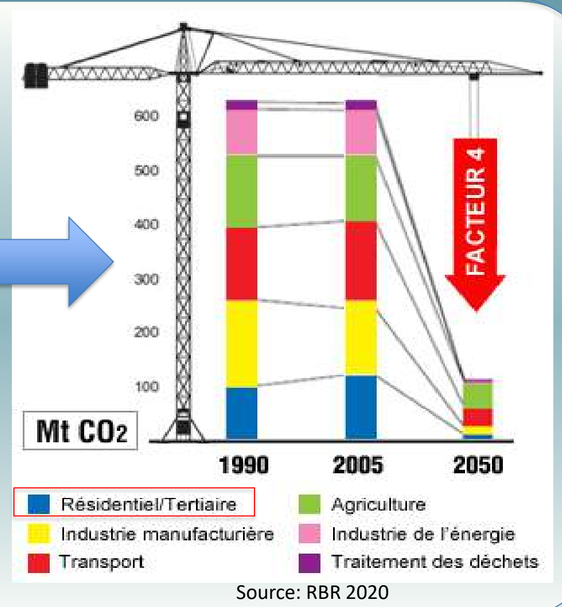

Source: RBR 2020

Problem statement

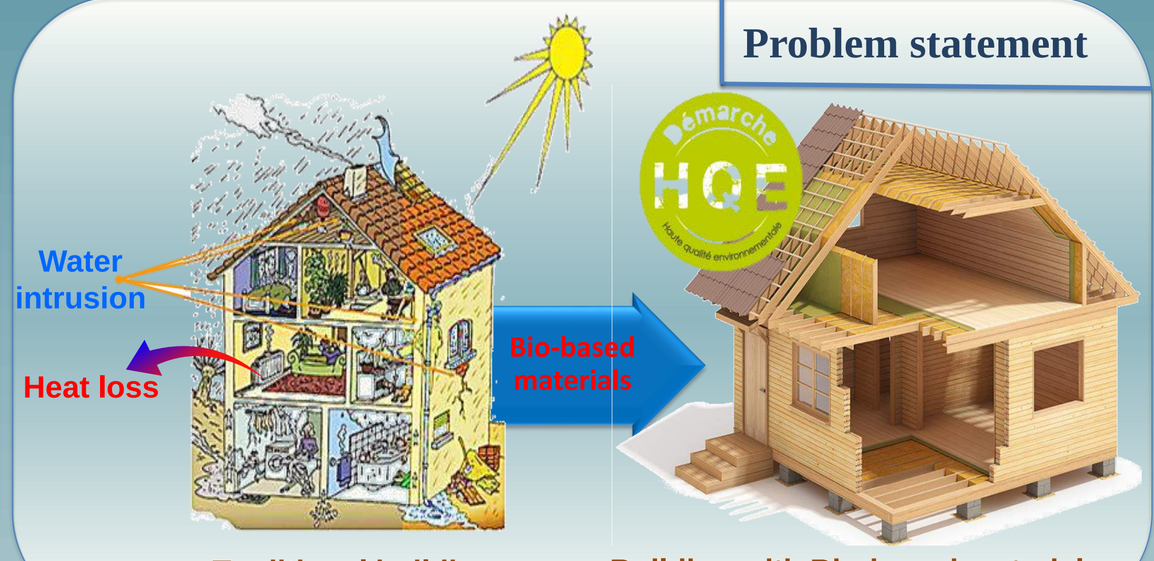

Hemp

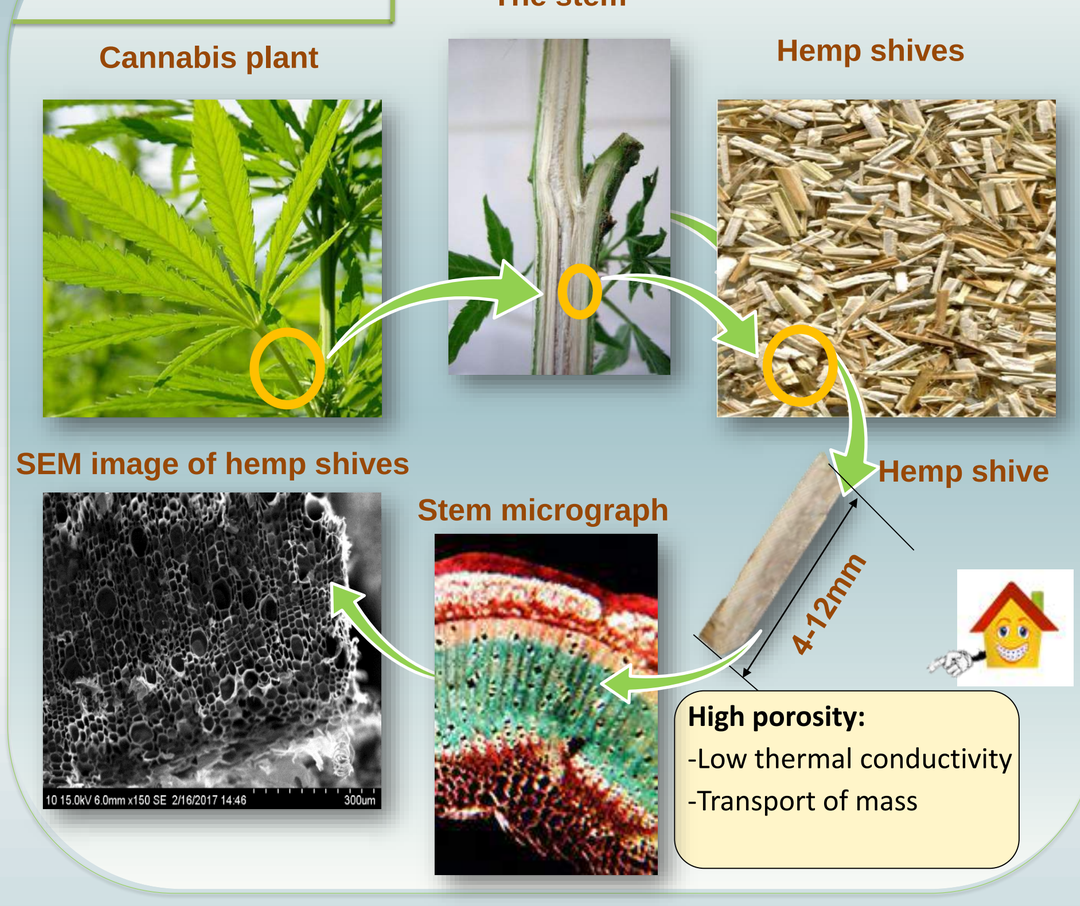

High porosity:
-Low thermal conductivity
-Transport of mass

Hemp concrete

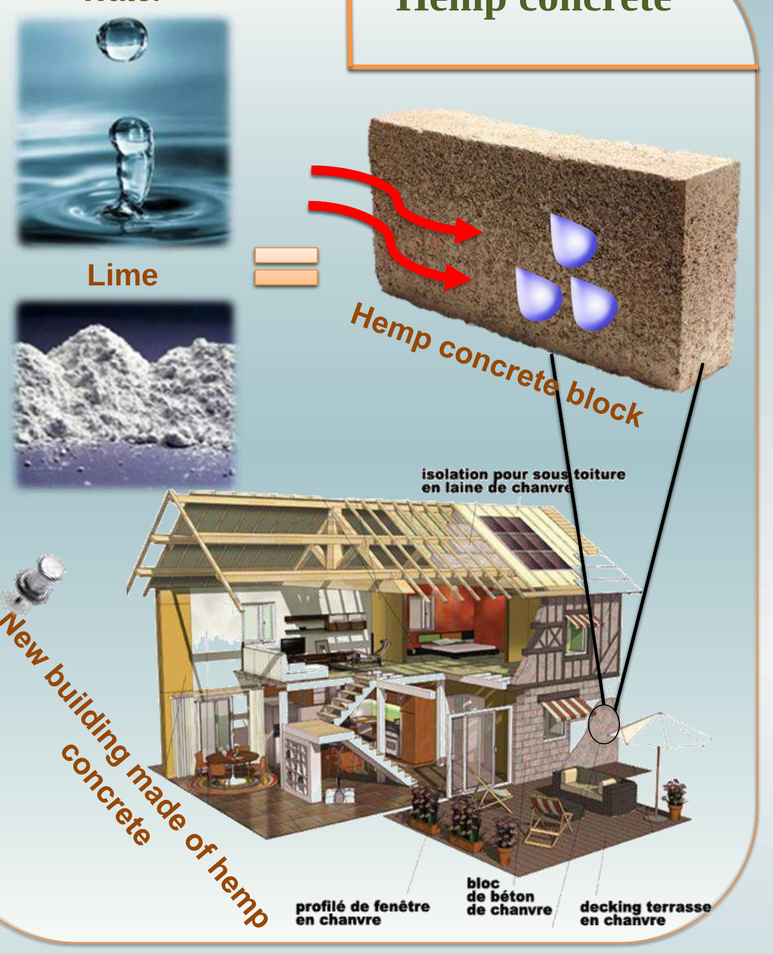

Experimental characterization of the material

Modelization

Numerical simulation

Confirmation

Experimental study at the wall scale

Research methodology

Experimental studies of the hygrothermal behavior of hemp wall

The bi-climatic heat chamber at the IUT of Montluçon

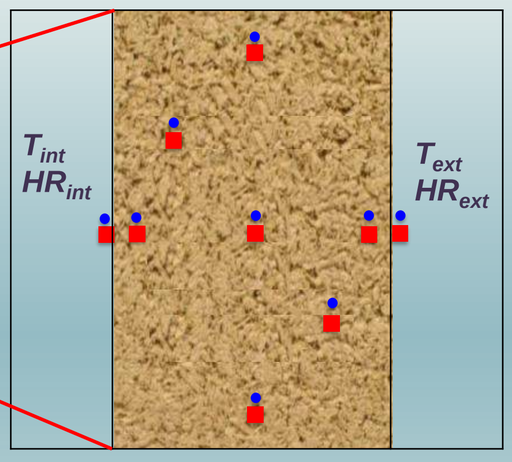

Hemp wall concrete (Implentation of the sensors within the wall)

- Experiments in a bi-climatic chamber will be performed on an instrumented wall of hemp concrete.
- Measurement sequences will be performed with constant temperature and humidity conditions on one side and representative of summer or winter conditions on the other.
- Evaluation of the pressure gradient impact on coupled heat and mass transfers.

Numerical studies of the hygrothermal behavior of hemp wall

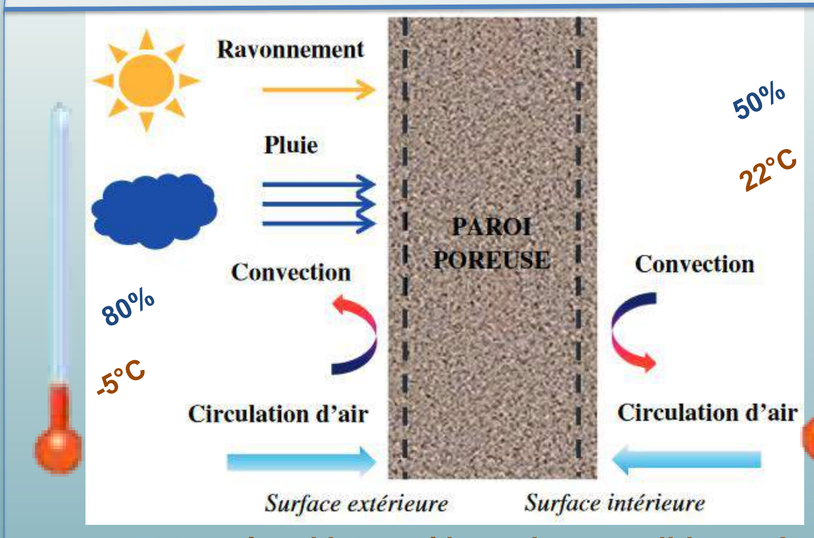

External and internal boundary conditions of a wall [AIT 2013]

$$* c_m \frac{\partial \omega}{\partial t} = div[d_m(\nabla \omega + \varepsilon \nabla T + K \nabla P)]$$

$$* C\rho_s \frac{\partial T}{\partial t} = div(a_t \nabla T + \delta_t \nabla \omega + \zeta \nabla P) + h_{lv}\, \rho_s\, \chi \frac{\partial \omega}{\partial t}$$

$$* h_a \frac{\partial P}{\partial t} = div(\lambda_f \nabla P) + \rho_s\, \chi \frac{\partial \omega}{\partial t}$$

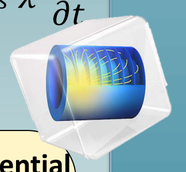

- A system of three strongly coupled partial differential equations.
- The model will be implemented on the Comsol software (finite element method).
- The measured evolutions of T (° C) and HR (%) within the wall will be compared to the numerical results that obtained by the proposed model.

Expected results

- An improvement of the HAM model (Heat, Air and Moisture) will be implemented on the Comsol multiphysics software by integrating various parameters (pressure, convection, thermo-transfer of the liquid phase and hysteresis).
- Obtain experimental data on the thermal and hydrous behavior of the material.
- Evaluation of the energy impact of hemp concrete on the energy performance of buildings and the comfort of users.

Visibility Restoration in a Scattering Medium Using Light-field Data

Ecole doctorale Sciences Pour l'Ingénieur

Maryam Ghaneizad, Frédéric Chausse, Céline Teulière, Christophe Blanc

Université Clermont Auvergne, CNRS, Institut Pascal

Introduction

In this work, we aim to develop a potentially real-time algorithm for improving the visibility of images captured in a scattering environment, such as turbid water. As will be seen later, the dehazing problem is highly correlated with depth. For this purpose, we propose light-field imaging realized by an affordable compact plenoptic camera, i.e. Lytro Illum [1].

Related work

Single image methods [2, 3] lack the depth information, hence they assume some priors to be able to solve the problem. Polarizer-based methods [4] demand the effort to capture multiple images while rotating the polarizer in front of the sensor and therefore, are obviously not real-time.

Contribution

Thanks to the plenoptic camera capturing an array of images in one shot, we develop a real-time algorithm for dehazing. In this framework, having increased the recorded input scene information without trading-off the time, we can apply our dehazing algorithm to any arbitrary scene with no priorities.

Plenoptic camera (Lytro Illum) [1]

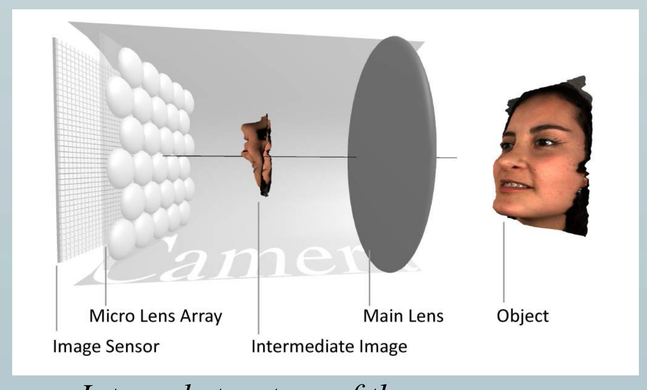

Internal structure of the camera [https://raytrix.de/]

Formulation

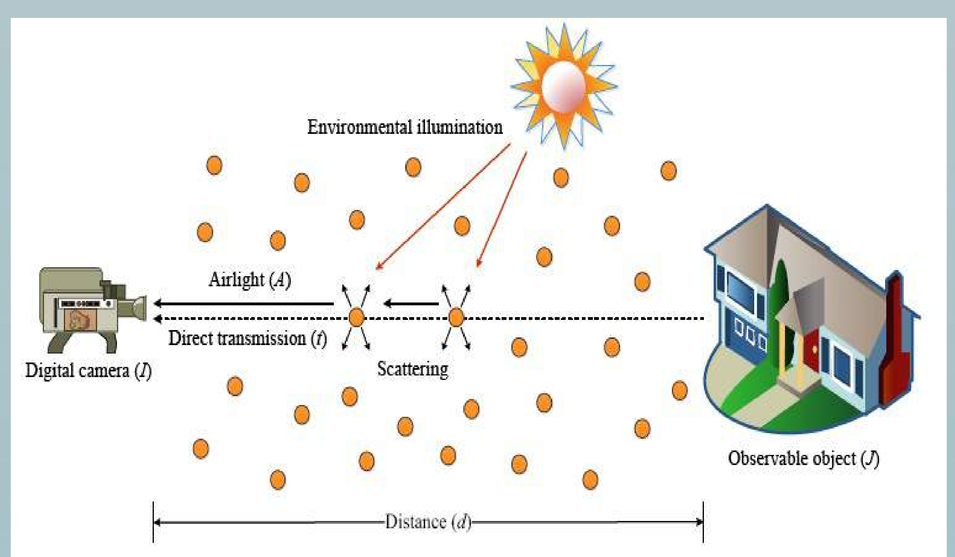

Schematic model of a imaging in a scattering environment [3]

$$I(\bar{x}) = J(\bar{x}).exp(-\beta d(\bar{x})) + A.(1 - exp(-\beta d(\bar{x})))$$

Proposed algorithm

Input: *I(x)* Captured image
Output: *J(x)* Dehazed image, *d(x)* Depth map

Given ambient light A and parameters of medium:

1. Initiating a fixed depth value *z_ref*
2. Deriving 1-order restored image *J1* based on *z_ref*
3. Using *J1* to compute a depth map *d1*
4. Enhancing depth map *d1* based on the transmission cue method in [5]
5. Using improved depth map to compute the finally restored image *J(x)*

Results taken from [5]

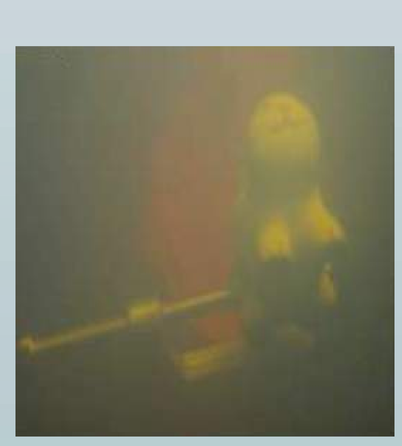

The center view image captured by camera (in turbid water)

The restored image

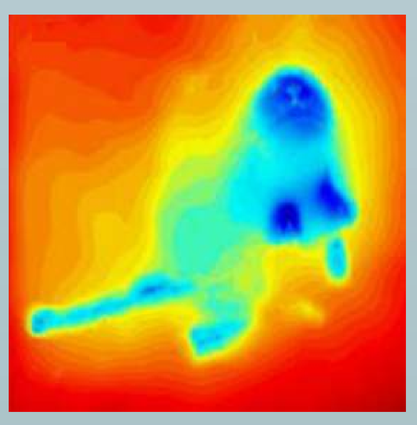

The restored depth map

Applications

1. Visibility enhancement of sea animals in aquariums
2. Visibility enhancement of roads for drivers

...

Bibliography

[1] *https://support.lytro.com/*
[2] R. T. Tan, et al. "Visibility enhancement for roads with foggy or hazy scenes," *Intelligent Vehicles Symposium*, IEEE, 2007.
[3] S. Huang, et al. "Visibility restoration of single hazy images captured in real-world weather conditions," *IEEE Transactions on Circuits and Systems for Video Technology* 24.10, 2014.
[4] S. Shwartz, et al. "Blind haze separation," *Computer Society Conference on Computer Vision and Pattern Recognition*, IEEE, 2006.
[5] J. Tian, et al. "Depth and image restoration from light field in a scattering medium," *International Conference on Computer Vision*, IEEE, 2017.

Applying the social-ecological system framework to construct a biophysical-social forest model: Application to the Quatre-Montagnes forest

Mojtaba HOUBALLAH[1], Jean-Denis MATHIAS[1], Thomas CORDONNIER[2]

[1] UR LISC, Laboratoire d'Ingénierie pour les Systèmes Complexes, IRSTEA - Clermont Ferrand

[2] UR LESSEM, Laboratoire Ecosystèmes et Sociétés En Montagne, IRSTEA - Grenoble

Ecole doctorale Sciences Pour l'Ingénieur

LISC-IRSTEA

Introduction

Forest policy and management are subject to various and often conflicting demands, which internationally have led to distinct policy responses and related management paradigms. The ever increasing demand on the forest ecosystem to produce wood and other goods and services poses a corresponding demand on a forest decision support system. Forest ecosystem components interact with each other and with the external environment in many different ways and over multiple spatial and temporal scales [Messier et al. 2013]. The capacity of societies to address forest sustainability hinges on their capacity to deal with several social dilemmas associated with integrating their activity and cooperating with respect to the provisioning and use of the forest and human-made infrastructure [Muneepeerakul and Anderies 2017]. Nevertheless, Forest ecological modelling studies often view humans as external disturbance or drivers of ecosystem processes while economic modelling studies often treat ecosystems only as input to a production process. Neither generally takes into account that humans and societies may or may not adapt their behavior as a response to ecological changes. The specific reconciliation and integration of both sides (social and ecological dimensions) of the spectrum have been at the center of scientific discussion on forest policy and management for several decades. Nevertheless, Ostrom [2009] proposed a framework that analytically combines these two aspects. The social-ecological system framework (SES) helps scholars and policy makers to accumulate knowledge from empirical studies and assessments of past efforts at reforms and to organize their analytical, diagnostic, and perspective capabilities. This research centers on understanding the nature of economic-social-ecological interactions through infrastructures point of view. Specifically we seek to study, by means of concise mathematical expressions, the interaction between infrastructures associated with different forest aspect within the dynamics of the robustness framework [Anderies 2004].

Methods

As the literature review the SES framework [Ostrom 2009] as an appropriate tool for examining forests, we first describe the Quatre-Montagne case study area through the SES subsystems lens, emphasizing characteristics that are known to affect the viability of common property institutions.

❖ Social-ecological system framework [Ostrom 2009]

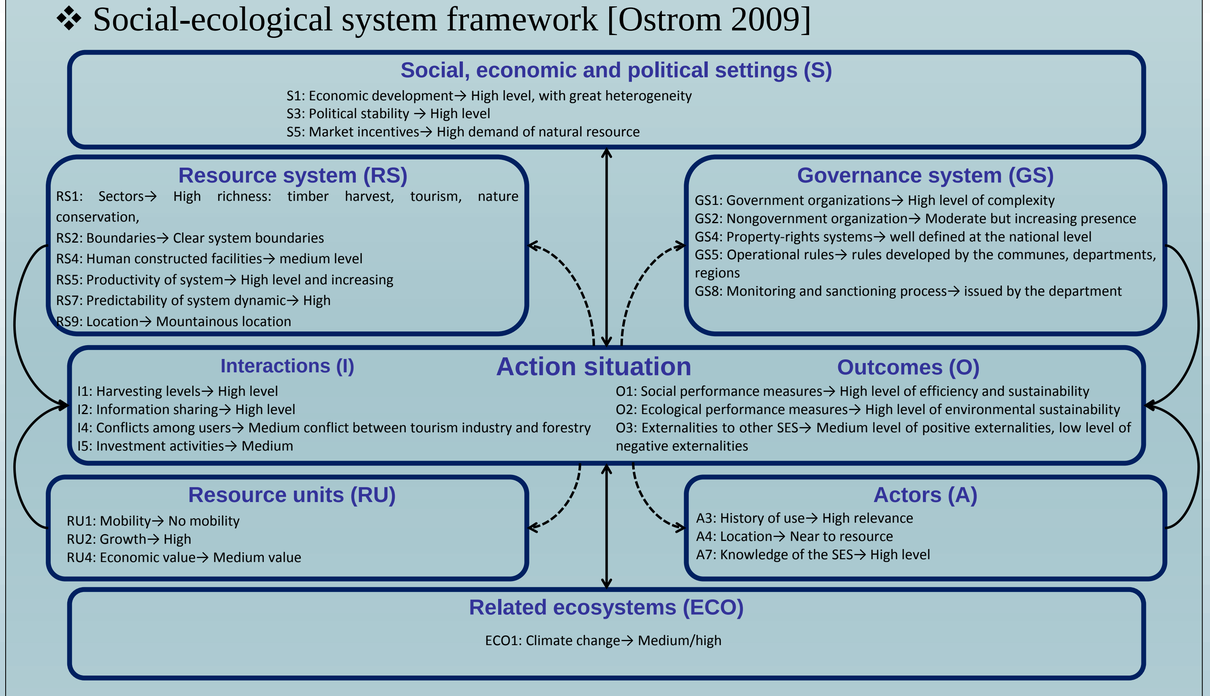

The main goal is to construct a mathematical model that operationalizes the robustness conceptual framework to analyze the interactions in the forest. Particularly, we seek to present the forest management through the lens of the robustness framework. The model brings to clear focus the exchange between diverse forest users, functionality of human-made infrastructure, dynamics of the forest, and governance influence. We derive a variety of trade-offs between investments in construction and maintenance of public infrastructure for forestry.

❖ Robustness framework [Anderies 2004]

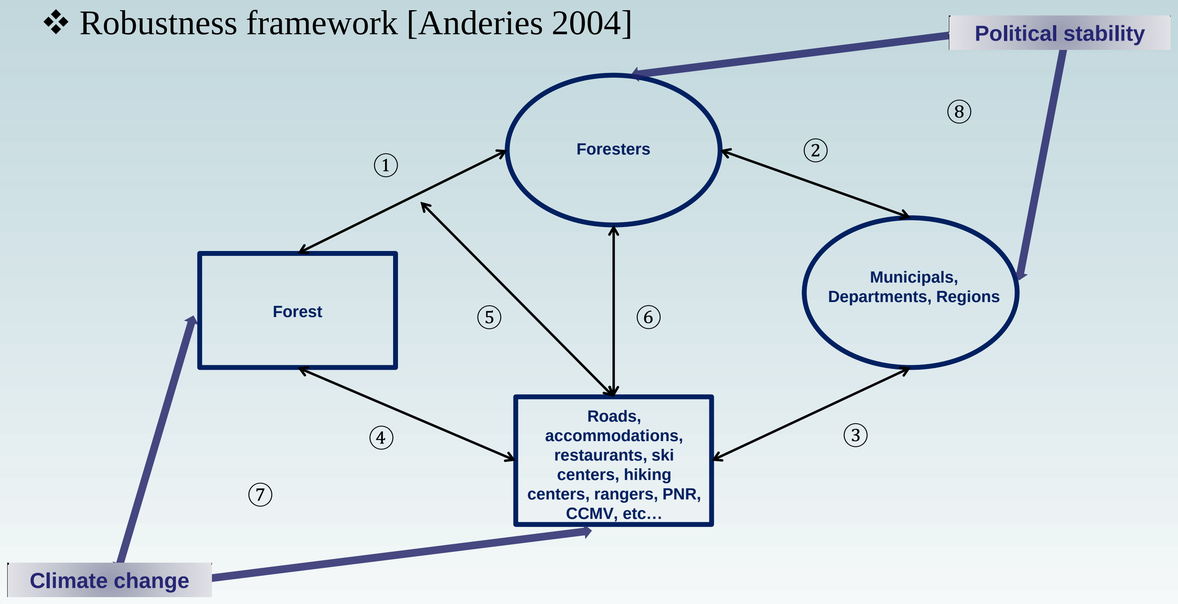

Results

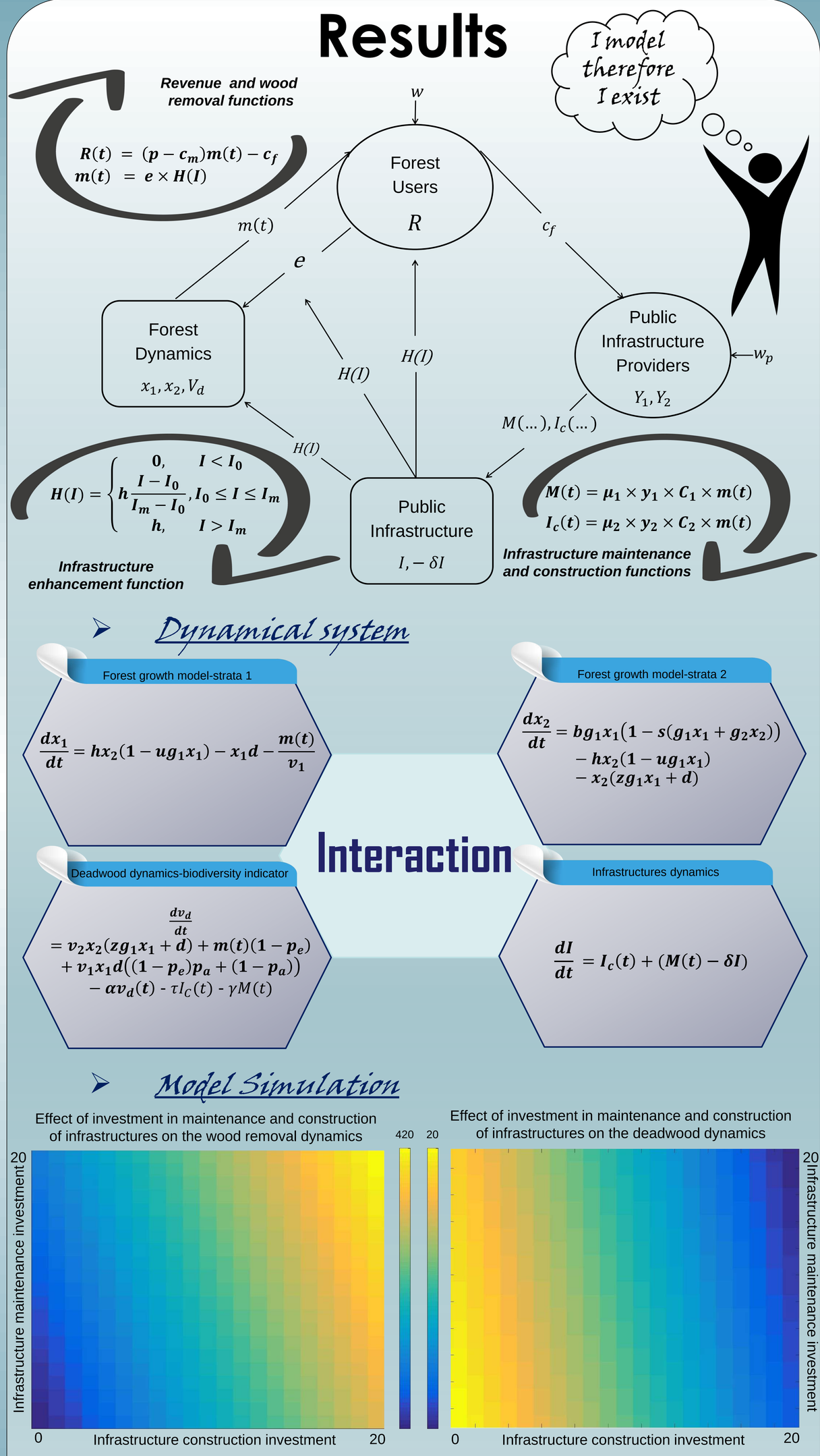

➢ Dynamical system

Forest growth model-strata 1

$$\frac{dx_1}{dt} = hx_2(1 - ug_1x_1) - x_1d - \frac{m(t)}{v_1}$$

Forest growth model-strata 2

$$\frac{dx_2}{dt} = bg_1x_1\big(1 - s(g_1x_1 + g_2x_2)\big) - hx_2(1 - ug_1x_1) - x_2(zg_1x_1 + d)$$

Interaction

Deadwood dynamics-biodiversity indicator

$$\frac{dv_d}{dt} = v_2x_2(zg_1x_1 + d) + m(t)(1 - p_e) + v_1x_1d\big((1 - p_e)p_a + (1 - p_a)\big) - \alpha v_d(t) - \tau I_C(t) - \gamma M(t)$$

Infrastructures dynamics

$$\frac{dI}{dt} = I_c(t) + (M(t) - \delta I)$$

➢ Model Simulation

Conclusions

We applied the SES framework to examine the multiple social and ecological factors that potentially affect the biophysical outcomes of the forest in Quatre-Montagne area, France, and we found out that the main aspect influencing the outcomes of the forest is the availability of infrastructure. Thus, we apply the robustness framework to enhance our infrastructural point of view of the forest. Nevertheless, we use the framework's conceptual map to guide our model development. The model shows a clear tradeoffs between maintenance and construction of infrastructures for forest biodiversity as well as wood removal.

Acknowledgment

This research has been funded by the ANR (Agence Nationale de la Recherche) under the VIRGO project (ANR-16-CE03-0003) and the region of Auvergne. Moreover, this research was conducted on the Long-Term Socio-Ecosystem Research platform LTSER "Zone Atelier Alpes", a member of the ILTER-Europe network.

Bibliography

1. Ostrom, E. (2009) A General Framework for Analyzing Sustainability of Social-Ecological Systems. Science 325: 419-422
2. Anderies, J. M., M. A. Janssen, and E. Ostrom. 2004. A framework to analyze the robustness of social-ecological systems from an institutional perspective. Ecology and Society 9(1): 18.
3. Muneepeerakul, R., and J. M. Anderies (2017), Strategic behaviors and governance challenges in social-ecological systems, Earth's Future, 5, 865–876, doi:10.1002/2017EF000562.
4. Messier C, Puettmann KJ, Coates KD (eds), 2013. Managing forests as complex adaptive systems: building resilience to the challenge of global change. Routledge, Oxon/New-York, pp. 327-341.

Hybrid Vehicular Communications Optimization For Cooperative Intelligent Transport Systems

Mouna Karoui[1] : First year phd student
Supervisors: Michel Misson[1], Gérard Chalhoub[1]
Co-Supervior: Antonio Freitas[1]
[1] *University of Clermont Auvergne*

Introduction

- The goal of this phd topic is to propose hybrid network architecture for C-ITS, that combines standards used for vehicular networks such as IEEE 802.11p/ETSI ITS-G5 and a cellular technology. Then a performance study of the proposed architecture will be done.
- We started by studying ETSI ITS-G5 European standardization dedicated for vehicular communications.
- We are focusing on Green Light Optimal Speed Advisory (GLOSA) application as a particular ITS service.
- We proposed an algorithm for GLOSA after studying several limitations in related work.

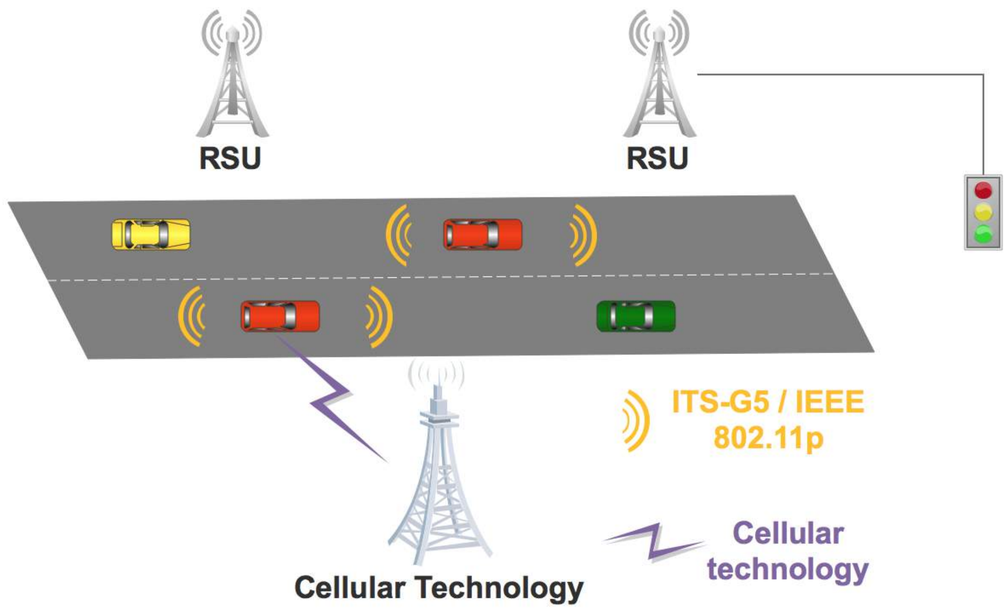

Speed Advisory Estimation

- We consider uniformly varied motion and Uniform straight movement.
- We consider both acceleration and deceleration cases as shown in the figure below.

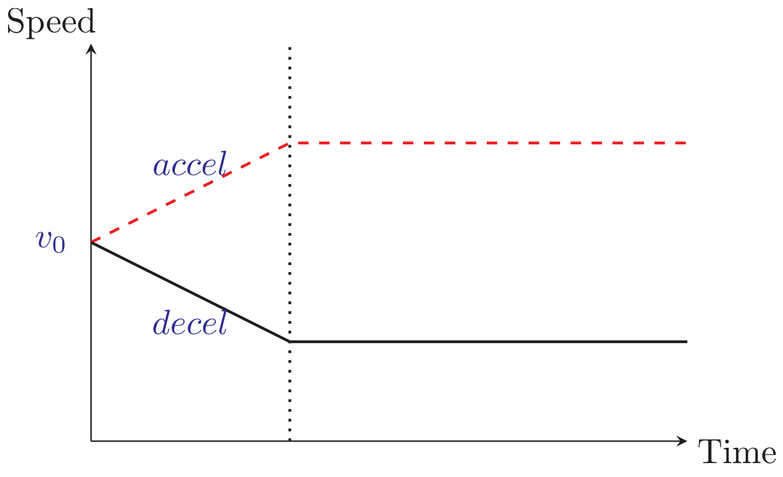

Equation (1) is obtained after resolving a system of equations. The below conditions should be verified.

$$v_{conseil}(t) = a * (t - \sqrt{t^2 - \frac{2(d - v_0 t)}{a}}) + v_0 \quad (1)$$

$$\begin{cases} If\ v_0 < \frac{d}{t} \Leftrightarrow a > 0 \\ If\ v_0 > \frac{d}{t} \Leftrightarrow a < 0 \end{cases}$$

$$\begin{cases} If\ a > 0,\ a > \frac{2*(d - v_0 t)}{t^2} \\ If\ a < 0,\ a < \frac{2*(d - v_0 t)}{t^2} \end{cases}$$

Speed Advisory Boundaries FINder Algorithm (SABIN)

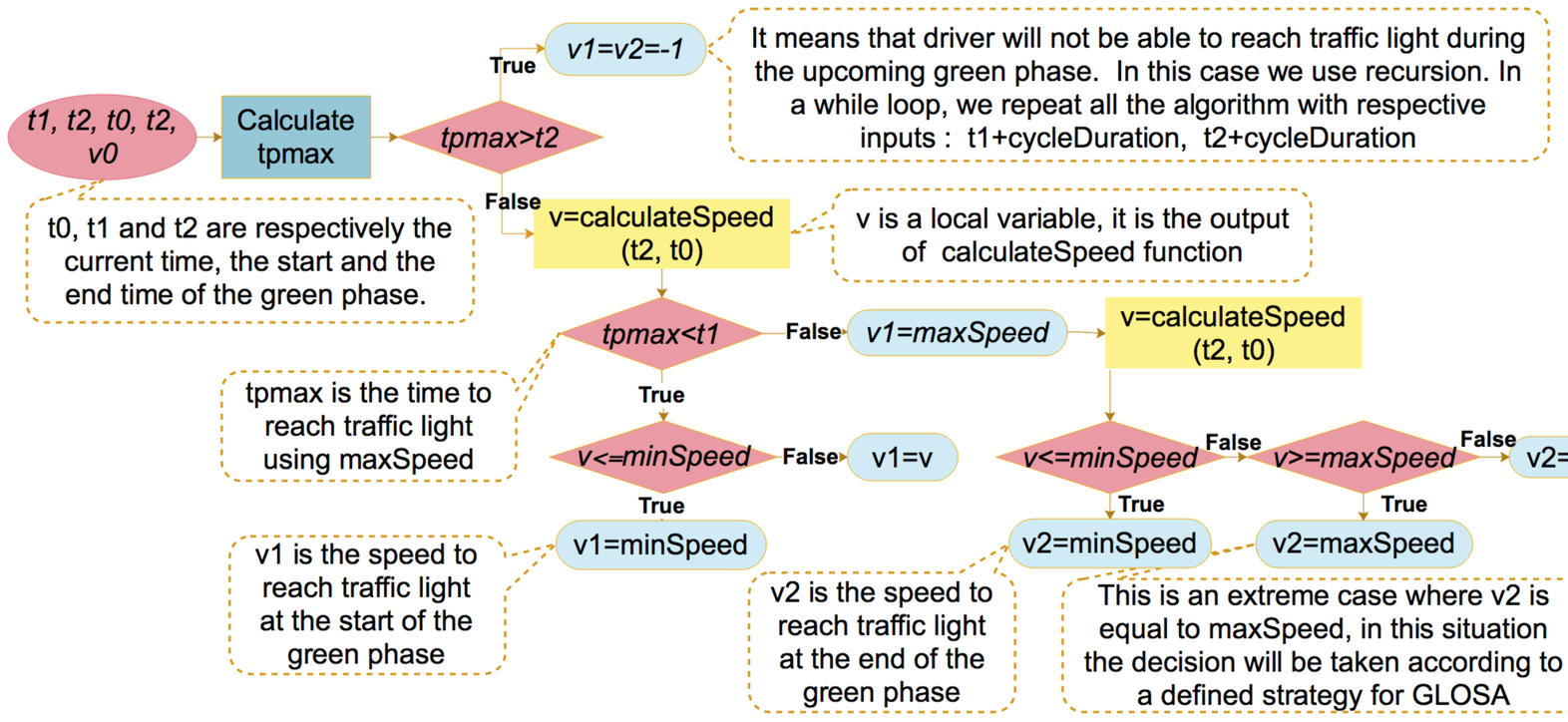

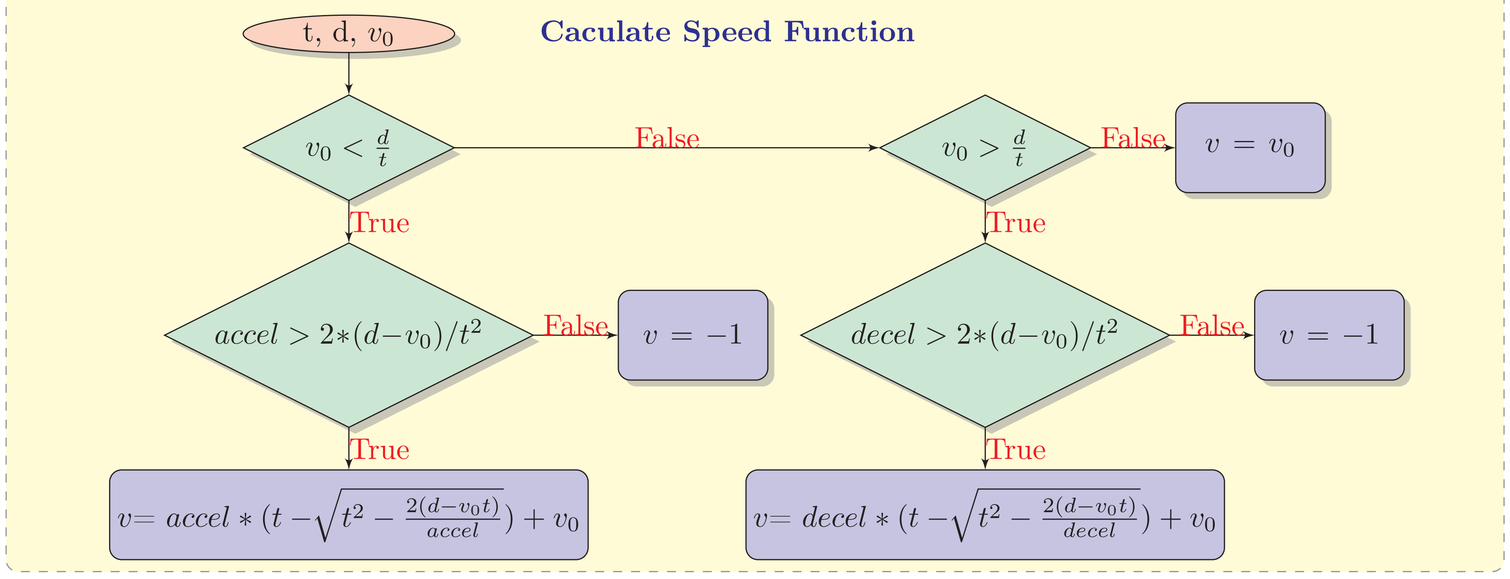

Future Work

- The proposed Algorithm "SABIN" for GLOSA will be tested for various scenarios and use cases in order to validate our implementation.
- Second, we will evaluate ITS-G5 network performance of ITS services (GLOSA, CAM, DENM etc..).
- We will study ETSI ITS-G5 limitations and then we will propose hybrid network architecture that combines ETSI ITS-G5 and a cellular technology.

Contact Information

- Email: mouna.karoui@uca.fr

Results

The results below are obtained using V_1 as speed advisory. Fuel consumption and speed comparison between GLOSA and non GLOSA systems are presented.

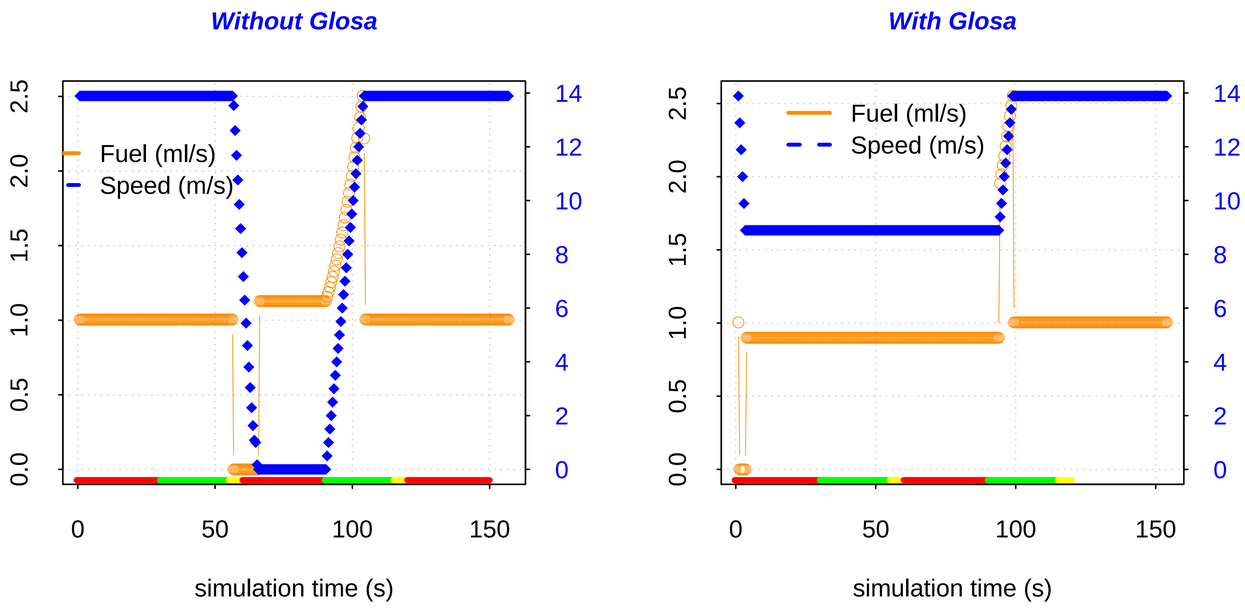

OPTIMIZATION OF PRESTRESSED CONCRETE BRIDGES

Ecole doctorale Sciences Pour l'Ingénieur

BY NADIM ABDEL NOUR

CHEC (CENTRE DES HAUTES ETUDES DE LA CONSTRUCTION), LEBANESE UNIVERSITY

Introduction

Road infrastructure is the basis of communication and transportation systems in both developed and under development countries. With the increasing evolution of socio-economic activity and urban growth, the improvement of communications becomes an obvious necessity. The construction of bridges has, since then, become essential to cross new communication routes.

Prestressed concrete bridges are frequently used in the motorway design when intersecting traffic occurs. Durability, aesthetics and ease of construction and maintenance are some advantages to their use.

In the design of a prestressed concrete bridge deck, the analysis and the rearrangement of the cables represent a very important task.

Most traditional procedures for structural concrete design select initial solutions based on material grades and cross-section dimensions derived from common practice and previous experiences. Once the structure is defined, the analysis is carried. Should the dimensions or reinforcement be insufficient, the structure is redefined on a trial-and-error basis. This process is not automatic and leads to safe design, but the cost of the concrete structure is highly dependent upon the experience of the structural engineer.

Optimization methods are a clear alternative to experience-based methods!! Many researchers have been working in this direction, and it can be clearly stated that applying optimization techniques to the concrete structures design has made the structural design more efficient.

Methodology Adopted

The objective of this research project is the development of a digital tool for the optimization of two types of prestressed concrete bridges:

Continuous bridge (sur cintres)

Cantilever bridge (encorbellement)

This year's study was conducted for the continuous bridge "construit sur cintres".

METHODOLOGY IS DIVIDED INTO 2 PARTS:

- **PRESTRESSED CONCRETE BRIDGE DESIGN**
- **OPTIMIZATION PROBLEM DEFINITION AND RESOLUTION**

1-PRESTRESSED CONCRETE BRIDGE DESIGN:

Main steps followed and accomplished

- **LOADING DEFINITION:** Given by the Eurocode EN-1991-2
- **ANALYSIS OF THE DECK** (tablier):
  - Longitudinally: the bridge is assumed a continuous beamlike structure supported on the piers. The analytical method consists of finding the envelop curves of the moment and shear under different load combinations, in order to design the bridge for the worst case
  - Transversally: the analysis of the transversal stress-resultants can be analyzed according to different methods (Guyon-Massonnet)
- **PRESTRESS ANALYSIS:** Computation of the prestressing force:
  - Concordant cable profile method: The cable layout is defined such that no secondary moments are developed in the continuous beam
- **PRESTRESSING LOSSES CALCULATIONS**

$$e_{oo} = \frac{M}{P} = e_o + \frac{M_{hyp}}{P}$$

- **VERIFICATION OF STRESSES AT SERVICE STATE AND ULTIMATE STATE**

RESULTS OF PRESTRESSED CONCRETE BRIDGE DESIGN:

- Establishing an Excel and a Word written document of the applied analytical method for the cable definition and the prestressing force calculation for a 10 span continuous beam
- Programming this method into Scilab software

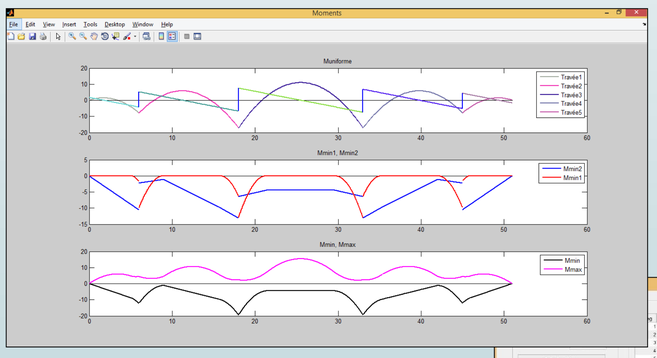

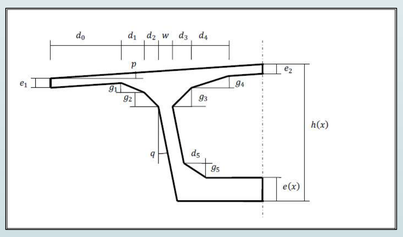

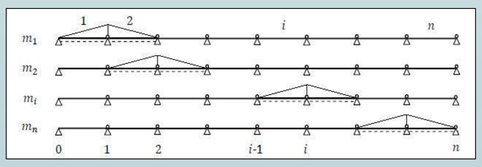

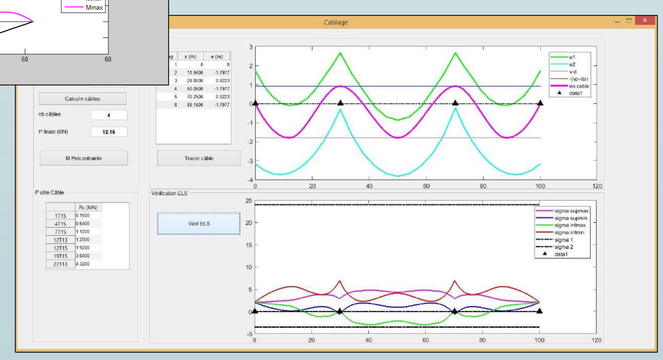

2-OPTIMIZATION PROBLEM DEFINITION AND RESOLUTION:

A literature review was conducted of the many published papers regarding the different optimization techniques adopted in the optimization of prestressed concrete bridge.

RESULTS:

Optimization problem can be stated in the following form:

Minimize {Cost of structure (Objective Function)}
While satisfying the constraints:
g1: Geometric constraints
g2: Serviceability limit states (deflection, stresses, …)
g3: Ultimate limit sates (Moment, shear, …)
g4: Tendon layout and configuration constraints
With the design variables:
-Geometric design variables (Structure dimensioning)
-Material strength
-Prestressing variables

Optimization methods can be divided into two main categories:

DETERMINISTIC OPTIMIZATION		STOCHASTICS AND METAHEURISTICS	
Kuhn-Tucker	Newton	Genetic Algorithm	Tabu Search
Simplex	Fibonacci	Simulated Annealing	Particle Swarm Opt
…		…	

PRESTRESSED CONCRETE BRIDGE OPTIMIZATION => NON LINEAR PROBLEM

RESOLUTION

LINEARIZATION AND SIMPLIFICATION OF THE PROBLEM => **SIMPLEX** **OR** **METAHEURISTICS**

What's Next?

MAIN TARGETS:

- ***Choosing the proper optimization technique for our problem***
- ***Listing all design variables and constraints***
- ***Apply the optimization problem to Scilab***
- ***Analyze results***
- ***Conduct parametric studies for the design variables***
- ***Jump to the Cantilever bridge analysis***

2D-3D Fusion for Road Object Detection and Tracking on Autonomous Vehicles

Ruddy THEODOSE[1], Dieumet DENIS[1], Christophe BLANC[2], Paul CHECCHIN[2]

[1]Sherpa Engineering, [2]Institut Pascal

Ecole doctorale Sciences Pour l'Ingénieur

Goals

- Explore merging methods between point clouds from **automotive LiDAR** and **camera** video stream with artificial neural networks
- Develop a **obstacle detection** system using **both** modalities
- **Track** obstacles from detections and predict their trajectories

Network Architecture

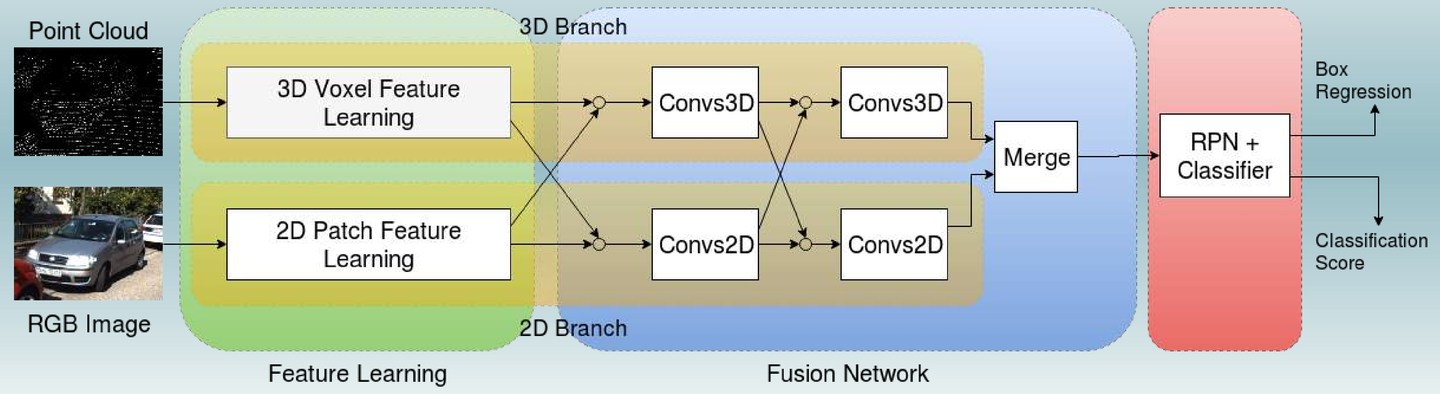

Detection System

- Image patches and corresponding 3D cells learn their own representation independently from the other patches/cells
- Spherical coordinates for Voxel Feature learning
- Voxels features augmented with probabilities inspired by occupancy grid approach
- Diffusion of each branch information to the other branch

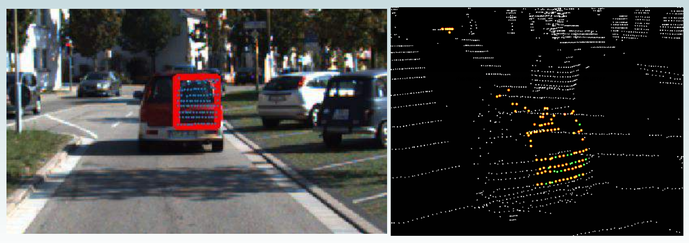

Experiments : Detection

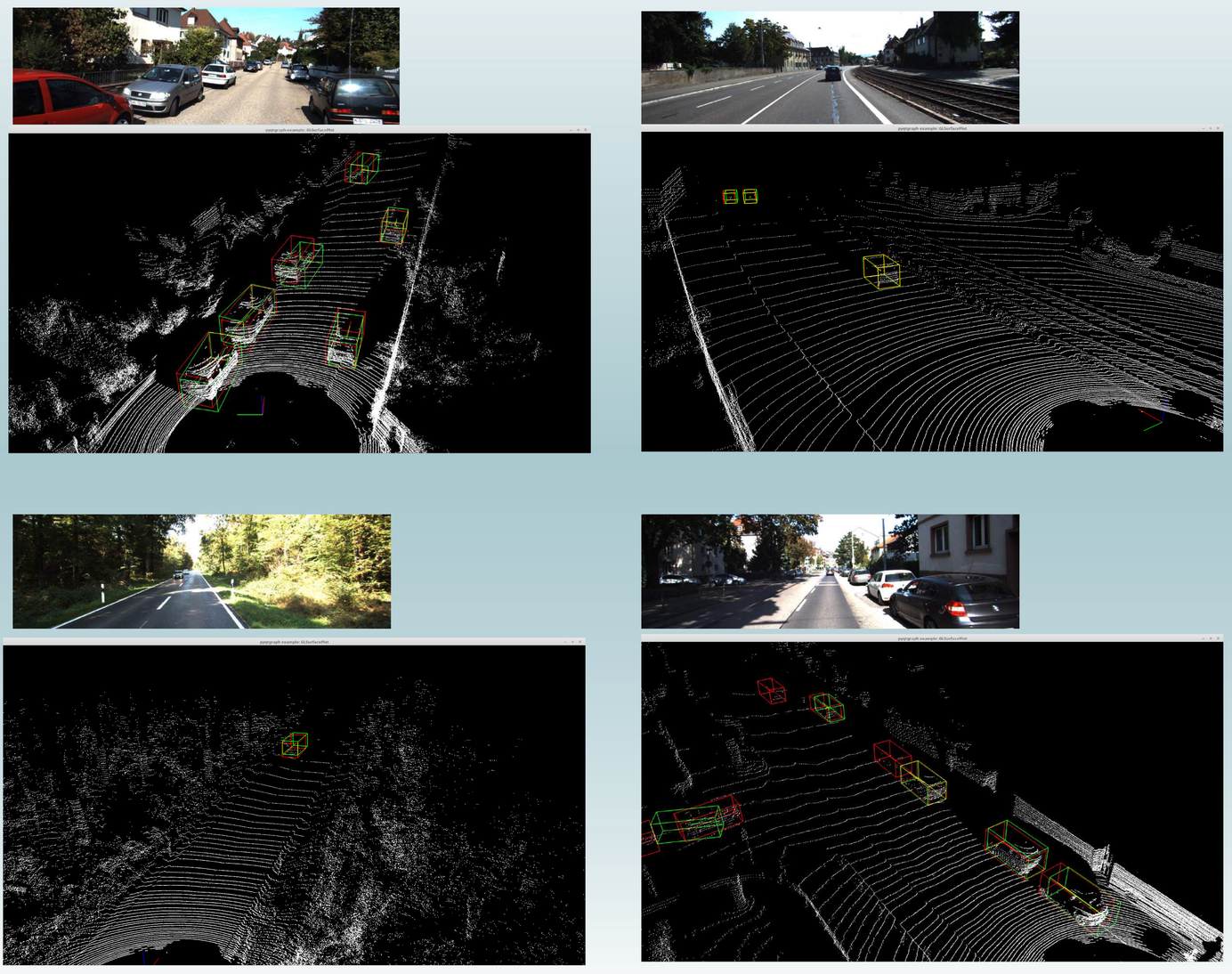

Cell Probabilities

- For each patch, the related space region is divided into 3 zones depending on the sensor values and the distance
- Region 1 : Obstacle probably present
- Region 2 : Obstacle probably missing
- Region 3 : Missing information

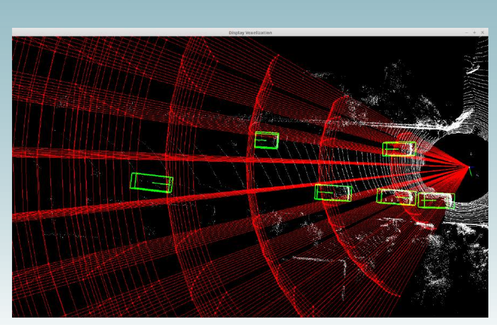

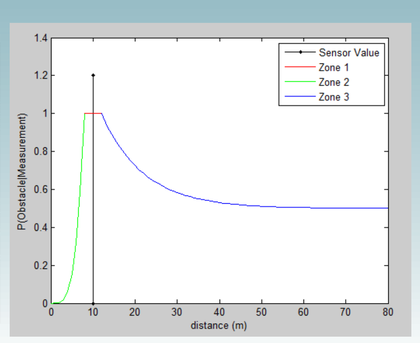

Future Work

- Improve accuracy, execution time and stability on sensor loss
- Adaptation to different types of LiDAR (resolution, FOV…)
- Data augmentation : Information Densification (Depth) or Prediction (Surface Normals, Ego Motion Pose…)
- Obstacle tracking and trajectory estimation

Bibliography

- Zhou, Y., & Tuzel, O. (2017). VoxelNet: End-to-End Learning for Point Cloud Based 3D Object Detection.
- Murphy, R., & Murphy, R. R. (2000). *Introduction to AI robotics*. MIT press.
- Ku, J., Mozifian, M., Lee, J., Harakeh, A., & Waslander, S. (2017). Joint 3D Proposal Generation and Object Detection from View Aggregation.
- Chen, X., Ma, H., Wan, J., Li, B., & Xia, T. (2017, July). Multi-view 3d object detection network for autonomous driving. In *IEEE CVPR* (Vol. 1, No. 2, p. 3).

EXPERIMENTAL VALIDATION OF A FINITE ELEMENT MODEL OF TRANSVERSALLY STIFFENED PANEL UNDER A DOUBLE PATCH LOADING

S. BOUGOFFA[1,2], S. DURIF[1], O. MEZGHANNI[2,3], A. BOUCHAÏR[1], A. DAOUD[2,3]

[1]Université Clermont Auvergne, Institut Pascal, BP 10448, F-63000 Clermont-Ferrand, France
[2]Université de Tunis El Manar, Ecole Nationale d'Ingénieurs de Tunis, LGC, BP 37, le Belvédère, 1002 Tunis, Tunisie
[3]Université de Sfax, Ecole Nationale d'Ingénieur de Sfax, Département de Génie Civil, Route de Soukra Km 3,5, BP 1173,3038, Sfax, Tunisie

Introduction

The transverse stiffeners are widely used in the field of steel construction. However, their design methods are poorly developed. In this study, the influence of the transverse stiffeners on the behavior of a cross-section under double localized compression is analyzed. Five configurations of transverse stiffeners are studied. They cover single and double stiffeners over a part or the whole height of the web panel. The stiffeners are welded or not to the flange. Real tests are performed to observe the behavior and to obtain the load-displacement curve of each configuration. Then, a finite element model is developed using Cast3m software with consideration of geometric and material nonlinearities. This numerical model is validated on the basis of the test results considering the resistance and the buckling modes of the tested panels.

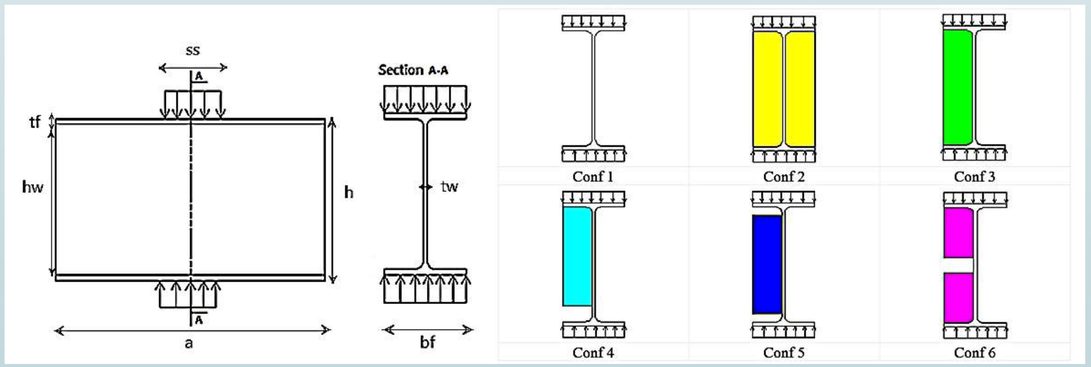

Configurations of tested transverse web stiffeners

Methods

TEST CAMPAIGN

Six specimens were tested at the MSGC platform (Pascal Institute and Polytech) of Clermont Auvergne University (dimensions summarized in the following table).

Geometric details of transverse web stiffeners

Model	h_w (mm)	t_w (mm)	t_f (mm)	b_f (mm)	$h_s^{(1)}$ (mm)	$t_s^{(2)}$ (mm)	Description
Conf. 1	278.6	7.1	10.7	150	--	--	Unstiffened
Conf. 2	278.6	7.1	10.7	150	278.6	8	double stiffener, all height
Conf. 3	278.6	7.1	10.7	150	278.6	8	simple stiffener, all height
Conf. 4	278.6	7.1	10.7	150	232.2	8	simple stiffener welded to a flange and a part of the web
Conf. 5	278.6	7.1	10.7	150	232.2	8	simple stiffener welded to the middle of the web
Conf. 6	278.6	7.1	10.7	150	232.2	8	simple stiffener welded to the two flanges and a part of the web

(1) h_s : the height of the stiffener
(2) t_s : the thikness of the stiffener

OPERATING MODE

The load is applied controlling the displacement rate to observe the post-failure modes (Testing machine with a capacity of 3000 kN). The load-displacement curves are continuously registered.

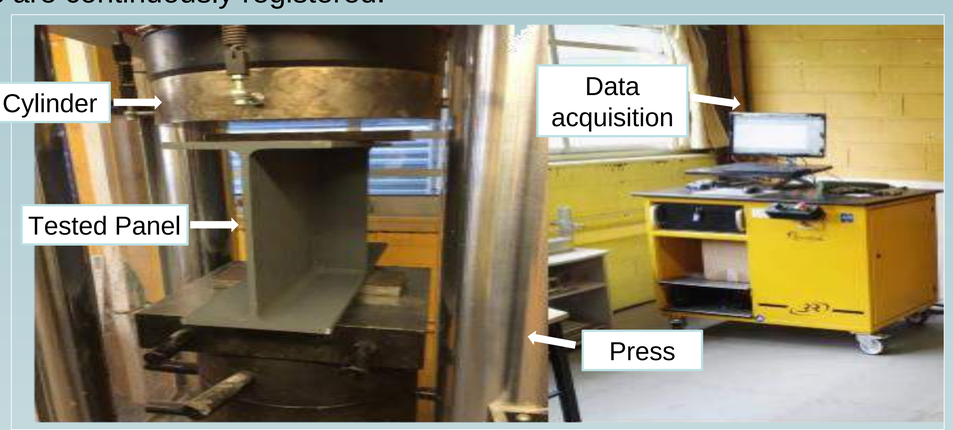

Experimental tests setup

FINITE ELEMENT MODELING

The finite element model is three-dimensional consisting of three-node DKT shell elements. The geometry is defined by the mean plane of each panel with the associated thickness of each element. The mesh density was chosen on the basis of a convergence study. The stiffeners are added considering their dimensions. The red part of the flange represents the loaded zone.

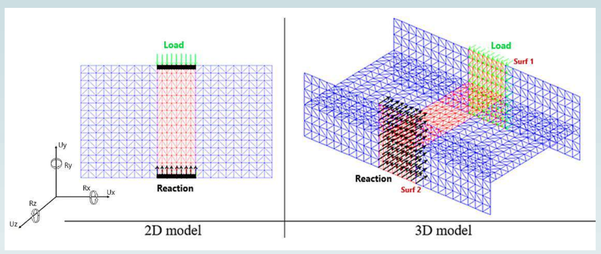

Finite element model

Boundary conditions

axis	Ux	Uy	Uz	Rx	Ry	Rz
Surf 1	◉		◉		◉	
Surf 2	◉	◉	◉	◉	◉	

◉ : blocked

Results

EXPERIMENTAL RESULTS

The test results concern mainly the load-displacement curves.

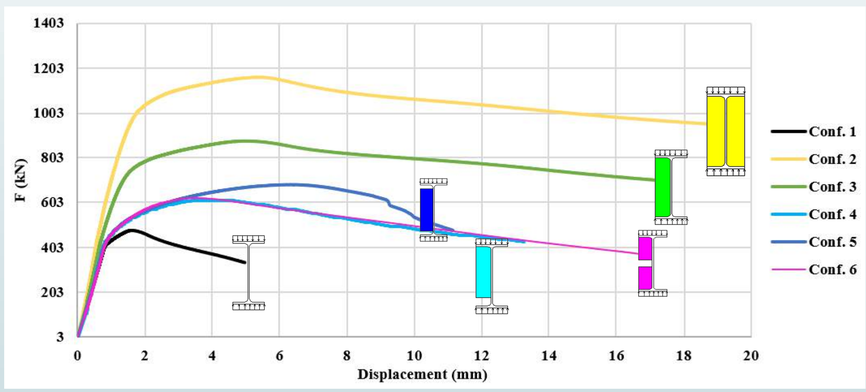

Load-displacement curves (experimental results)

VALIDATION OF THE FINITE ELEMENT MODEL

The numerical model is validated by comparison of its results with those of the tests (the load-displacement curves and the buckling modes).

load-displacement curves

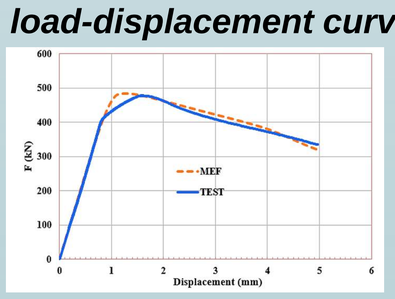

Load-displacement curves of Conf. 1

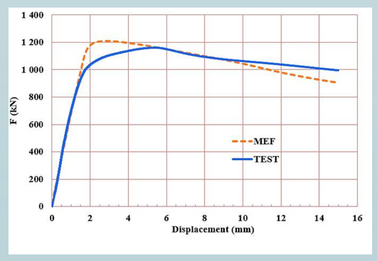

Load-displacement curves of Conf. 2

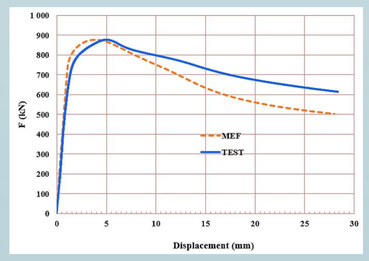

Load-displacement curves of Conf. 3

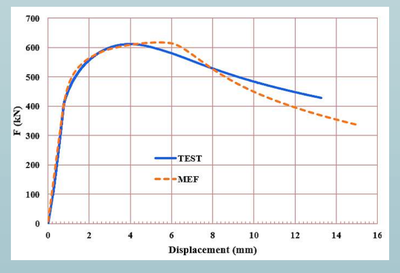

Load-displacement curves of Conf. 4

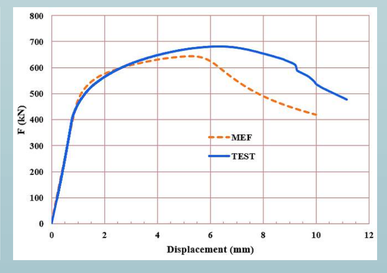

Load-displacement curves of Conf. 5

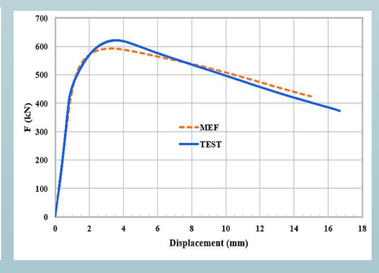

Load-displacement curves of Conf. 6

Buckling modes

real deformation of Conf. 1

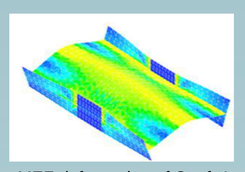

MEF deformation of Conf. 1

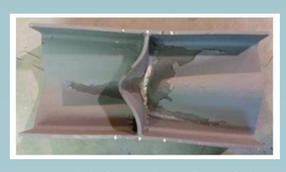

real deformation of Conf. 2

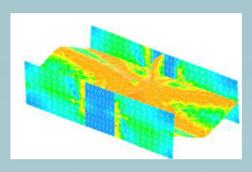

MEF deformation of Conf. 2

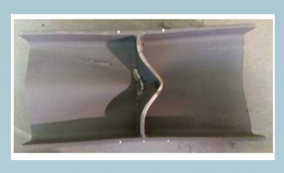

real deformation of Conf. 3

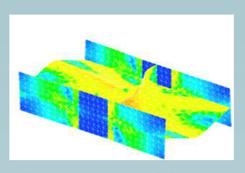

MEF deformation of Conf. 3

real deformation of Conf. 4

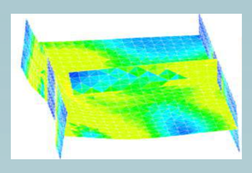

MEF deformation of Conf. 4

real deformation of Conf. 5

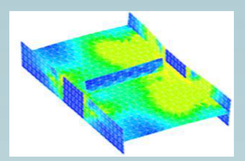

MEF deformation of Conf. 5

real deformation of Conf. 6

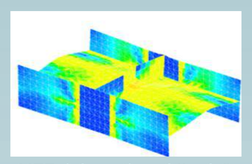

MEF deformation of Conf. 6

Conclusions

The present study analyzed the behavior of transverse stiffened web panels subjected to an opposite patch loading. A numerical model is developed using the CAST3M software and calibrated using the results of an experimental study. The behaviors of different shapes of stiffeners are examined showing that the addition of a transverse stiffener in all cases increases the strength of the panel. An analytical model is under development on the basis of a large parametric study performed using the validated finite element model.

Bibliography

1. **EN-1993-1-5 (2006), Eurocode 3 - Design of steel structures - Part 1-5: General rules: Plated structural elements.**
2. **EN-1993-1-8 (2006), Eurocode 3 - Design of steel structures - Part 1-8: Design of joints.**
3. **O. Mezghanni, J. Averseng, A. Bouchaïr, H. Smaoui, Behavior of beam web panel under opposite patch loading, J. Constr. Steel Res. 83 (2013) 51–61.**
4. **Sung C. Lee, Doo S. Lee, Chai H. Yoo, "Design of intermediate transverse stiffeners for shear web panels", Engineering Structures 75 (2014) 27-38.**

Elaboration of new polymer/nanocarbon hybrid materials : application as sensing materials for the detection of H_2S and NH_3

S. SAAD ALI, A. NDIAYE, A. PAULY, C. VARENNE, J. BRUNET
Université Clermont Auvergne, CNRS, Sigma Clermont, Institut Pascal, F-63000 Clermont-Ferrand, France

Institut de Chimie de Clermont-Ferrand

Ecole doctorale Sciences Pour l'Ingénieur

Introduction

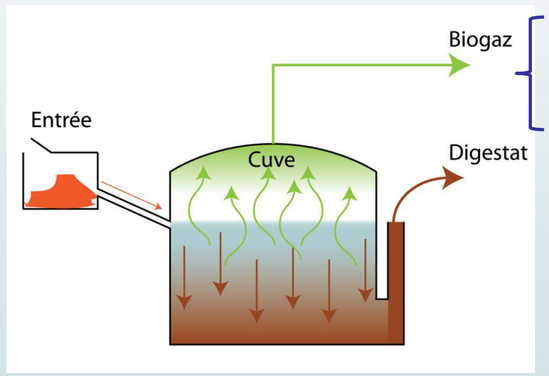

➢ *Control and monitoring of pollution of industrial sites (gas leaks)*

H_2S: highly toxic and flammable gas (toxicity threshold ~ 10-20ppm 6-7h)

NH_3 : Irritant and harmful gas (toxicity threshold ~ 50ppm 7h)

Make sensors sensitive to these gases below threshold toxicity

Methods

(1) Polyaniline

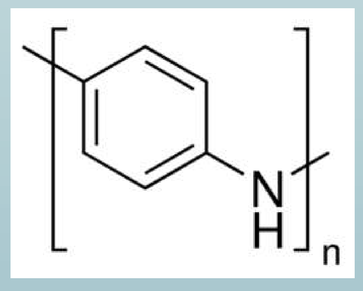

+

(2) Carbon Nanotubes

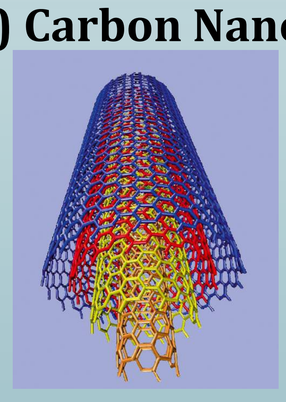

Functionalization

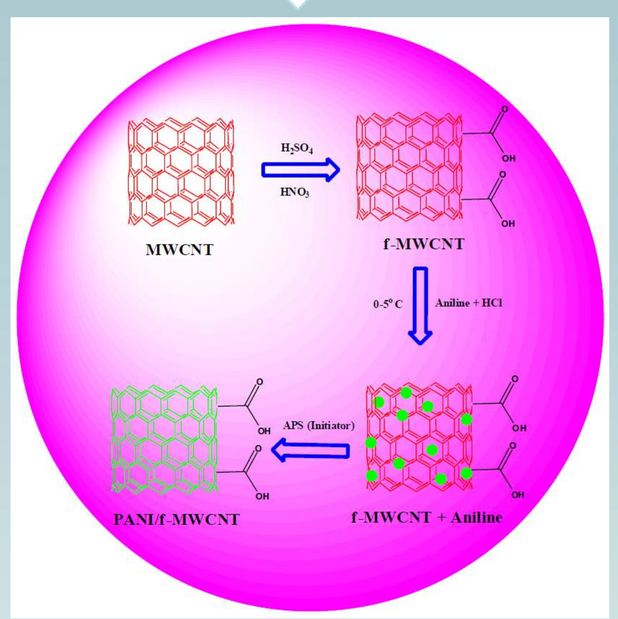

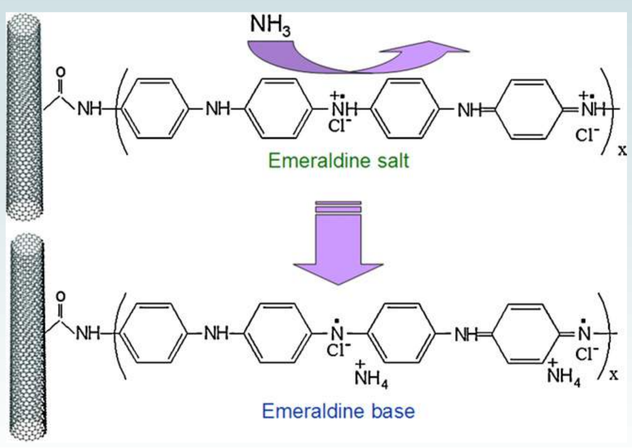

Results

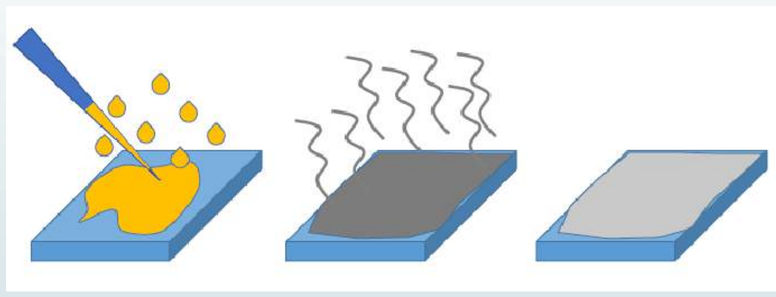

Deposition process

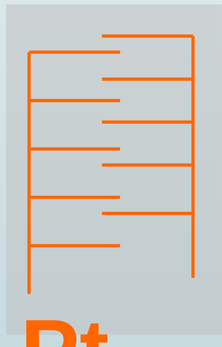

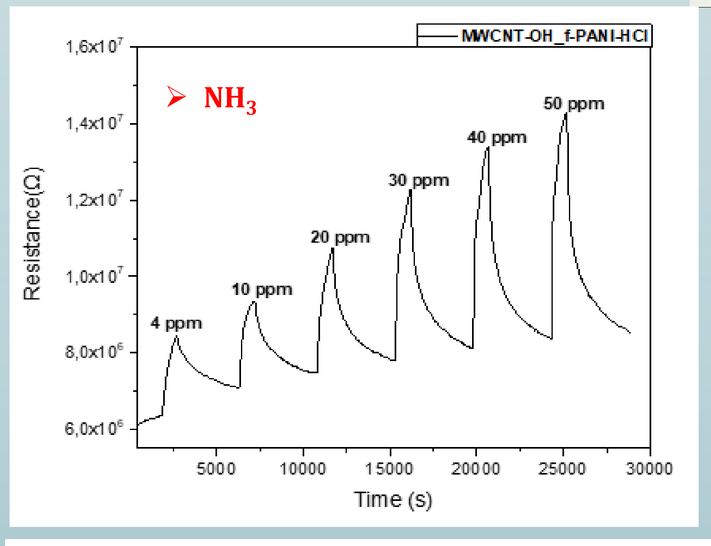

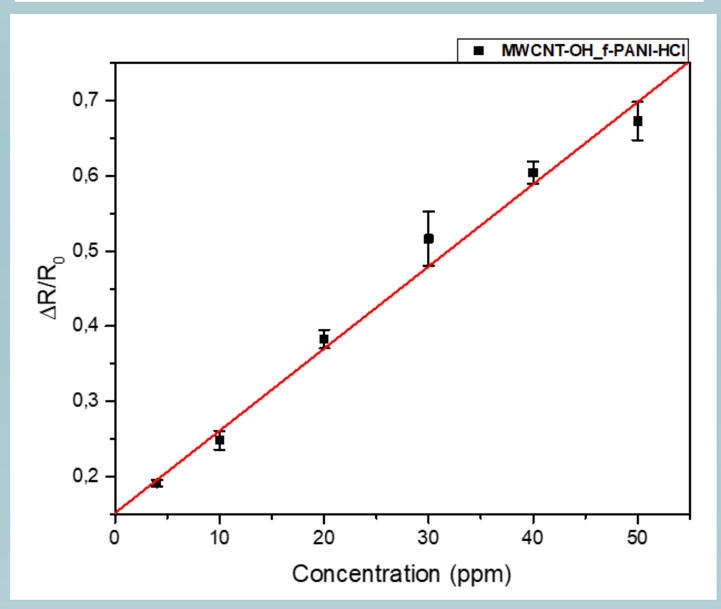

Conclusions

✓ **Functionalization PANI with MWCNT-OH➔ Increased performance of sensor (sensivity, stability, reproducibility)**

✓ **Interaction between PANI and MWCNT-OH ➔ Facilites electron delocalisation in the composites**

✓ **Real test condition, in air and room temperature**

Acknowledgement

This work was carried out within the **framework** of LABEX IMobS3 (Innovative Mobility: Smart and Sustainable Solutions) supported by the National Centre for Scientific Research (CNRS), the Regional Council Auvergne, the European Regional Development Funds (ERDF/FEDER) and the National Research Agency (ANR) (Grant No. ANR-10-LABX-16-01).

Embedded real-time system for motion and deformation measurement

Seyfeddine BOUKHTACHE

Institut Pascal : ISPR

Introduction

- Digital image correlation (DIC) is a popular and efficient technique for motion and deformation measurements as it provides sub-pixel accuracy. But it represents a significant drawback, extremely huge computational (iterative algorithm, ...).
- The current solution consists on off-line processing

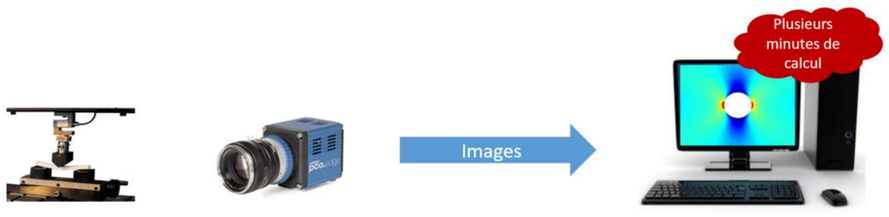

Figure 1: Current solution

Objectives

- Field-Programmable Gate Array (FPGA) for real-time: parallelism, pipeline

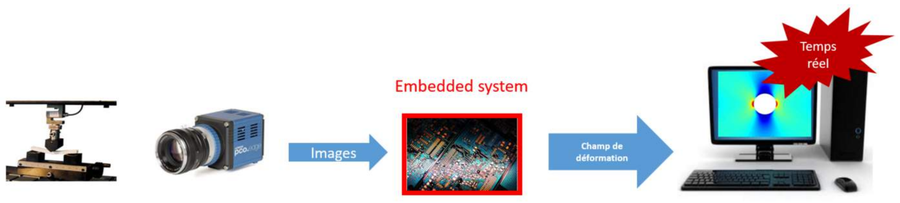

Figure 2: smart camera

1. Real-time
2. Achieve high-accuracy $\mathbf{(10^{-3})}$
3. Optimal architecture (Logic, DSP, memory, area and operating frequency)

DIC principle

- Track each image pixel by comparing gray level values of the images taken before and after deformation.
- Many pixels in the deformed image may have the same gray level value, hence neighboring pixels are used.

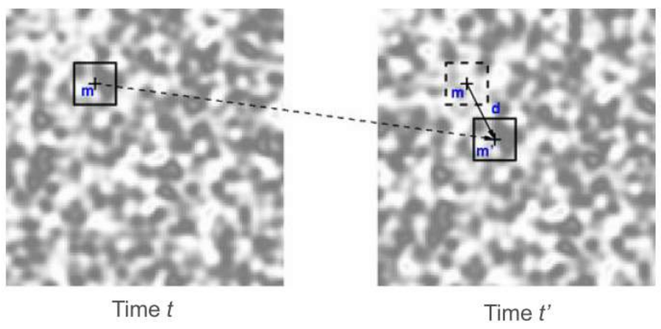

Figure 3: Subset Tracking

- DIC is based on minimizing the gray value difference between a reference subset and deformed subset [1].

$$U(X_0) = argmin \sum_{RoI} [f(X_0) - g(X_0 + U(X_0))]^2 dX_0 \qquad (1)$$

Algorithm

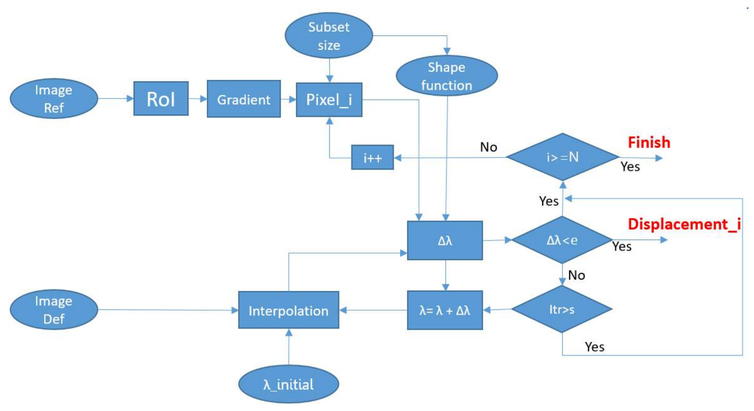

Figure 4: DIC algorithm

Interpolation

Method	Bi-linear	Bi-cubic	B-spline
Complexity	Low	Complex	Difficult to implement
Accuracy	Low	High	Excellent

Table 1: Interpolation methods [2]

Results (Matlab)

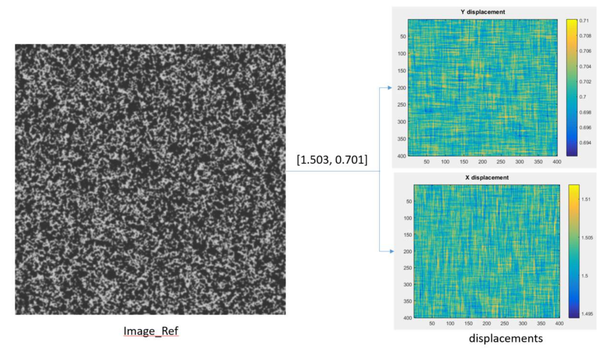

Figure 5: Translation of [1.503,0.701]

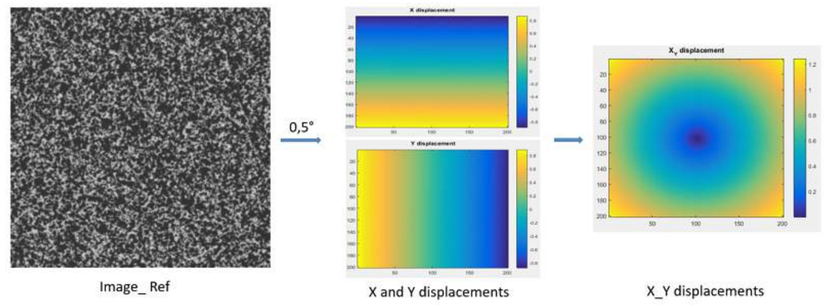

Figure 6: Rotation of 0.5°

Implementaion of Bi-cubic interpolation

- Hardware architecture
  - ▷ Mathematic reformulation
  - ▷ Avoiding redundant computations
- Coefficients block
- 5 bi-cubic sub-block

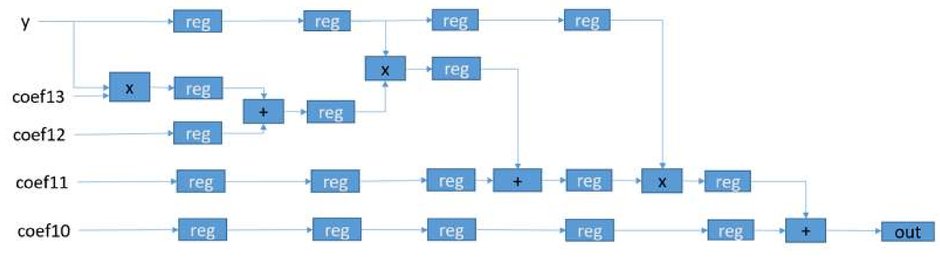

Figure 7: Bi-cubic sub-block

- The algorithm is coded in VHDL and implemented into FPGA Cyclone V

Image size	Frequency max	DSP(18x18)	Logic (ALMs)	Memory (bits)
1024x1024	204 MHz	15 (17%)	1786 (6%)	30657 (< 1%)

Table 2: Resources utilization report

Conclusion and perspectives

- Bi-cubic interpolation is selected because it represents the best trade-off between complexity and accuracy. Our proposed architecture improves the operating frequency [3] and it is well suited for practical real-time applications such as DIC.
- As a perspective, the implementation of DIC based on bi-cubic interpolation is envisaged.

References

[1] Michael A. Sutton, Jean-Jos Orteu and Hubert W. Schreier. *"Image Correlation for Shape, Motion and Deformation Measurements"*. *Springer, 2009*

[2] Han, D. *"Comparison of Commonly Used Image Interpolation Methods"*. *2nd International Conference on Computer Science and Electronics Engineering (ICCSEE 2013), (Iccsee), 15561559.*

[3] G.Mahale, H.Mahale, R.B.Parimi, S.K.Nandy, S.Bhattacharya. *"Hardware Architecture of Bi-Cubic Convolution Interpolation for Real-time Image Scaling"*. *International Conference on Field-Programmable Technology (FPT) 2014 .*

Contact Information

- Email: seyfeddine.boukhtache@uca.fr

Conception of robotic hands with electormyographic signals

Kirchhofer Simon

Institut Pascal / UCA / SIGMA / CHU de Clermont-Ferrand

Ecole doctorale Sciences Pour l'Ingénieur

Introduction

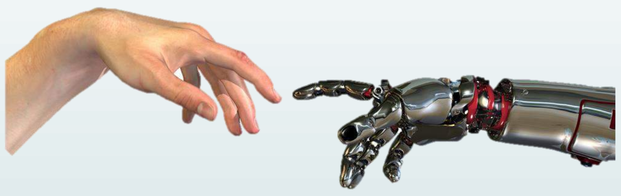

Robotic hands turn on revolutionary perspectives for people with disabilities. However, numerous technical issues are still hard to override in order to design systems as efficient as the human hand. The main difficulties are the human-machine interface and the conception that must be compact, powerful and precise. Nowadays, electromyographic signals seem to be relevant to control such systems but the design is isolated from the signal processing. Robotics hands are developed only with a biomechanical approach [1][2][3][4] and the signals used for the control are ignored. The goal of this PhD is to use the EMG signal in order to get a conception in line with the control capabilities.

Methods

The first step is to understand the link between the electromyographic signal and the motion of a human hand. This is needful to create the control of a prosthetic device from EMG.

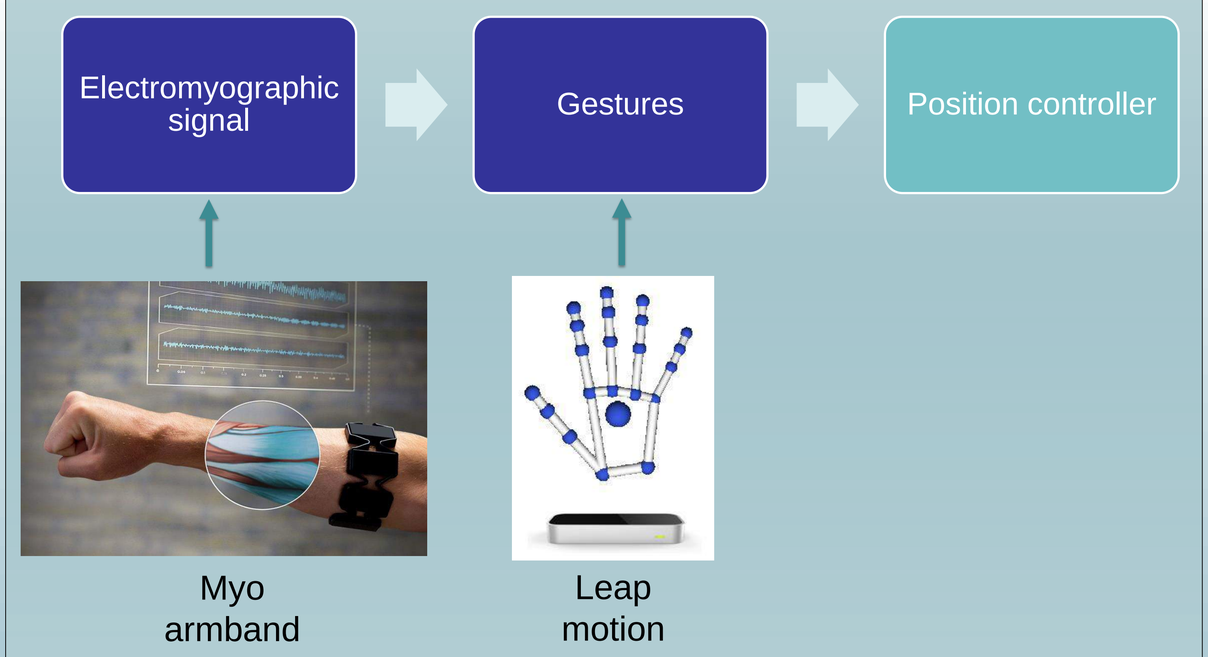

Then, an initial design of the hand will be developed. It will be used as the starting point of an optimization loop. Reinforcement learning algorithms are likely to be used.

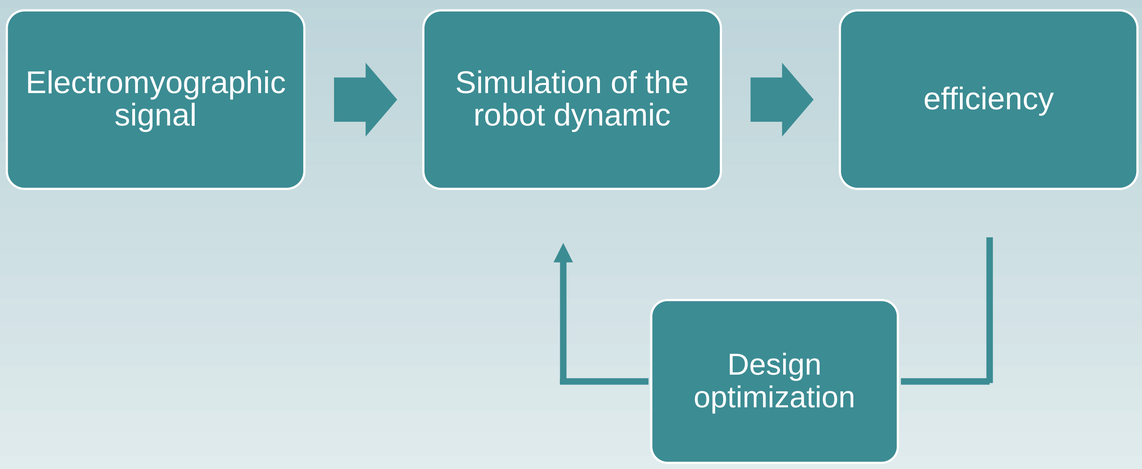

Results

The state of the art in electromyographic processing focuses on the classification of gestures with EMG [5]. As the number of gesture is limited (usually pronation/supination, flexion/extension of the wrist and opening/closing of the hand), we tackle the issue with a regression analysis that estimates the joint coordinates of the hand from the EMG signal. A Kinematic model was developed and the regression was build with a recurrent network.

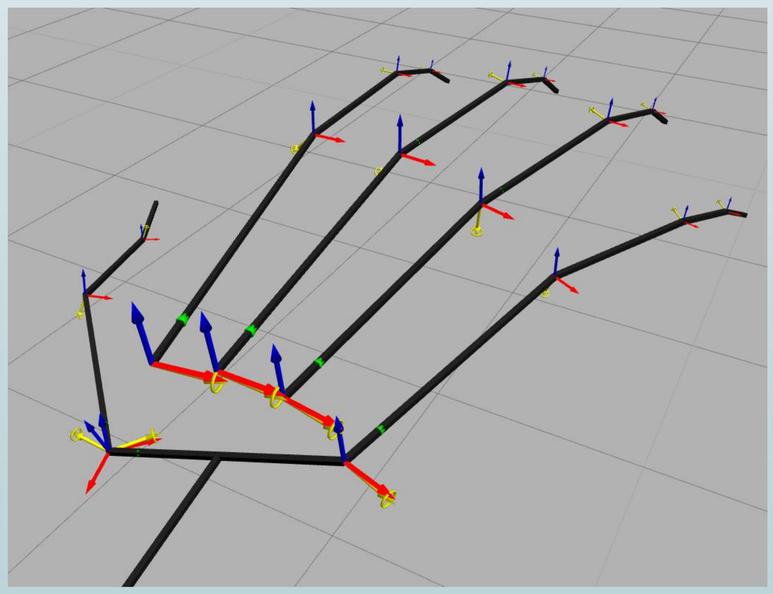

Kinematic model

Preliminary results

With a small dataset (record of 1 person for several minutes), the training converges. We need to create a database to validate the concept and evaluate the robustness via the study of the differences between people, the impact of muscle fatigue, the importance the sensor positioning, etc.

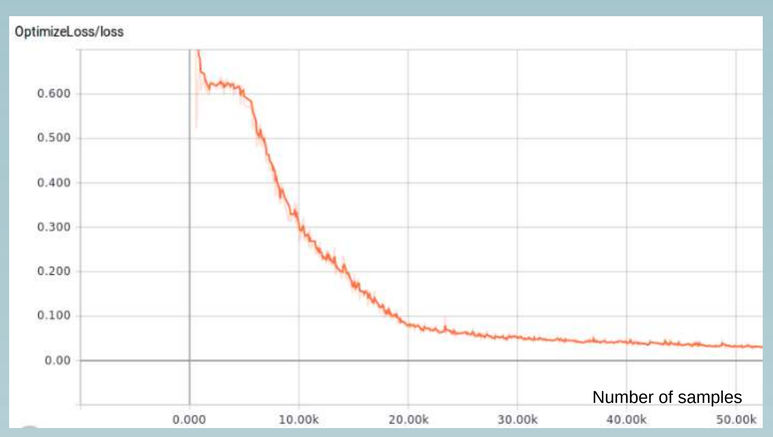

Conclusions

First results are hopeful, they match the current evolution of the state of the art. Nevertheless, we must keep in mind that a lot of shortcomings still need to be addressed. Mainly, the forces generated by the fingers are not measured or estimated. It seems relevant to include it in the signal processing as the force is significant for the success of grasping tasks.

Bibliography

[1] **LTD S.R.**C., "Shadow hand Website." [Online]. Available: https://www.shadowrobot.com/products/dexterous-hand/ (Accessed 2016-12-24).

[2] **H. Liu, K. Wu, P. Meusel, N. Seitz, G. Hirzinger, M. Jin, Y. Liu, S. Fan, T. Lan, and Z. Chen**, *"Multisensory five-finger dexterous hand: The dlr/hit hand ii,"* in IEEE/RSJ International Conference on Intelligent Robots and Systems, 2008, pp. 3692-3697.

[3] **D. Keymeulen and C. Assad**, *"Investigation of the harada robot hand for space,"* in IEEE RAS Internation Conference on Humanoid Robots University International Conference Center, Tokyo, Japan, 2001, pp. 749-754.

[4] **"Prensilia Srl webpage." [Online]**. Available: http://www.prensilia.com/index.php?q=en/node/40 (Accessed 2016-12-15).

[5] **U. Côté-Allard, C. Latyr Fall, A. Drouin** "Deep Learning for Electromyographic Hand Gesture Signal Classification by Leveraging Transfer Learning" in CoRR, feb 2018, vol abs/1801.07756 http://arxiv.org/abs/1801.07756

Diagnosis of optimal solutions in refinery planning

UNIVERSITÉ Clermont Auvergne

Ecole doctorale Sciences Pour l'Ingénieur

Stéphane GERMAIN

LIMOS

The refinery planning problem

Scope :

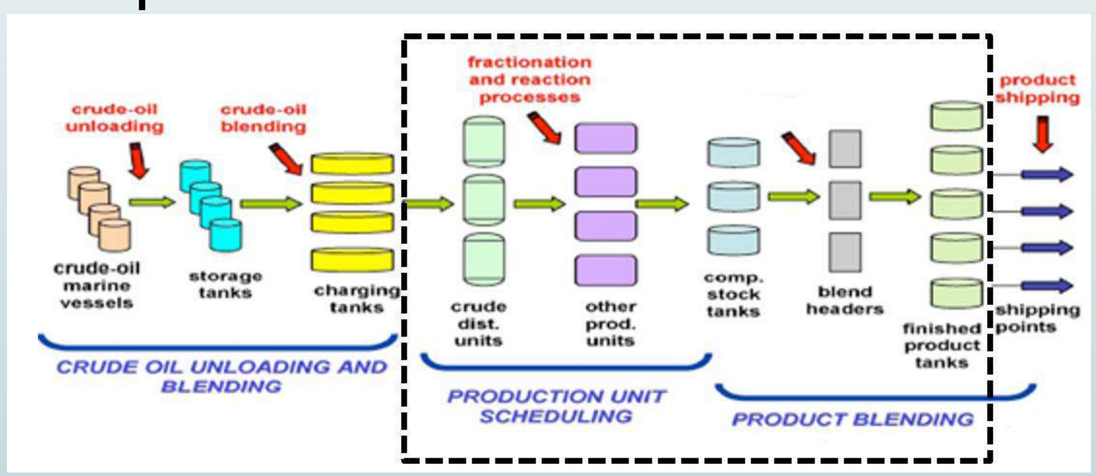

Input :

- Graph of the refinery (cf below)
- Set of crude oil
- Initial stock
- Parameters, prices and contracts

Ouput :

- Process units tuning
- State (quantity and qualities) of all the stream

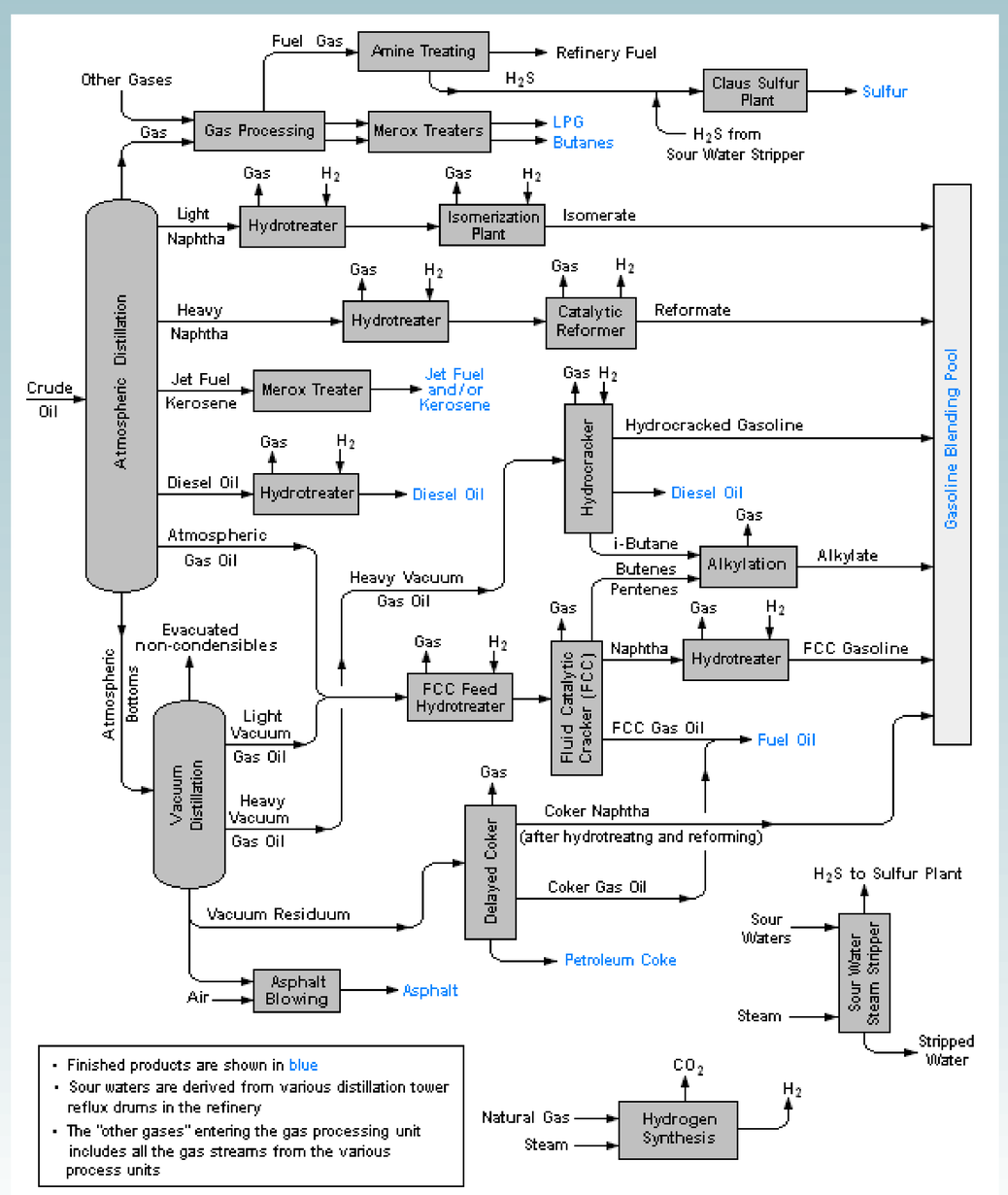

Problem formulation

x_b^F	Quantity of crude oil b sent to the CDU
$x_{b,m}^F$	Quantity of crude oil b distilled in mode m
y_v	Quantity in the node v
$x_{u,v}$	Quantity of the stream between nodes u and v
q_v^t	Value of quality t at node v
$q_{u,v}^t$	Value of quantity t between the nodes u and v

$$
P_{PGM}\begin{cases}
min & \sum_{b\in\mathcal{B}} c_b x_b^F + \sum_{u\in\mathcal{U}} h_u(y_u) - \sum_{p\in\mathcal{P}} c_p y_p & \\
s.t. & & \\
(1) & x_b^F = \sum_{m\in\mathcal{M}} x_{b,m}^F & \forall b\in\mathcal{B} \\
(2) & \sum_{b\in\mathcal{B}} x_b^F \le \overline{CDU} & \\
(3) & \sum_{b\in\mathcal{B}}\sum_{m\in\mathcal{M}} a_{j,m} x_{b,m}^F \le \overline{PC_j} \sum_{b\in\mathcal{B}} x_b^F & \forall j\in[1..|\mathcal{K}|+1] \\
(4) & \sum_{b\in\mathcal{B}}\sum_{m\in\mathcal{M}} a_{j,m} x_{b,m}^F \ge \underline{PC_j} \sum_{b\in\mathcal{B}} x_b^F & \forall j\in[1..|\mathcal{K}|+1] \\
(5) & y_k = \sum_{b\in\mathcal{B}}\sum_{m\in\mathcal{M}} \alpha_{b,m}^k x_{b,m}^F & \forall k\in\mathcal{K} \\
(6) & q_k^t y_k = \sum_{b\in\mathcal{B}}\sum_{m\in\mathcal{M}} q_{k,b,m}^t x_{b,m}^F & \forall k\in\mathcal{K}, \forall t\in\mathcal{Q} \\
(7) & y_k = \sum_{v\in succ_k} x_{k,v} & \forall k\in\mathcal{K} \\
(8) & q_{k,v}^t = q_k^t & \forall t\in\mathcal{Q}, \forall v\in succ_k \\
(9) & y_u = \sum_{v\in pred_u} x_{v,u} & \forall u\in\mathcal{U} \\
(10) & q_u^t y_u = \sum_{v\in pred_u} q_{v,u}^t x_{v,u} & \forall u\in\mathcal{U}, \forall t\in\mathcal{Q} \\
(11) & x_{u,v} = f_0^{u,v}(q_u, In_u) y_u & \forall u\in\mathcal{U}, \forall v\in succ_u \\
(12) & q_{u,v}^t = f_t^{u,v}(q_u, In_u) & \forall u\in\mathcal{U}, \forall t\in\mathcal{Q}, \forall v\in succ_u \\
(13) & Out_u = f_{Out}^{u,v}(q_u, In_u) & \forall u\in\mathcal{U}, \forall v\in succ_u \\
(14) & y_c = \sum_{v\in pred_c} x_{v,c} & \forall c\in\mathcal{C} \\
(15) & q_c^t y_c = \sum_{v\in pred_c} q_{v,c}^t x_{v,c} & \forall t\in\mathcal{Q}, \forall c\in\mathcal{C} \\
(16) & y_p = \sum_{c\in\mathcal{C}_p} x_{c,p} & \forall p\in\mathcal{P} \\
(17) & q_p^t y_p = \sum_{c\in\mathcal{C}_p} q_{c,p}^t x_{c,p} & \forall p\in\mathcal{P}, \forall t\in\mathcal{Q} \\
(18) & q_p^t \le S_p^t & \forall p\in\mathcal{P}, \forall t\in\mathcal{Q} \\
(19) & y_p \ge D_p & \forall p\in\mathcal{P} \\
(20) & \underline{OP_u^i} \le OP_u^i \le \overline{OP_u^i} & \forall u\in\mathcal{U}, \forall i\in Out_u
\end{cases}
$$

First results

Tool under development to visualize the impact of desaturating a constraint.

Saturated constraint in a solution : dual value of 7$/t.

7 = Impact on purchases + impact on sales

How much and why ?

Bibliography

1. **Pinto, J. M., Joly, M., & Moro, L. F. L. (2000). Planning and scheduling models for refinery operations. Computers & Chemical Engineering, 24 (9), 2259-2276**
2. **Mouret, S. (2010). Optimal scheduling of refinery crude-oil operations. PhD thesis, Carnegie Mellon University**
3. **Greenberg, H. J. (1992). Intelligent analysis support for linear programs. Computers and chemical engineering, 16 (7), 659-673**
4. **Borgonovo, E., and Plischke, E. (2016). Sensitivity analysis : A review of recent advances. European Journal of Operational Research, 248(3), 869-887**

Image Segmentation on Laparoscopic Images using Deep Learning for Augmented Reality

Tom FRANCOIS - Supervisors: Adrien BARTOLI, Lilian CALVET and Damien SABOUL.

Université Clermont Auvergne, CHU Clermont-Ferrand, CNRS, SIGMA Clermont, Institut Pascal, F-63000 Clermont-Ferrand, France

Introduction

- Numerous diseases are nowadays treated using minimal invasive surgery to access the internal anatomy of the patient. Contrary to open surgery which requires a large incision of the abdominal wall to gain access to a lesion, laparoscopic surgery requires smaller incisions and is less traumatizing.

Figure 1: Laparoscopic surgery.

- One of the goals of medical Augmented Reality (AR) is to reveal the hidden anatomy, such as a tumour or major blood vessels within an organ. The EnCoV team has developped an AR system for gynecology to augment tumors inside the uterus.

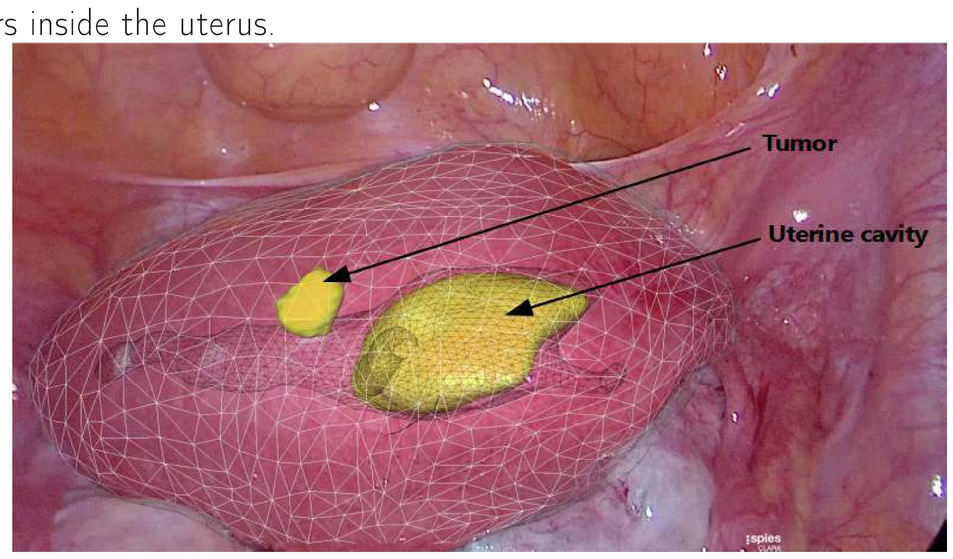

Figure 2: Augmentation of an uterus during a surgery.

- The current AR system requires manual inputs like annotating the live video to locate the organ. The goal on this project is to replace these manual steps using deep learning approaches. Convolutional Neural Networks (CNN) can now solve challenging computer vision issues.

Creation of a Custom Dataset

- No public dataset is available for uterus segmentation in laparoscopy.
- We are currently collecting data from surgeries performed by members of EnCoV. An annotated dataset containing laparoscopic images of gynecologic operations is being built based on these live videos. Still images are extracted and manually annotated. Compared to common object datasets (the COCO dataset contains more than 200K annotated images), ours is currently really small (350 annotated images).

First Results

- Transfer learning: Transfer learning is a way of reusing a model trained on a first dataset by finetuning on another specific dataset. In our case, we reused a model trained on the COCO Dataset [1] (persons, vehicles, animals, ...) and finetuned an instance segmentation system [2] with our custom dataset. These results of this approach can be seen in Figure 3. This approach is currently limited by the low quantity of annotated data available.

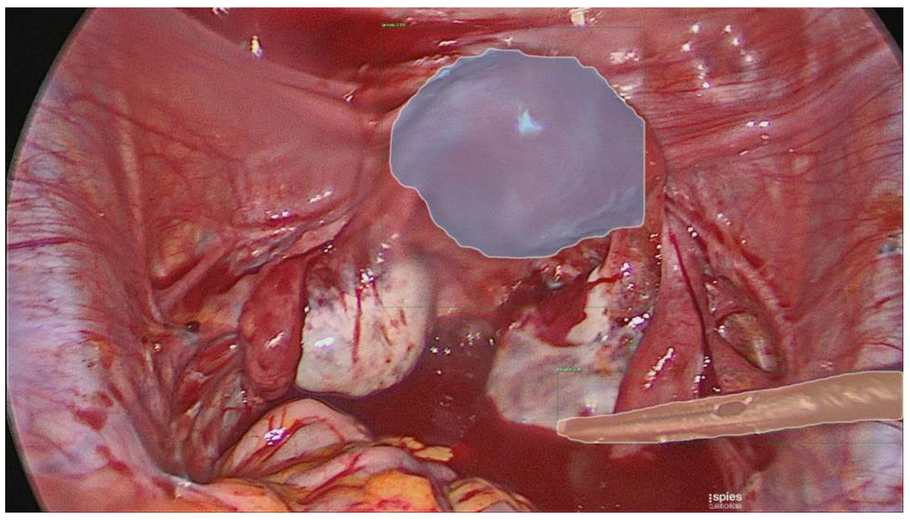

Figure 3: Automatic detection and segmentation of the uterus (blue) and surgical tool (yellow).

Current Approach

- The AR system need to register the preoperative data, that contain the 3D model of the uterus and the tumors (b), with the intraoperative video stream of the surgery (c) (see Figure 4). One of the cues we are using to perform this is the occluding contours of the uterus. We want to develop a deep learning algorithm to extract these contours from frames extracted of the video stream.

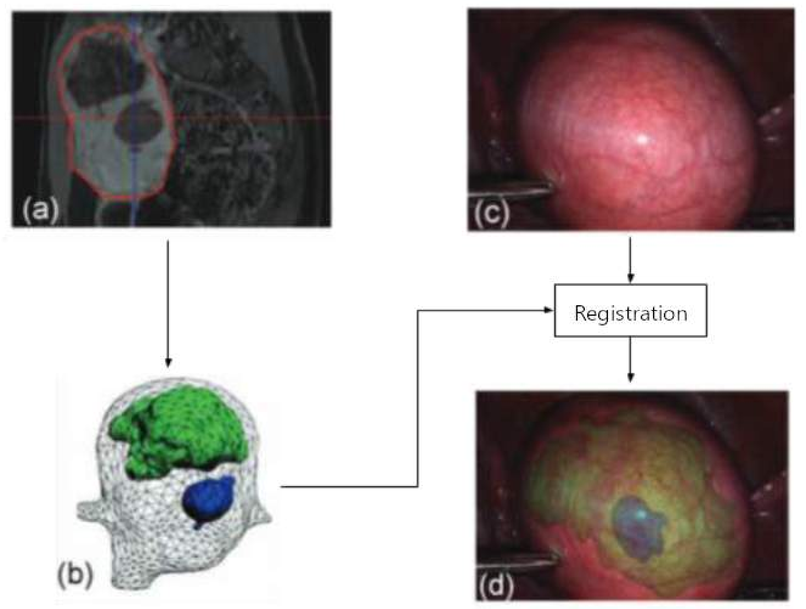

Figure 4: Diagram of the process of our AR system

- In order to pretrain our CNN, we use an external contours extractor to create the annotated data. Once our model is trained, we finetune this to detect different type of contours : occluding contours of the uterus, surgical tool contours, etc. (see Figure 5).

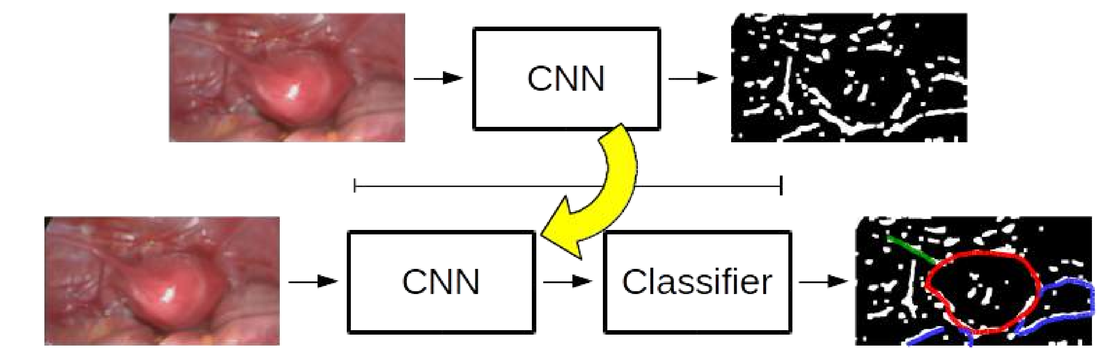

Figure 5: The top row illustrate a first learning phase to train a CNN to extract contours from laparoscopic images. The bottom row presents a second learning phase using the previous CNN models to classify contours (uterus occluding contours, surrounding organ contours, etc).

Conclusion

Using deep learning methods on the augmented reality system could help clinicians perform their surgery more precisely and eventually faster.

Next steps

- Increase the size of our laparoscopic dataset.
- Complete and improve our solution to automatically classify and extract contours of the organ to perform the 3D registration between preoperative and intraoperative data.

Acknowledgments

- This research is conducted within a CIFRE convention between Almerys (Be-Studys) and EnCoV (Institut Pascal).

References

[1] Tsung-Yi Lin, Michael Maire, Serge Belongie, James Hays, Pietro Perona, Deva Ramanan, Piotr Dollár, and C Lawrence Zitnick.
Microsoft coco: Common objects in context.

[2] Kaiming He, Georgia Gkioxari, Piotr Dollár, and Ross Girshick.
Mask r-cnn.

[3] Carl Doersch, Abhinav Gupta, and Alexei A. Efros.
Unsupervised visual representation learning by context prediction.

Modeling psychological and social mechanisms involved in transformational adaptation

Y.de Cacqueray Valmenier, G.Deffuant, S.Huet

Laboratory of Engineering for Complex Systems (LISC)

Objective

- Simulating the dynamics of transformational adaptation at the level of a population by synthesizing literature of adaptation psychology and sociology in an agent-based model

Introduction

- Climate change, biodiversity decline, change in nitrogen cycle and many others widening issues have already a decisive impact on economic development and social stability
- All these evolutions, combined with the unprecedented connectivity and complexity of societies, are shaping a context in which crises are increasingly frequent, intense, and unpredictable
- Responses mainly irrelevant and counterproductive in long-term since worldviews of decision-makers not in line with global context
- Transformational adaptation are often required to change the decision context of actors, and thus enable to engage persistently in pathway to sustainability

Materials

- Factors of Change:
  - internal (values, worldviews)
  - external (social network, overall situation)
- Barriers to Adaptation:
  - psychological (unfavorable attitude)
  - social (unfavorable institutions)
  - technical (unfavorable facilities)
- Considering Transformational Options:
  - more likely in multi stressors context
  - first incremental adaptations, then transformational
- Adopting Transformational Options :
  - Theory of Planned Behavior [1] for capturing all motivational factors
  - Intention to adopt depends on attitude, subjective norm and perceived behavioral control

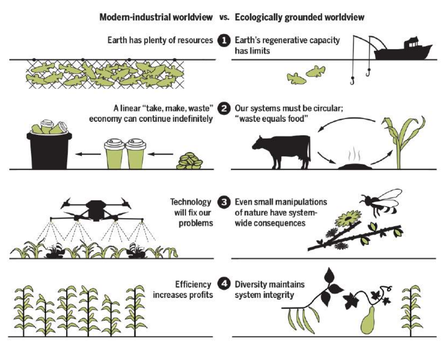

Figure 1: Example of psychological barrier in farming context [2]

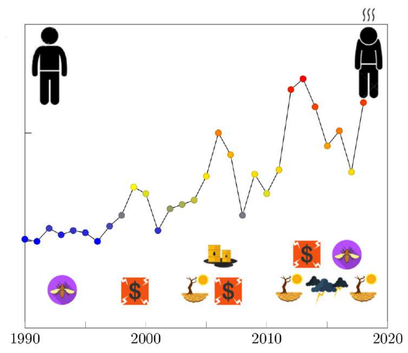

Figure 2: Illustration of increasing need for change in farming context

Methods

Implementation of process of transformational adaptation in an agent-based model.

- Proposed Process:
  1. habitual routine :
     - evaluation through current worldview and social group
  2. perturbation :
     - change of environment and social influences
  3. possible responses :
     - search informations
     - consider alternative from neighbor
  4. when considering
     - evaluation through both worldviews and social groups
  5. adoption and internalization
     - new behavior, worldview and social group
     - return to habitual routine
- Cognitive Elements:
  - Value : Reference for evaluating a practice, for considering alternatives and for searching informations. Constant during the simulation.
  - Worldview : bounds attitude of agent. Two types of worldview possibles : one based on beliefs oriented toward resilience (worldview R), one based on beliefs toward narrow efficiency (worldview E).

Mathematical Section

Cognitive functions

- Attitude:

$$\text{Att(practice)} = \begin{cases} \mathbf{0.5} \times \text{value(practice)} + 0.5 \text{ if worldview R} \\ \mathbf{0.5} \times \text{value(practice)} \text{ if worldview E} \end{cases} \quad (1)$$

- Subjective Norm:

$$\text{Sn(practice)} = \begin{cases} \text{mean of Att(practice) of similar neighbors} \\ \mathbf{0.5} \text{ if no similar neighbor} \end{cases} \quad (2)$$

- Perceived Behavioral Control:

$$\text{Pbc(practice)} = \mathbf{1} - \text{ Impact } * \mathbf{(1} - \text{Level of resilience of the practice}\mathbf{))} \quad (3)$$

- Evaluation:

$$\text{E(practice)} = \begin{cases} 1/3 \times (\text{ Att(practice)} + \text{Sn(practice)} + \text{Pbc(practice)} \text{)} \\ 1/2 \times (\text{ Att(practice)} + \text{Sn(practice)} \text{) if no info on pbc} \end{cases} \quad (4)$$

Response to perturbation

$$\text{if E(current practice)} < \text{value, then search information and consider} \quad (5)$$

$$\text{if} \left\{ \begin{array}{c} \text{PBC(current practice)} < \text{value} \\ \text{alternative in local network} \end{array} \right\} \text{ then consider} \quad (6)$$

Adoption of the alternative

$$\text{if E(current practice)} < \text{E(alternative practice), then adoption} \quad (7)$$

Results

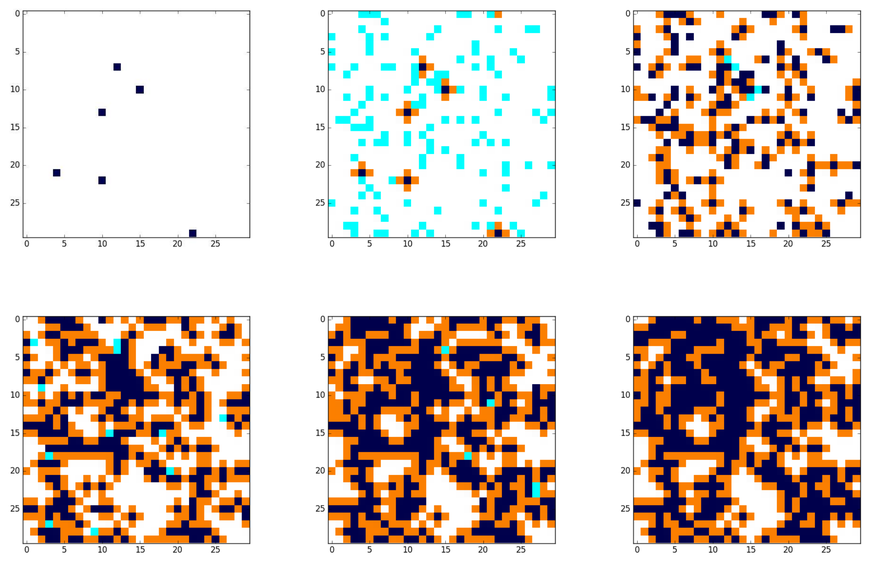

Figure 3: Maps of the population where each pixel represents an agent. Shock triggered on the first map. White : no adoption, orange : considered, light blue : informed, dark blue : adopted.

Conclusion

- Adopters are first the ones with high value, then the ones in high difficulty
- Some agents do not adopt because of low value or no access to information

References

[1] Icek Ajzen.
The theory of planned behavior.
Organizational behavior and human decision processes, 50(2):179–211, 1991.

[2] Elise Amel, Christie Manning, Britain Scott, and Susan Koger.
Beyond the roots of human inaction: Fostering collective effort toward ecosystem conservation.
Science, 356(6335):275–279, 2017.

Acknowledgments

- We acknowledge funding from the Auvergne-Rhône-Alpes region (France)

Contact Information

- Web: http://www.irstea.fr/lisc
- Email: yannick.de-cacqueray-valmenier@irstea.fr

Visual SLAM with automatic map update in a dynamic environment

Youssef Bouaziz, Eric Royer, Guillaume Bresson and Michel Dhome

Institut Pascal, University of Clermont Auvergne

Introduction

- In recent years, Simultaneous Localization and Mapping (SLAM) has emerged as a powerful algorithm for real-time localization of smart vehicles in urban environments. Current algorithms are adapted to an environment supposed to be rigid and static in time. But the environment is constantly changing. Automatic updating of the 3D model is a difficult problem but crucial from an application point of view. There are several types of changes that need to be treated differently. Typically in an urban scene:
  - Some elements are long-term stable (buildings, streets, floor, ...). These elements are modified rarely and for long durations.
  - Some elements are temporary like parked cars but are always in the same areas.
  - Other elements have a stable geometry but change their appearance (for example an advertising board which displays is changed).

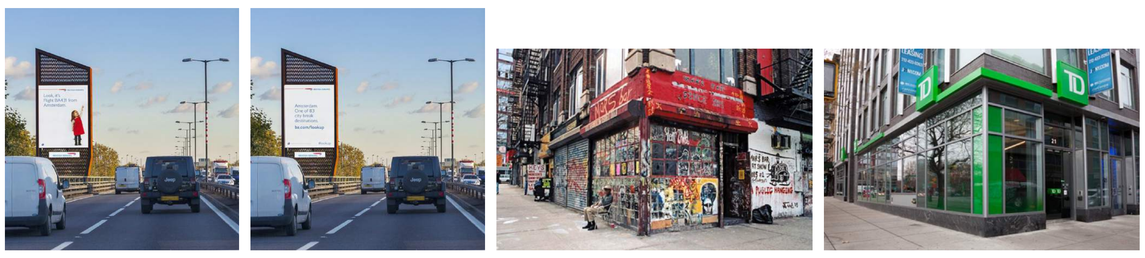

Challenges

- Seasons
- Day/Night
- Viewpoint

Loop closure

- Loop-closure detection is crucial for enhancing the robustness of both topological and metrical SLAM algorithms. This problem consists in detecting when the robot has returned to a past location after having discovered new terrain for a while. Such detection makes it possible to increase the precision of the actual pose estimate. Recognizing previously mapped locations can also be relevant for addressing the global localization problem. Hence, solving the loop-closure detection problem not only improves SLAM performances, but it enables additional capabilities to mobile robots.

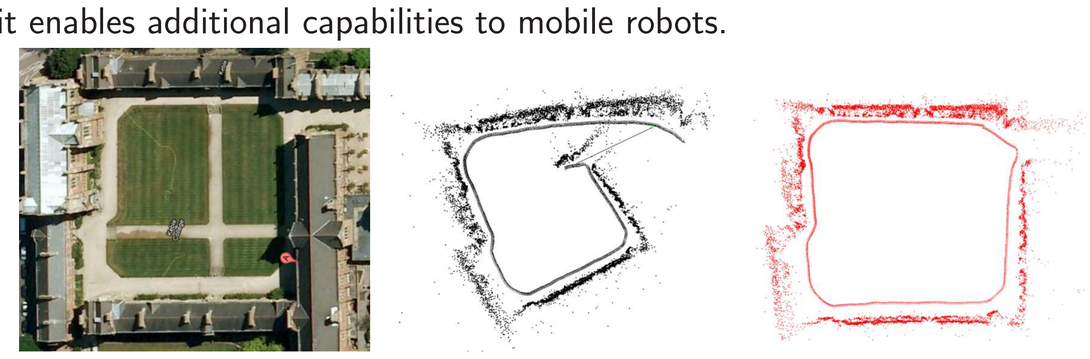

(a) Aerial photo (b) Before loop closure (c) After loop closure

SeqSLAM

- A loop closing is performed when the robot revisits a familiar place. In order to detect if the current location is already visited in the past or if it is a new place, we use SeqSLAM[1] which consists of calculating the best candidate matching location within every local navigation sequence. Localization is then achieved by recognizing coherent sequences of these local best matches.

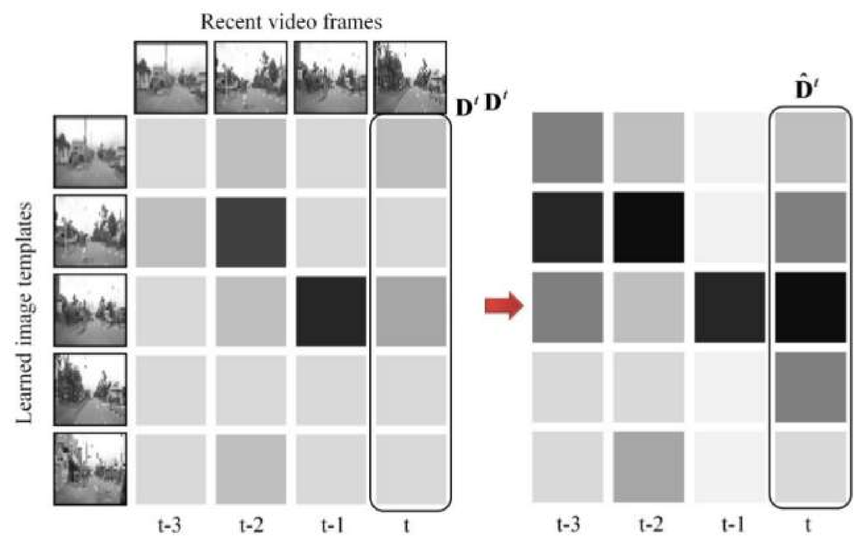

Results:

- We applied the algorithm on different datasets. We have obtained the following matching and similarity matrix on the University of Bonn dataset[2].

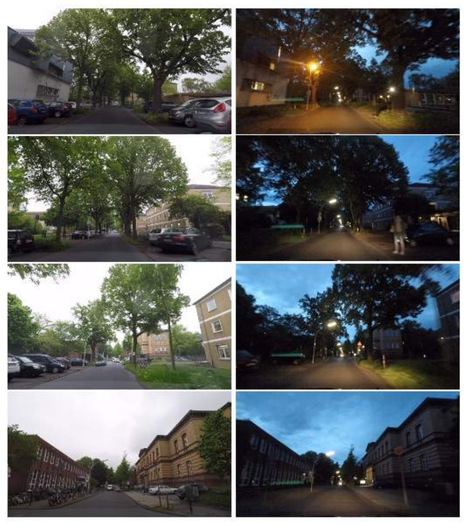

Corresponding frames

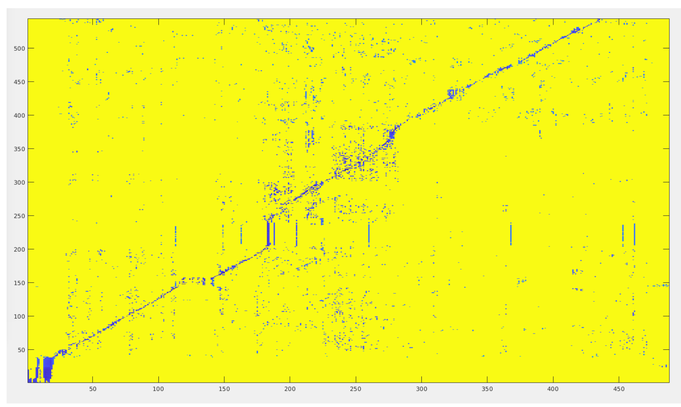

Smiliarity matrix

Conclusion

- SeqSLAM has shown good performance on recognizing places across seasons and under luminosity changes (example : day/night). However, most of global image descriptors lack viewpoint invariance, which may lead to undetecting familiar places on the revisit and thus, loop closure will not be performed when necessary.
- Future work will try to fuse global image descriptor and local feature descriptor together to improve the performance when viewpoints changes.

References

[1] M. J. Milford and G. F. Wyeth.
Seqslam: Visual route-based navigation for sunny summer days and stormy winter nights.
pages 1643–1649, May 2012.

[2] Olga Vysotska and Cyrill Stachniss.
Lazy data association for image sequences matching under substantial appearance changes.
2016.

Contact Information

- Email: youssef.bouaziz@etu.uca.fr
- Phone: +33 6 35 52 84 70

Modeling and Analysis of Electrophysiological Activity Using Matrix Pencil Method

Ecole doctorale Sciences Pour l'Ingénieur

Z. MIZOURI[1], K. EL KHAMLICHI DRISSI[1], L. MONCONDUIT[2], C. PASQUIER[1], B. SION[2] and F. GABRIELLI[2]

[1] Pascal Institute, CNRS, SIGMA Clermont, Clermont-Auvergne University

[2] NEURO-DOL Laboratory, INSERM, Clermont-Auvergne University

Introduction

This work is achieved in collaboration between two interdisciplinary laboratories, Neurol-Dol for health sciences and Pascal Institute for engineering sciences. The subject is to develop a high resolution signal processing tool in order to have a better understanding of pain message and its propagation from the peripheral to the central nervous system.

Electro-stimulation is one of the most used techniques in analyzing neural activity. Recorded signal are always contaminated by the appearance of stimulus artifact. In order to eliminate this useless information and to focus only on neural response, we propose to use a high resolution Matrix Pencil Method (MPM).

The choice of Matrix Pencil Method is based on three criteria: allowing a lossless data compression, providing robustness to measurement noises and the ability to reconstruct truncated signal (useful in the case of stimulus artifact saturation).

Method

✓ **Diagram of experimental procedure**

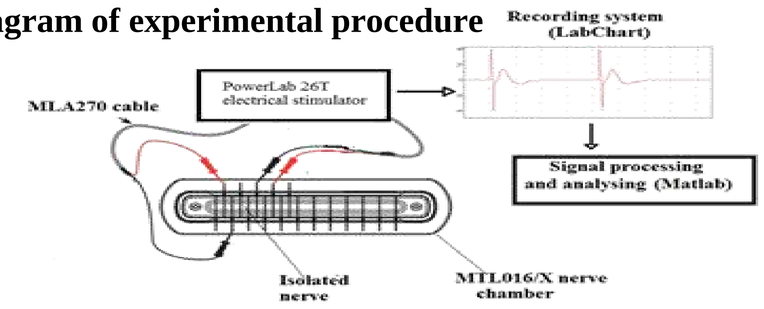

Fig.1 Diagram of experimental procedure

Our data is composed of signals recorded in vitro on the sciatic nerve of a rat, stimulations ranged from 20 to 400 mV (20mV step) with a duration of 200µs and 500 µs, and were repeated 3 times (represented by Test 1 to 3 in result figures).

✓ **Matrix Pencil Method:**

In our case, we use Matrix Pencil Method for measured signal identification. The signal *y(t)* can be written in the following form:

$$y(t) = x(t) + w(t) = \sum_{j=1}^{M} R_j e^{s_j t} + w(t)$$

Matrix Pencil is based on the identification of the number of M significant poles, the complex value of each poles s_j and the complex value of each corresponding amplitude R_j. *w(t)* represents the measurement noise.

✓ **Stimulus artifact removal:**

Our method propose to decompose stimulus artifact into two symmetrical [A] an [B] parts (Fig. 2). In the case where stimulus artifact and response are clearly separated (Fig. 3). , the duration between artifact peaks allows us to ascertain the duration of [A] an [B] parts.

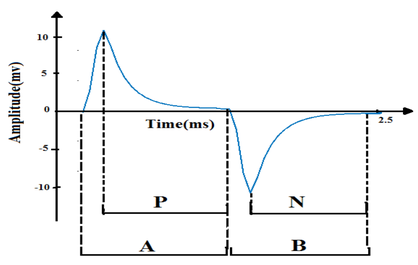

Fig.2 Stimulus artifact wave form

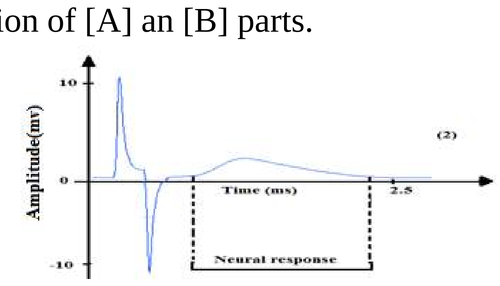

Fig.3 Example of signal with neural response

Under the hypothesis that [A] and [B] are symmetrical, the proposed method reconstructed the exponential part (N) of [B] from the corresponding exponential decay part (P) of [A] and prolong it with the series of M damped exponentials.

In the case of stimulus artifact saturation, it corresponds to input signal overloaded. Only late part of the exponential decay [P] is treated.

In this case, we reconstructed the late part of decay exponential [a2] from the portion [a1] (Fig. 4).

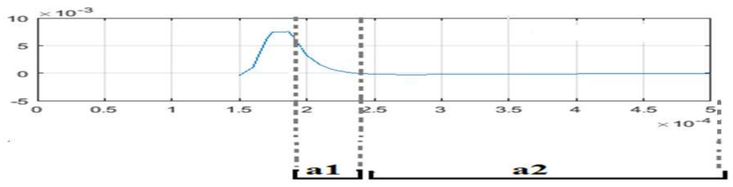

Fig.4 Example of truncated signal

Hypothesis validation and reconstruction quality was assessed with normalized mean square error (NRMSE) .

Results

✓ **Symmetry hypothesis validation**

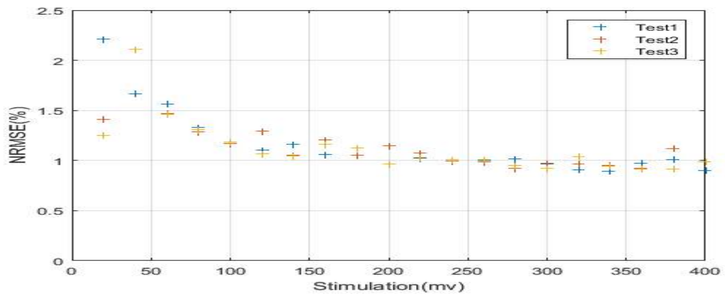

Fig.5 Difference between [A] and [-B] part of artifact, pulse width 200µs, pulse amplitude from 20 to 400mV (increment of 20mV), (Experience is repeated 3 times for the same experimental conditions: Tests 1 to 3)

An NRMSE with a mean of 1,3% and a standard deviation of 0,5% was obtained between [A] and [-B] for the range of electrical stimulations. This result validate our hypothesis of symmetry.

✓ **Quality of reconstruction**

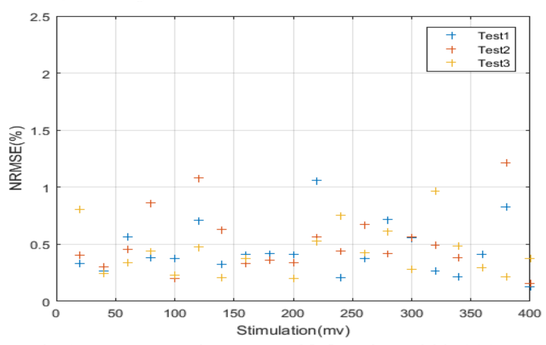

Fig.6 Reconstruction error of [A], pulse width 200µs

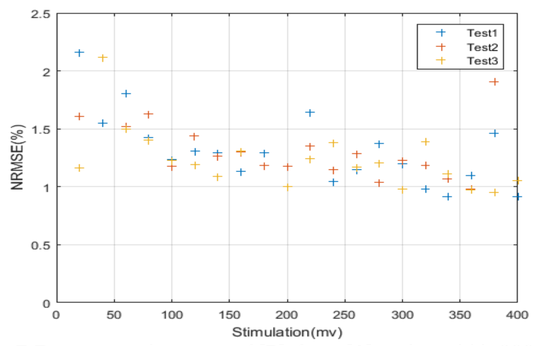

Fig.7 Reconstruction error of [B] from [A], pulse width 200µs

With only three significant poles, an NRMSE with a mean of 0,47% and a standard deviation of 0,25% was obtained for the reconstruction of [A]. For the reconstruction of [B] from [A], an NRMSE with a mean of 1,45% and a standard deviation of 0,54% was obtained (Fig.6 & Fig.7).

✓ **Truncated signal**

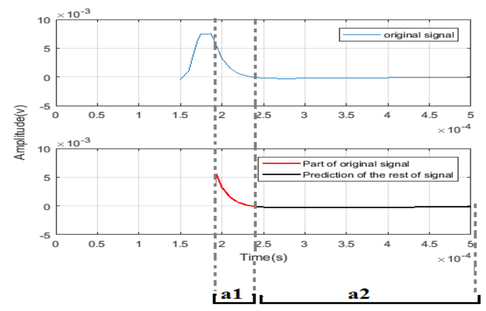

Fig.8 Truncated signal reconstruction, pulse width 500µs, pulse amplitude 400mV

The Matrix Pencil Method is already efficient in identifying truncated signals (Fig.8).

✓ **Stimulus artifact removal**

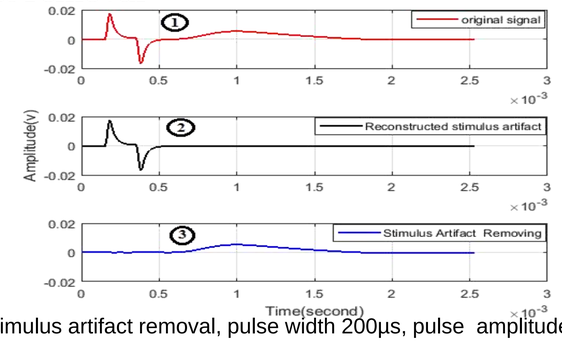

Fig.9 Stimulus artifact removal, pulse width 200µs, pulse amplitude 400 mv

Those results show clearly the potential of our technique in stimulus artifact removal.

Conclusions

- Identification mean error by using Matrix Pencil Method is less than 1,5%.
- Matrix Pencil predict late part of the signal based on few samples.
- Stimulus artifact removal is achieved successfully.

In term of perspectives, we suggest to extend the prediction of late part of artifact in the case when the stimulus artifact is contaminated by the neural response.

Later on, we will classify neural responses in different clusters.

Bibliography

- JA. Freeman, "An electronic stimulus artifact suppressor", Electroencephal Clin Neurophysiol, 1971.
- M. Khodjet-Kesba, K. El Khamlichi Drissi, S. Lee, K. Kerroum, C. Faure and C. Pasquier, "Comparison of Matrix Pencil Extracted Features in Time Domain and in Frequency Domain for Radar Target Classification", International Journal of Antennas and Propagation, 2014